University of Alberta

Violet Diode Laser for Fluorescence Detection in Capillary Electrophoresis

by

Jeremy Edward Melanson

A thesis submitted to the Faculty of Graduate Studies and Research in partial fulfillment of the requirements for the degree of Doctor of Philosophy.

Department of Chemistry

Edmonton, Alberta

Spring 2002

National Library of Canada
Acquisitions and Bibliographic Services
395 Wellington Street
Ottawa ON K1A 0N4
Canada

Bibliothèque nationale du Canada
Acquisitions et services bibliographiques
395, rue Wellington
Ottawa ON K1A 0N4
Canada

Your file Votre référence

Our file Notre référence

The author has granted a non-exclusive licence allowing the National Library of Canada to reproduce, loan, distribute or sell copies of this thesis in microform, paper or electronic formats.

L'auteur a accordé une licence non exclusive permettant à la Bibliothèque nationale du Canada de reproduire, prêter, distribuer ou vendre des copies de cette thèse sous la forme de microfiche/film, de reproduction sur papier ou sur format électronique.

The author retains ownership of the copyright in this thesis. Neither the thesis nor substantial extracts from it may be printed or otherwise reproduced without the author's permission.

L'auteur conserve la propriété du droit d'auteur qui protège cette thèse. Ni la thèse ni des extraits substantiels de celle-ci ne doivent être imprimés ou autrement reproduits sans son autorisation.

0-612-68605-1

Canada

University of Alberta

Library Release Form

Name of Author: Jeremy Edward Melanson

Title of Thesis: Violet Diode Laser for Fluorescence Detection in Capillary Electrophoresis

Degree: Doctor of Philosophy

Year this Degree Granted: 2002

Permission is hereby granted to the University of Alberta Library to reproduce single copies of this thesis and to lend or sell such copies for private, scholarly or scientific research purposes only.

The author reserves all other publication and other rights in association with the copyright in the thesis, and except as herein before provided, neither the thesis nor any substantial portion thereof may be printed or otherwise reproduced in any material form whatever without the author's prior written permission.

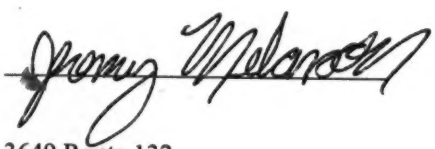

3649 Route 132
Scoudouc Road, New Brunswick
E4P 3M3

Dec. 17, 2001
Date

University of Alberta

Faculty of Graduate Studies and Research

The undersigned certify that they have read, and recommend to the Faculty of Graduate Studies and Research for acceptance, a thesis entitled "Violet Diode Laser for Fluorescence Detection in Capillary Electrophoresis" submitted by Jeremy Edward Melanson in partial fulfillment of the requirements for the degree of Doctor of Philosophy.

Supervisor, Dr. Charles Lucy, Dept. of Chemistry

Dr. D. Jed Harrison, Dept. of Chemistry

Dr. Gary Horlick, Dept. of Chemistry

Dr. Wolfgang Jaeger, Dept. of Chemistry

Dr. Xing-Fang Li, Dept. of Public Health Sciences

External Examiner, Dr. Edward Yeung,
Dept. of Chemistry, Iowa State University

Dec 14, 2001
Date

ABSTRACT

In October of 1999, Nichia Corporation of Japan launched the commercial sale of their InGaN-based violet diode laser. Operating near 400 nm with an output power of 5 mW, this laser presents numerous opportunities for laser induced fluorescence detection (LIF) in capillary electrophoresis (CE). The laser offers significant advantages over conventional red diode lasers and fills a void in the 400-nm region of the electromagnetic spectrum where a suitable laser line for LIF detection had not been available.

To demonstrate the suitability of the violet diode laser for LIF detection in CE, amino acids labeled with the common fluorogenic probe naphthalene-2,3-dicarboxaldehyde were chosen as test compounds. Detection limits of 3 – 8 nM were achieved with a commercial instrument and over 10-fold lower using a home-built LIF detector. This sensitivity is comparable to that achieved previously with the HeCd laser, making the violet diode laser an attractive alternative for this application.

Exploiting the high stability of diode lasers and the numerous fluorescent probes that excite near 400 nm, the violet diode laser was evaluated for indirect LIF detection. Inorganic anions were determined using 8-hydroxypyrene-1,3,6-trisulfonic acid as the indirect detection probe with limits of detection ranging from 0.4 – 0.6 μM. A series of phosphonic acids were detected using tetrakis-(4-sulphophenyl)porphine as the indirect detection probe and detection limits of 0.2 μM were achieved . Baseline stability observed with the violet diode laser was excellent, with dynamic reserve values greater than 1000.

The highly intense Soret excitation band of porphyrins near 400 nm makes them an ideal target for sensitive detection using the violet diode laser. A limit of detection of 20 pM was achieved for urinary porphyrins, which represents a gain in sensitivity of more than two orders of magnitude over previously reported values. This high sensitivity allowed for up to a 100-fold dilution of urine prior to analysis, compared to the pre-concentration steps required in previously reported methods.

Exploiting its high sensitivity for porphyrins, the violet diode laser was used for LIF detection of porphyrin-containing or 'heme' proteins. After reconstitution with a more fluorescent porphyrin, the limit of deteciton for myoglobin was 1 nM.

ACKNOWLEDGEMENTS

I would like to express my sincere thanks to my supervisor, Charles Lucy, for his continual support and friendship throughout the duration of my graduate work. Current and former members of the Lucy group are also gratefully acknowledged. In particular, Ken Yeung, Nicole Baryla, and Panos Hatsis provided daily assistance and created an enjoyable working environment. Further, numerous colleagues in the Department of Chemistry provided immeasurable support. Specifically, I would like to thank Bernd Keller and Rob Polakowski for helpful discussions. Finally, much of the work described in this thesis would not have been possible without the ingenuity of Al Chilton of the departmental electronics shop.

Financial support from the Natural Sciences and Engineering Council of Canada, The Department of National Defense Canada, and the Department of Chemistry of the University of Alberta is gratefully acknowledged.

TABLE OF CONTENTS

Chapter One – Introduction

1.1 Principles of capillary electrophoresis 1
1.1.1 History 1
1.1.2 Basic CE instrumentation 2
1.1.3 Electrophoretic mobility 2
1.1.4 Electroosmotic flow 4
1.1.5 Modes of operation 5
1.1.5.1 Capillary zone electrophoresis 5
1.1.5.2 Micellar electrokinetic chromatography 8

1.2 Detection in CE 12
1.2.1 History 12
1.2.2 Absorbance detection 13
1.2.3 Fluorescence detection 13
1.2.3.1 Theory 14
1.2.3.2 Fluorescence instrumentation 14
1.2.3.2.1 Conventional excitation sources 14
1.2.3.2.2 Diode lasers 16
1.2.3.2.3 Frequency doubling of diode lasers 18
1.2.3.2.4 The quest for the violet/blue laser diode 19

1.3 Thesis overview 20

1.4 Literature cited 24

Chapter Two – Detection of NDA-Labeled Amino Acids

2.1 Introduction 26

2.2 Experimental 31
2.2.1 Apparatus 31
2.2.2 Commercial CE-LIF system 31
2.2.3 High-sensitivity LIF detector 34
2.2.4 Reagents 37
2.2.5 Derivatization procedure 38
2.2.6 Separation conditions – MEKC using commercial CE-LIF 38
2.2.7 Separation conditions – MEKC and CZE using high-sensitivity CE-LIF ... 39

2.3 Results and discussion 39
2.3.1 Detection of NDA-labeled amino acids with MEKC using commercial CE-LIF instrument 39
2.3.2 Detection of NDA-labeled amino acids with MEKC using high-sensitivity CE-LIF instrument 42

2.3.3 Detection of NDA-labeled amino acids with CZE using high-sensitivity CE-LIF instrument 44
2.3.5 Effect of laser power on signal-to-noise of NDA-amino acids 46

2.4 Conclusion 46

2.5 Literature cited 49

Chapter Three – Indirect LIF Detection Using a Violet Diode Laser
3.1 Introduction 51

3.2. Experimental 55
3.2.1 Apparatus 55
3.2.2 Violet diode laser setup 56
3.2.3 HeCd laser setup 56
3.2.4 Reagents 57
3.2.5 Procedures 57

3.3 Results and discussion 58
3.3.1 Selection of indirect fluorescent probes 58
3.3.2 Detection of inorganic anions with HPTS 63
3.3.2.1 Choice of buffering agent 63
3.3.2.2 Separation optimization 65
3.3.2.3 Figures of merit 65
3.3.3 Detection of phosphonic acids with TSPP 67
3.3.4 Baseline stability and dynamic reserve 71

3.4 Conclusions 74

3.5 Literature cited 76

Chapter Four – Analysis of Urinary Porphyrins
4.1 Introduction 79

4.2 Experimental 83
4.2.1 Apparatus 83
4.2.2 Reagents 84
4.2.3 Procedures 84

4.3 Results and discussion 85
4.3.1 Separation of the urinary porphyrins 85
4.3.1.1 Literature methods 85
4.3.1.2 Method optimization 85
4.3.1.3 Porphyrin mobility behaviour 88
4.3.2 Calibration and detection limits 90
4.3.3 Detection of porphyrins in urine 93

4.4 Conclusions 98

4.5 Literature cited 99

Chapter 5 – Trace Analysis of Myoglobin after Reconstitution with a Fluorescent Porphyrin

5.1 Introduction 101

5.2 Experimental 103
5.2.1 Apparatus 103
5.2.2 Reagents 104
5.2.3 Reconstitution procedure 104
5.2.4 Separation conditions 104

5.3 Results and discussion 105
5.3.1 Structure of myoglobin 105
5.3.2 Optical properties of the heme group 108
5.3.3 Demetalation or transmetalation of the heme 110
5.3.4 Reconstitution of myoglobin with a fluorescent porphyrin 112
5.3.4.1 Reconstitution of *apo*-myoglobin with PPIX 114
5.3.4.2 Reconstitution of *apo*-myoglobin with Zn-PPIX 117
5.3.4.3 Potential sensitivity for reconstituted myoglobin 119

5.4 Conclusions 121

5.5 Literature cited 122

Chapter Six – Conclusions and Future Work

6.1 Conclusions 124

6.2 Future work 125
6.2.1 Myoglobin 125
6.2.1.1 Implementation of non-denaturing capillary coatings 125
6.2.1.2 Extension of reconstitution procedure to *holo*-myoglobin 126
6.2.3.1 Enhancement of native myoglobin fluorescence 128
6.2.2 Other proteins 129
6.2.2.1 Hemoglobin 129
6.2.2.2 Cytochromes 129

6.3 Literature cited 131

Appendix

Curriculum vitae 132

LIST OF TABLES

2-1. Fluorescent probes potentially compatible with the violet diode laser 48
3-1. Spectral properties of HPTS and TSPP 62
5-1. Fluorescence excitation and emission maxima for PPIX and Zn-PPIX in aqueous buffer and bound within hemoglobin 113

LIST OF FIGURES

1-1. Schematic of a capillary electrophoresis instrument 3
1-2. Depiction of the movement of anions, cations, and neutral compounds under CZE conditions and the corresponding theoretical electropherogram 7
1-3. Schematic of the separation mechanism of MEKC and the corresponding theoretical electropherogram 10
1-4. Schematic of a diode laser 17
1-5. Structure of the InGaN based laser diode 21
1-6. Picture of the violet laser diode from Nichia 22
2-1. Structures of some common fluorogenic probes 27
2-2. Fluorescence excitation and emission spectra of NDA-labeled glycine in pH 9.5 borate buffer 29
2-3. Schematic of the optical setup of the Beckman LIF detector 32
2-4. Side view schematic of the violet diode laser 35
2-5. Schematic of the laser induced fluorescence detector 36
2-6. MEKC separation of NDA-amino acids using the commercial CE-LIF instrument 40
2-7. MEKC separation of NDA-amino acids using the high-sensitivity CE-LIF instrument 43
2-8. CZE separation of NDA-amino acids using the high-sensitivity CE-LIF instrument 45
3-1. Depiction of the mechanism of indirect detection 52
3-2. Schematic of the mechanism of electrodispersion 59
3-3. Structures HPTS and TSPP 61
3-4. Separation of inorganic anions using HPTS 66
3-5. Degradation pathways of some common nerve agents 69
3-6. Separation of the chemical warfare agent degradation products using TSPP 70
3-7. Comparison of baseline stability of the HeCd laser and violet diode laser 73
4-1. Structures of urinary porphyrins 80
4-2. Absorption spectrum of a typical porphyrin 82
4-3. The effect of SDS concentration on the urinary porphyrin separation 87
4-4. Optimized separation using the high-sensitivity instrument 91
4-5. Calibration curves for coproporphyrin and uroporphyrin 92
4-6. Separation of urine sample diluted 10-fold 95
4-7. Blow-up of 7 to 10 min region of the separation of the urine sample diluted 10- and 100-fold 96
5-1. Three dimensional structure of myoglobin 106
5-2. Structure of the heme group of myoglobin and coordination of the Fe atom 107
5-3. Electropherogram of 5 μM native myoglobin 109
5-4. The separation of the reaction mixture of 70 nM *apo*-myoglobin with 100 nM PPIX and the injection of 100 nM PPIX 115
5-5. The separation of the reaction mixture of 70 nM *apo*-myoglobin with 100 nM Zn-PPIX and the injection of 100 nM Zn-PPIX 118
5-6. The separation of the reaction mixture of 7 nM *apo*-myoglobin with 10 nM Zn-PPIX 120

Chapter One – Introduction

1.1 Principles of capillary electrophoresis

1.1.1 History

Electrophoresis refers to the separation of solutes based on their differential migration in an electric field. The velocity of charged solutes is proportional to the applied voltage. Thus high voltage is theoretically desirable for fast and efficient separations. In practice, the use of high electric fields is limited due to the unwanted peak broadening generated by Joule heating. As a result, early electrophoresis was performed in anti-convective media; e.g., polyacrylamide gel, with low applied electric potentials. The analytes were also limited to macromolecules with low diffusion coefficients. Today, polyacrylamide gel electrophoresis (PAGE) has become a classical technique in biochemistry laboratories for separating macromolecules such as proteins, peptides and nucleic acids.

Owing to the use of viscous gel media and low applied voltage, gel electrophoresis suffers from long analysis times and low efficiencies. Alternatively, the use of narrow bore tubes or capillaries was proposed as it provides good heat dissipation, allowing the electrophoresis to be performed in solution instead of gel. Capillary electrophoresis (CE) was first demonstrated by Hjertén with 3 mm tubes in 1967 [1]. As the technology advanced, capillaries with smaller inner diameter (i.d.) were used in electrophoretic separations to achieve higher resolutions and efficiencies [2, 3]. Today, CE is mostly performed in 10 to 100 μm inner diameter (150 to 375 μm outer diameter) fused silica capillaries. This fragile capillary is protected by a polyimide outer coating

which makes the capillary flexible and easy to handle. The high surface-to-volume ratio of the narrow capillaries allows for very efficient dissipation of Joule heating. In addition the use of capillaries in electrophoresis allows separation of a wide variety of analytes ranging from small inorganic ions to large biomolecules.

1.1.2 Basic CE instrumentation

A schematic diagram of a capillary electrophoresis instrument is shown in Figure 1-1. Typical capillary lengths range from 10 to 100 cm, and capillary inner diameters (i.d.) are 10 to 100 μm. Each end of the capillary is immersed in an electrolyte reservoir, which are connected to the high voltage power supply via electrodes.

To perform a CE separation, the capillary is filled with the electrolyte by applying an external pressure to the inlet reservoir. Then the inlet reservoir is replaced with a sample reservoir, from which a small plug of sample is pushed into the capillary by either applying a small pressure or voltage. Typical injection volumes are on the order of 1 – 10 nL. Next the inlet reservoir is put back in place, and separation begins upon the application of an electric field. Typical applied voltages are 100 to 1000 V/cm. Ions in the sample migrate with an electrophoretic mobility determined by their charge and mass. Photometric detection is usually performed on capillary near the outlet reservoir. A window for optical detection is created by removing a section of the polyimide coating. Data is typically collected and stored by computer.

1.1.3 Electrophoretic mobility

Separation by electrophoresis is based on the differences in the solutes' electrophoretic mobility. The electrophoretic mobility of an ion is proportional to the

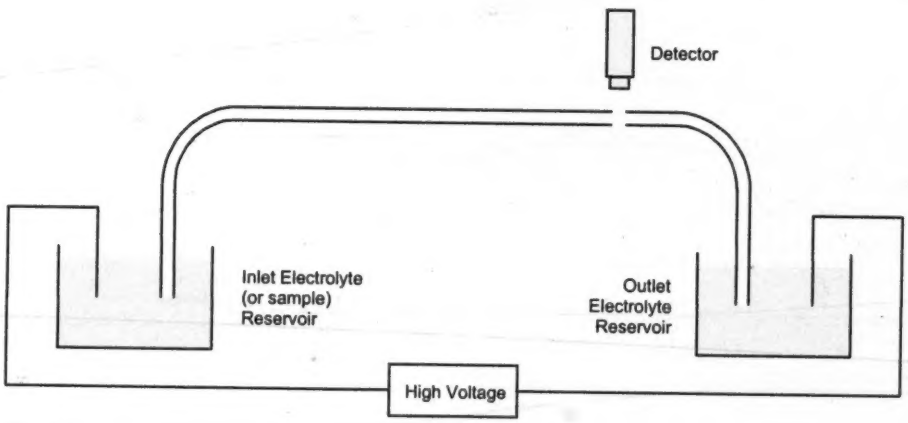

Figure 1-1. Schematic of a capillary electrophoresis instrument.

electric force that the ion experiences and inversely proportional to its frictional drag through the medium. Electrophoretic mobility can be expressed as

$$\mu_e = \frac{q}{6\pi\eta r} \qquad \text{(Eqn. 1-1)}$$

where q is the net charge of the ion, η is the viscosity of the medium, and r is the radius of the ion. Therefore, electrophoretic separation occurs for solutes with different mobilities, or charge-to-size ratios.

1.1.4 Electroosmotic flow (EOF)

In addition to the electromigration of analyte ions, electroosmotic flow also occurs upon application of an electric field in CE. The inner walls of fused silica capillaries possess an intrinsic negative charge due to the presence of weakly acidic silanol groups (–SiOH) ($pK_a \sim 5.3$ [4]). Cations in solution build up near the capillary surface to balance this charge, thus forming an electrical double layer. Upon the application of an electric field across the length of the capillary, the cations in the diffuse portion of the double layer migrate toward the negative electrode (cathode). Since these cations are hydrated, they induce a bulk flow of solution within the capillary toward the cathode that exhibits a flat flow profile. The magnitude of this EOF is generally described by the Smoluchowski equation:

$$\mu_{eof} = -\frac{\varepsilon\zeta}{\eta} \qquad \text{(Eqn. 1-2)}$$

where ε and η are the dielectric constant and viscosity of the solvent, and ζ is the zeta potential. The zeta potential is the potential slightly off the silica surface at the plane of shear, and is a function of the deprotonation of the silanols, ion adsorption onto the

surface, and the ionic strength of the buffer. Manipulation of the magnitude and/or the direction of the EOF can yield either rapid [5] or high-resolution [6] separations.

1.1.5 Modes of operation

Capillary electrophoresis is a general term that is used to describe a number of different separation techniques. Capillary zone electrophoresis (CZE) is the classic technique and is therefore usually referred to as just CE. Other techniques include micellar electrokinetic chromatography (MEKC), capillary isoelectric focusing (CIEF), and capillary isotachophoresis (CITP). CZE and MEKC are the predominant techniques and are those used herein, so only they will be discussed in detail here.

1.1.5.1 Capillary zone electrophoresis (CZE)

As described above, charged analytes in CZE experience both their electrophoretic mobility (μ_e) and also the electroosmotic flow mobility (μ_{eo}). The net or apparent mobility is given by

$$\mu_{app} = \mu_e + \mu_{eof} = \frac{L_d}{t_m E} \qquad \text{(Eqn. 1-3)}$$

This apparent mobility can be easily calculated with the capillary length to the detector (L_d), the migration time of the analyte (t_m), and the electric field strength (E).

In general, most analytes separated by CE possess an electrophoretic mobility less than that of the EOF mobility (μ_{eof} is typically 5×10^{-4} to 8×10^{-4} cm^2/(V s) at neutral pH). This allows for simultaneous determination of both positively and negatively charged species when the detector is placed at the cathodic (negative) end of the capillary. In this case, cations migrate in the same direction as the EOF (co-EOF) and anions migrate opposite to the direction of the EOF (counter-EOF). As long as anions have electrophoretic mobilities less than that of the EOF ($\mu_e < \mu_{eof}$), they are swept by the

EOF towards the detector. Figure 1-2A shows a schematic of a CZE separation and Figure 1-2B displays the corresponding theoretical 'electropherogram'. Note that CZE is incapable of separating neutral compounds.

In the case of high-mobility analytes such as inorganic anions, μ_e values are comparable or even greater than that of μ_{eo}. For instance, common anions such as chloride, bromide, and sulfate have electrophoretic mobilities of 7.92, 8.09, and 8.29 $\times$ 10^{-4} $cm^2/(V\ s)$, respectively. Thus these anions migrate faster than the EOF but in the opposite direction. As a consequence they would not be detected in the normal configuration described above (detector at cathode). Rather one would need to inject at the cathode and place the detector at the anode to detect these ions. This reversed configuration will be used in Chapter 3.

The major source of band-broadening in CZE is longitudinal diffusion. Longitudinal diffusion refers to the axial diffusive spreading of the solute from the solute zone into the bulk solution as it travels down the capillary. The variance in peak width contributed by longitudinal diffusion is given by

$$\sigma^2_{diff} = 2\,D\,t_m \qquad \text{(Eqn. 1-4)}$$

where D is the diffusion coefficient of the solute and t_m is the migration time. Hence, longitudinal diffusion is proportional to the time the solute spends in the capillary, and longitudinal diffusion is more severe for solutes with large diffusion coefficients.

Neglecting all other sources of band-broadening, the maximum theoretical efficiency (N_{max}) due to longitudinal diffusion alone is

$$N_{max} = \frac{\mu_e V}{2D} \qquad \text{(Eqn. 1-5)}$$

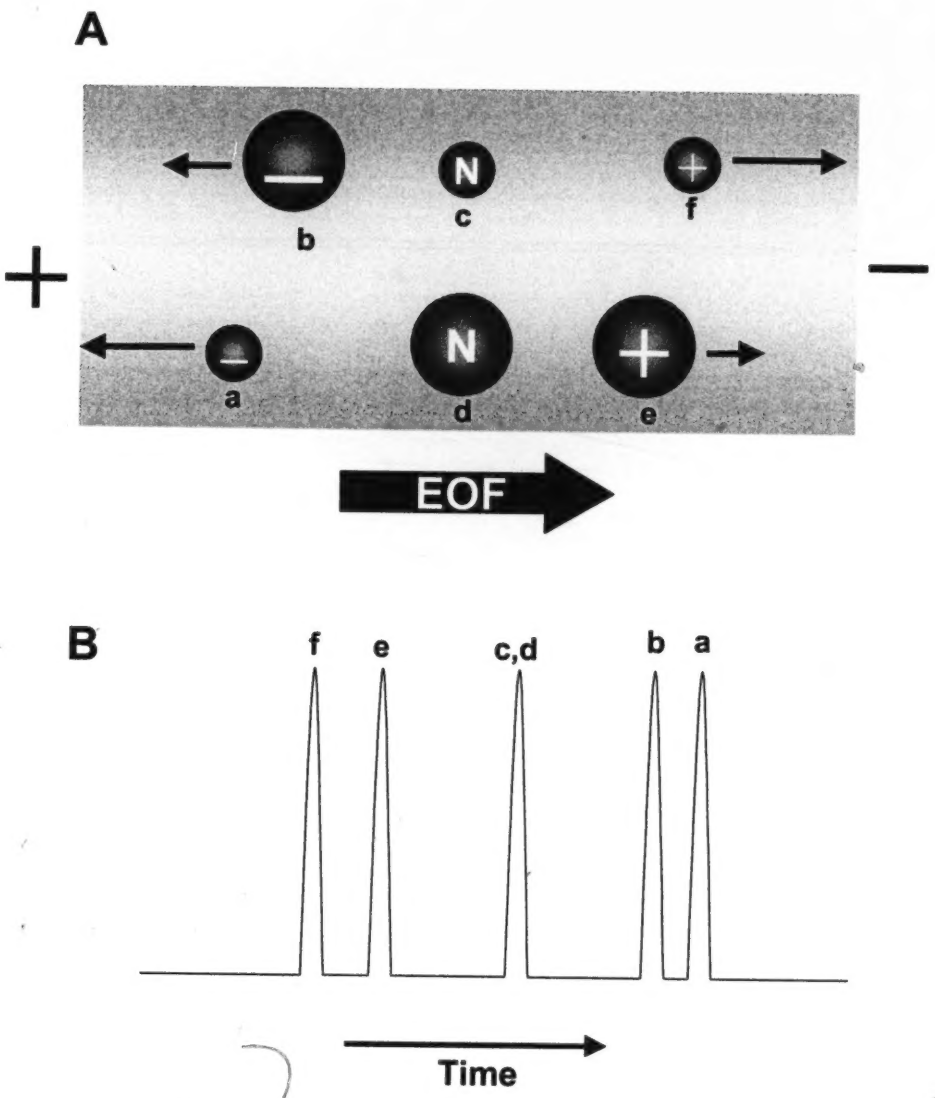

Figure 1-2. Depiction of the movement of anions, cations, and neutral compounds under CZE conditions (A) and the corresponding theoretical electropherogram (B).

where V is applied voltage. Therefore, it is desirable to use large applied voltages in CE. However, if excessive current is generated in the capillary (i.e. using high-conductivity buffers or large i.d. capillaries), Joule heating can limit the maximum electric field strength used. Joule heating creates a radial temperature gradient, with higher temperatures at the center of the capillary than at the walls. This temperature gradient gives rise to viscosity differences in the buffer and leads to band-broadening, as analyte molecules in the center of the capillary travel faster those near the walls.

The high efficiency achievable by CE (typically >100,000 plates) also enhances its resolving power. The resolution (R) of two components achievable in CZE is expressed by

$$R = \frac{1}{4}\sqrt{N}\,\frac{\Delta\mu}{\overline{\mu}_{app}} \qquad \text{(Eqn. 1-6)}$$

where N is the efficiency, $\Delta\mu$ is the mobility difference between the ions and $\overline{\mu}_{app}$ is the mean apparent mobility of the ions.

1.1.5.2 Micellar electrokinetic chromatography (MEKC)

First reported in 1984 by Terabe and co-workers, micellar electrokinetic chromatography (MEKC) is a hybrid of electrophoresis and chromatography [7]. Its main strength is its ability to separate both charged and neutral compounds.

Separation by MEKC is based on the differential partitioning of solutes into a 'pseudo'-stationary phase. In general, the pseudo-stationary phase is formed simply by the addition of surfactants to the background electrolyte. Above their critical micelle concentration (CMC), surfactant molecules aggregate in such as fashion as to minimize the contact of their hydrophobic tails with water. Spherical aggregates are the most

common result, with the hydrophobic tails oriented towards the center and the hydrophilic head groups on the exterior. A schematic of a micelle is shown in Figure 1-3A. The anionic surfactant sodium dodecyl sulfate is the classic surfactant employed for MEKC and has a CMC of ~ 8 mM and an aggregation number of ~ 60 [7].

A schematic of the separation mechanism of MEKC is shown in Figure 1-3A and Figure 1-3B displays the corresponding theoretical chromatogram. Briefly, the negatively charged SDS micelles migrate toward the anode (positive), which is in the opposite direction of the EOF. At neutral or basic pH, the EOF velocity will be fast enough such that the net movement of the micelles will be toward the cathode (negative). A completely unretained (hydrophilic; no interaction with micelles) neutral analyte will migrate with the EOF and will elute at t_0, as shown in Figure 1-3B. Conversely, a neutral analyte that is completely retained by the micelles will elute at t_{mc}, which corresponds to the time it takes a micelle to travel from the capillary inlet to the detector. Any neutral analytes with any degree of retention falling between these two extremes must then elute bewteen t_0 and t_{mc}, with more highly retained compound eluting after less retained compounds (Figure 1-3B). The length of this time window ($t_{mc} - t_0$) is significant in MEKC in that it dictates the peak capacity. Thus it is advantageous to use micelles having high mobility in the direction opposite of the EOF.

Retention of neutral solutes in MEKC is essentially chromatographic and can be described using modified chromatographic relationships. The capacity factor, $\widetilde{k'}$, is given by

$$\widetilde{k'} = \frac{(t_r - t_0)}{t_0\left(1 - \frac{t_r}{t_m}\right)} \qquad \text{(Eqn. 1-7)}$$

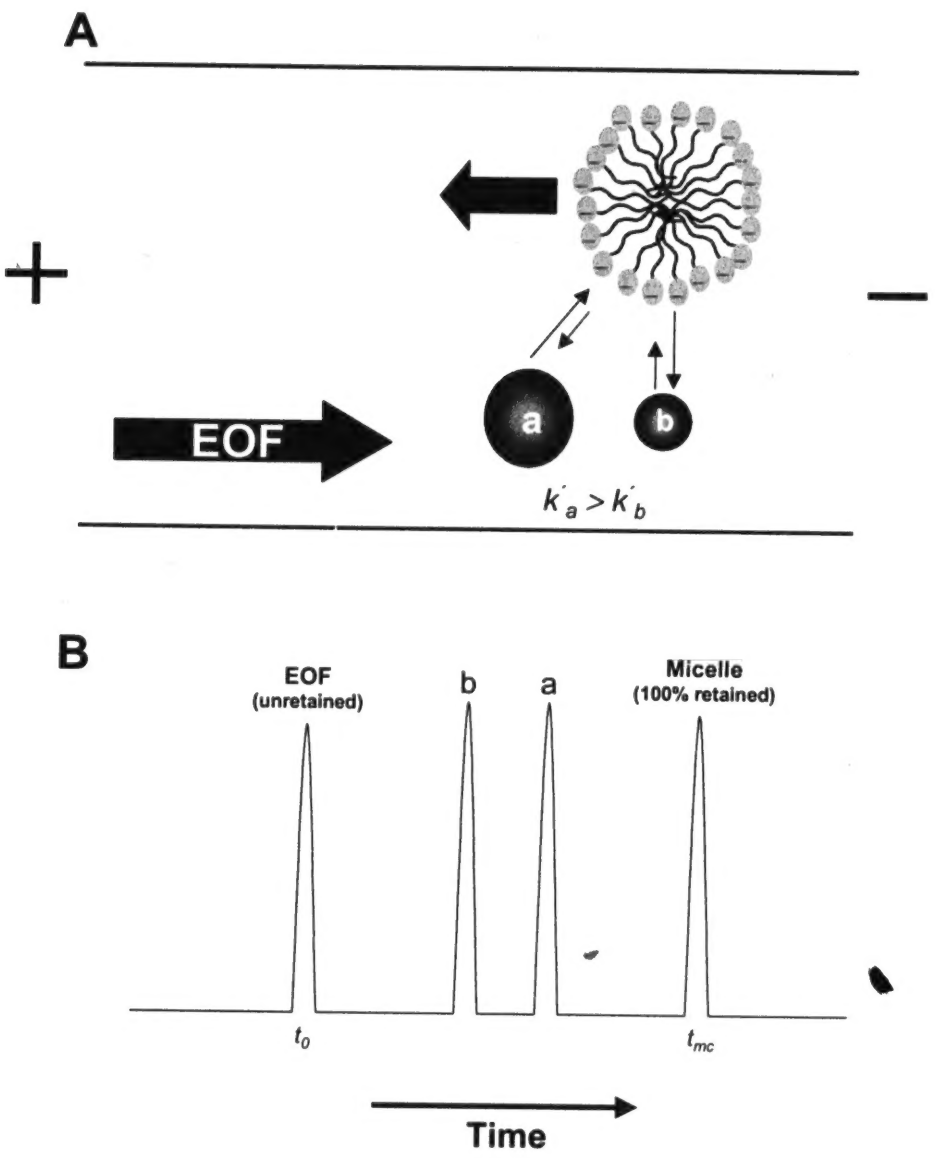

Figure 1-3. Schematic of the separation mechanism of MEKC (A) and the corresponding theoretical electropherogram (B).

where t_r is the rentention time of the solute, t_0 is the retention time of an unretained solute (dead time), and t_{mc} is the micelle elution time (100% retained compound). This equation is modified from the standard chromatographic form to account for the movement of the pseudo-stationary phase. Retention is most easily adjusted in MEKC by varying the surfactant concentration. Generally, the capacity factor increases linearly with surfactant concentration. However, the range of ionic surfactant concentrations is limited, since high concentrations can produce excessive current and thus lead to Joule heating in the capillary (temperature gradient). The typical concentration range for SDS is 20 – 100 mM.

Resolution of two components in MEKC is given by

$$R = \left(\frac{\sqrt{N}}{4}\right)\left(\frac{\alpha - 1}{\alpha}\right)\left(\frac{k_2'}{k_2' + 1}\right)\left(\frac{1 - \left(\frac{t_0}{t_m}\right)}{1 - \left(\frac{t_0}{t_m}\right)k_1'}\right) \qquad \text{(Eqn. 1-8)}$$

where N is the number of theoretical plate (typically 100,000 – 200,000) and α is the separation factor (k_2'/k_1'). By far the most powerful term in this equation for increasing resolution is the selectivity term (α-1/α). Altering the surfactant type is an effective way to alter selectivity. Zwitterionic surfactants and bile salts such as cholate have both been used effectively. Buffer additives such as cyclodextrins have also been used to alter selectivity in MEKC. Cyclodextrins introduce a shape or orientation component into the overall retention mechanism and can be used in conjunction with surfactants to fine-tune separations. Generally speaking, the resolving power of MEKC is such that separation can be achieved for a pair of analytes with α as low as 1.02.

The discussion so far has dealt strictly with neutral compounds in MEKC. MEKC will be used in this manner in Chapter 2. However, MEKC is also effective in enhancing selectivity of charged compounds that have a hydrophobic moiety. The net retention of these types of compounds is thus based on a combination of both electrophoretic and chromatographic behaviours. Thus MEKC is used to separate charged porphyrins in Chapter 4.

1.2 Detection in CE

1.2.1 History

As early as the rebirth period of capillary electrophoresis in the early 1980s, Jorgenson and co-workers recognized the need for highly sensitive detectors for CE [3]. It was quickly realized that the adaptation of conventional HPLC detectors would be problematic due to the small dimensions of CE.

Numerous techniques have been reported for detection in CE over the past 20 years [8]. Optical techniques such as absorbance and fluorescence have seen by far the most widespread use and will be discussed in detail below. Electrochemical techniques such conductivity, amperometry, and potentiometry have all been applied successfully to detection in CE with detection limits in the range of 10^{-5} to 10^{-8} M [8,9]. However, practical problems with the precise placement of microelectrodes and the grounding of the electrophoretic current prior to the point of detection have restricted their development into standard methodology. Electrospray ionization mass spectrometry (ESI) has also been implemented successfully as a detection system in CE separations [10].

1.2.2 Absorbance detection

On-column UV absorbance detection is by far the most common method of detection in CE today. Many compounds of interest absorb light to some extent in the UV region without any chemical modification. Detector components are fairly robust and inexpensive, and little operator skill is required. For these reasons, most commercial CE instruments are equipped with a standard UV absorbance detector [11].

Ironically, while being the most popular detection scheme used in CE, absorbance detection is arguably the least compatible with CE. A fundamental limitation of absorbance detection is that one is looking for a small difference between two relatively large signals. This problem is amplified as the amount of absorbing material in the light path becomes small. According to Beer's law, absorbance (*A*) is given by

$$A = \log \frac{I_0}{I} = \varepsilon bc \qquad \text{(Eqn. 1-9)}$$

where I_0 is the intensity of the incident radiation on the sample, I is the intensity of light transmitted through the sample, ε is the molar extinction coefficient of the sample, b is the optical path length, and c is the molar sample concentration. Therefore the optical path length directly impacts the sensitivity that can be achieved with absorbance detection. The 10 – 100 μm i.d. of capillaries used in CE yield rather disappointing detection limits of 10^{-5} M to 10^{-6} M [8].

1.2.3 Fluorescence detection

Without a doubt, fluorescence has emerged as the most sensitive detection technique in CE. In particular, laser induced fluorescence (LIF) has quite commonly achieved detection limits in the low pM range. Unlike absorbance detection, the sensitivity that can be achieved by fluorescence is not strictly pathlength dependent.

1.2.3.1 Theory

In fluorescence, a molecule absorbs a photon of light and sometimes will return to the ground state by emitting a photon (fluorescence). When self-absorption is negligible, fluorescence intensity (F) is directly proportional to concentration, c, and given by

$$F \propto P_0 k \Phi_f c \qquad \text{(Eqn. 1-9)}$$

where P_0 is the incident excitation power, k is the extinction coefficient or absorptivity, and Φ_f is the quantum yield (fraction of the excited molecules that emit photons). For the most highly fluorescent fluorophores, such as fluorescein and rhodamine, the quantum yield can approach 1. Another important parameter for fluorescence measurements is the photostability of the fluorophore, which is often quantified as the average number of excitation/emission cycles that a molecule can undergo before being destroyed or 'photobleached'. For fluorescein, a photostability of 8000 cycles has been reported [12]. However, many fluorescent molecules exhibit much lower photostability.

1.2.3.2 Fluorescence instrumentation

Fluorescence instrumentation is relatively simple and generally consists of an excitation source, focusing optics, collection optics, emission filter(s), and a detector (photomultiplier tube, PMT). A schematic of a typical fluorescence detector is shown in Figure 2-5 (page 36). The excitation light source is the focus of the work described in the following chapters so will be discussed in detail below.

1.2.3.2.1 Conventional excitation sources

Jorgenson and co-workers' initial CE system over 20 years ago employed a high-pressure mercury arc lamp for excitation of dansyl and fluorescamine labeled amines [3]. It was quickly realized that the focusing of light from such lamps down to the small

dimensions of the capillary was problematic. It was not until 1985 that Zare and co-workers demonstrated the first laser-based fluorescence detector for CE [13]. Using a 325-nm HeCd laser, and optical fibers for excitation beam delivery and fluorescence collection, detection limits of ~0.1 μM were achieved for dansylated amino acids. Since that original work, laser induced fluorescence (LIF) has been the method of choice for fluorescence detection in CE. Lasers are particularly well suited for focusing intense light onto small capillaries. Further, monochromatic laser light produces narrower Rayleigh scatter and more simple Raman features that are more easily filtered from the desired fluorescence signal than those produced by broad-band sources [14].

Since the introduction of LIF detection, the Ar-ion [15, 16], HeNe [17] and HeCd [18] lasers have dominated applications. These lasers have emission lines that are compatible with common fluorescent reagents. For instance, the 488-nm line of the Ar-ion laser works fairly well with the ever-popular fluorescein family of dyes. Similarly, the 543-nm line of the HeNe laser is effective for the excitation of rhodamine derivatives. Using these lasers coupled with appropriate fluorescent probes, detection limits generally range from 10^{-9} to 10^{-12} M [14].

Despite the success of these conventional gas-based lasers for LIF detection, they suffer from numerous shortcomings. Primarily, conventional lasers such as the Ar-ion and HeCd are generally expensive and have limited lifetimes (~ 5 000 h). These lasers are also relatively bulky, making them unattractive for miniaturized instruments. Finally, sensitivity achieved with conventional lasers may be limited by the instability of their output (typically 1% noise [19]).

1.2.3.2.2 Diode lasers

Semiconductor or diode lasers are a promising alternative to conventional lasers. Diode lasers are cheap, require no maintenance, and have lifetimes approaching 50 000 h [20]. These lasers are also extremely compact and can run off battery power. Further, the output stability of diode lasers is significantly better than that of conventional lasers (0.01% vs. 1% noise [19]). These properties suggest that diode lasers are ideally suited for LIF detection.

Diode lasers take advantage of the properties of a junction between positively doped (p-type) and negatively doped (n-type) semiconductors constructed from the same material. The p-type semiconductor contains 'holes' and the n-type semiconductor contains excess electrons. When a voltage is applied across the semiconductor, electrons flow from the n to the p region and positive holes flow in the opposite direction. This creates a population inversion in the junction region, leading to laser action. Figure 1-4 is a schematic of a diode laser. Laser diodes are typically only a few millimeters long and a couple microns thick. The two ends of the diode are polished to increase internal reflection. As a consequence of the small size and rectangular configuration of the cavity, the resulting beam diameter is very small (~1 μm), beam divergence is quite high (20 – 40°), and the beams are astimagtic and elliptical (typically 3:1 or greater). This is likely the most significant shortcoming of diode lasers, though beam shape can be corrected with the appropriate optics.

Also, diode laser output has been limited to the near-IR and more recently the red region (635 nm) of the electromagnetic spectrum. The red diode laser has been used successfully in a number of CE-LIF applications [21-23]. However, despite the advantage of

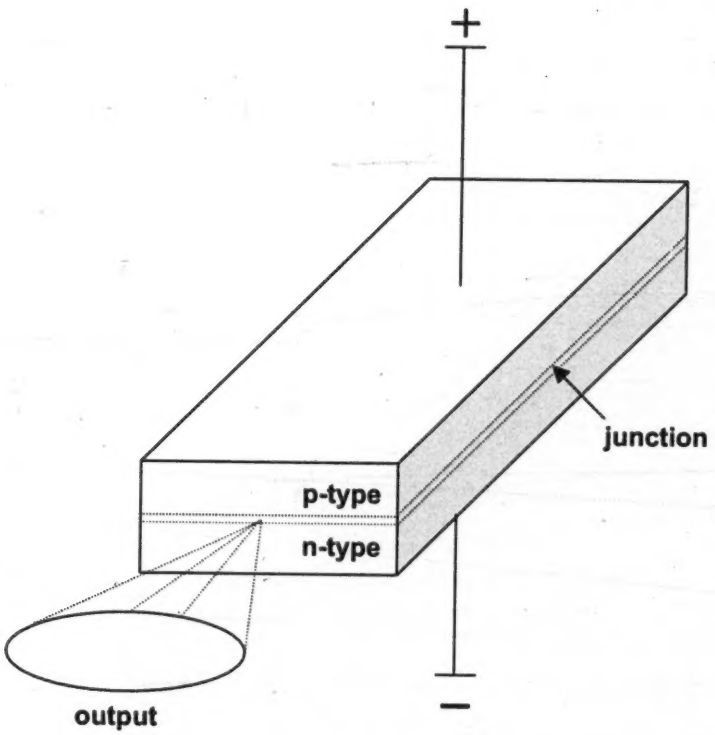

Figure 1-4. Schematic of a diode laser.

low Raman background signals in this region of the spectrum, use of the 635-nm diode laser has been limited. Very few commercially available dyes are excited in this region. Further, those that are available tend to be rather large molecules that are water insoluble and/or complicate separations. Thus diode lasers emitting at much shorter wavelengths would be extremely desirable.

1.2.3.2.3 Frequency doubling of diode lasers

Efforts have been made to shorten the wavelengths of diode lasers through second harmonic generation (SHG) [24, 25]. Unfortunately, SHG can be a very inefficient process, with conversion efficiencies as low as 2.5×10^{-6}. [26] For instance, Imasaka *et al.* frequency-doubled a 40 mW 830-nm diode laser using a $LiNbO_3$ waveguide to produce blue light at 415 nm [24]. Unfortunately, they ultimately found that the 0.01 to 0.05 mW of output power was too weak to be useful for many LIF applications [27]. More promising results were achieved by Jansson *et al.* who focused a diode laser (848 nm, 150 mW) through a potassium titanyl phosphate (KTP) waveguide to produce 0.5 mW of blue light (424 nm) [25]. Jansson *et al.* claimed that 0.5 mW was more than sufficient for LIF detection of derivatized amino acids in CE, and yielded detection limits of 5.9 nM [25]. Similarly, diode-pumped Nd:YAG lasers operating at 532 nm (second harmonic of YAG) have also been employed for detection in CE [27]. These lasers have sufficient power (several mW), are relatively small, and are now commercially available. However, these diode-based lasers have numerous shortcomings. Firstly, the use of non-linear optics adds substantially to the cost of these lasers. Secondly, the low SHG conversion efficiency requires rather large input power, adding both to the cost and to the size of

these lasers. Thus these diode-based lasers exhibit only moderate advantages over conventional gas-based lasers.

1.2.3.2.4 The quest for the violet/blue laser diode

The quest for a short-wavelength diode laser began in the late 1960s when it became evident that group III nitride materials (AlN, GaN, InN) possessed band gap energies capable of producing violet-blue light [28, 29]. Corporations such as AT&T, IBM, and RCA recognized the potential for such devices and implemented research programs. However, most of these programs were later cancelled due to the inability to solve several key technological problems. Specifically, GaN substrates were highly defective due to poor crystal growth technology. It was not until the mid-1980s that these problems began to be resolved, due in large part to the efforts of Isamu Akasaki at Nagoya University and Shuji Nakamura at Nichia Chemical Company (now Nichia Corporation). The technique of metalorganic chemical vapor deposition (MOCVD) was developed for depositing GaN films onto sapphire substrates [30]. These structures exhibited remarkable improvements in optical properties, ultimately leading to the development of high-brightness blue and green light emitting diodes (LEDs) [31].

In the mid-1990s, Nichia Corporation pumped an unprecedented 1.5 % of its annual revenue into Nakamura's research. In 1995, Nichia achieved room temperature pulsed operation of an InGaN-based laser diode with an emission wavelength of 410 nm. In 1996, Nakamura demonstrated room temperature continuous-wave (cw) operation of InGaN laser diodes, but lifetimes were limited to 1 s due to the generation of large amounts of heat [32]. Further optimization of the InGaN structure led to the reduction of the threshold current and voltage, initially increasing lifetimes to the tens of hours and

then up to nearly 10 000 hours in 1997. A schematic of the InGaN structure is shown in Figure 1-5.

In October of 1999, Nichia launched the commercial sale of their InGaN-based violet laser diode. Figure 1-6 is a picture of the laser diode from Nichia. The diode operates at 405 nm with a power output of 5 mW and has an estimated lifetime of 2 000 to 5 000 hours. It is anticipated that this laser will revolutionize technologies such as laser printing, telecommunications, and high-density data storage. For instance, Pioneer Electronics Corporation has already demonstrated an optical disk that holds 27.4 gigabytes (enough to store 4 hours of high-definition video) of data using the Nichia diode. Pioneer Electronics plans to use this technology for the next generation of DVD players. Current DVDs have a capacity of 8.54 gigabytes, not nearly enough to store an adequate length of high-definition video.

1.3 Thesis overview

The following chapters explore the use of the violet diode laser for laser induced fluorescence detection in capillary electrophoresis. Chapter 2 describes the first application of the violet diode laser for chemical analysis. Amino acids labeled with the common fluorescent reagent naphthalene-2,3-dicarboxaldehyde (NDA) were chosen as test analytes to evaluate the performance of the laser. In Chapter 3, the high stability of diode lasers is exploited for indirect fluorescence detection. Novel indirect fluorescent probes are used to detect inorganic anions and the degradation products of chemical warfare agents. Chapter 4 describes the analysis of urinary porphyrins using the violet diode laser for excitation. Until now, a practical laser has not been available for

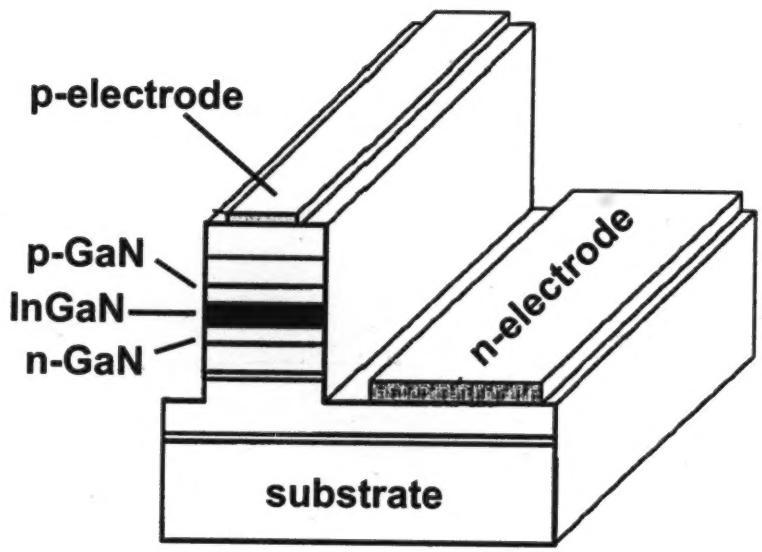

Figure 1-5. Structure of the InGaN based laser diode.

Figure 1-6. Picture of the violet laser diode from Nichia.

porphyrins, which are a large class of biologically important compounds. The high sensitivity achieved for porphyrins is then exploited for the detection of porphyrin containing (heme) proteins in Chapter 5. This preliminary work describes methodology to enhance the fluorescence of these proteins.

1.4 Literature cited

(1) Hjerten, S. *Chromatogr. Rev.* **1967,** *9*, 122.

(2) Mikkers, F. E. P.; Everaerts, F. M.; Verheggen, T. P. E. M. *J. Chromatogr.* **1979,** *169*, 11.

(3) Jorgenson, J. W.; Luckacs, K. D. *Anal. Chem.* **1981,** *53*, 1302.

(4) Schwer, C.; Kenndler, E. *Anal. Chem.* **1991,** *63*, 1801.

(5) Melanson, J. E.; Lucy, C. A. *J. Chromatogr. A* **2000,** *884*, 311.

(6) Yeung, K. K.-C.; Lucy, C. A. *Electrophoresis* **1999,** *20*, 2554.

(7) Terabe, S.; Otsuda, K.; Ichikawa, K.; Tsuchiya, A.; Ando, T. *Anal. Chem.* **1984,** *56*, 111.

(8) Albin, M.; Grossman, P. D.; Moring, S. E. *Anal. Chem.* **1993,** *65*, 489A.

(9) Haber, C. In *Handbook of Capillary Electrophoresis*; Landers, J. P., Ed.; CRC Press: Boca Raton, 1997, pp 425.

(10) Severs, J. C.; Smith, R. D. In *Handbook of Capillary Electrophoresis*; Landers, J. P., Ed.; CRC Press: Boca Raton, 1997, pp 791.

(11) DeFrancesco, L. *Anal. Chem.* **2001,** *73*, 497A.

(12) Hirschfeld, T. *Applied Optics* **1976,** *15*, 3135.

(13) Gassman, E.; Kuo, J. E.; Zare, R. N. *Science* **1985,** *230*, 813.

(14) Pentoney, S. L.; Sweedler, J. V. In *Handbook of Capillary Electrophoresis*; Landers, J. P., Ed.; CRC Press: Boca Raton, 1997, pp 379.

(15) Wu, S.; Dovichi, N. J. *J. Chromatogr.* **1989,** *480*, 141.

(16) Yeung, E. S.; Wang, P.; Li, W.; Giese, R. W. *J. Chromatogr. A* **1993,** *608*, 73.

(17) Chen, D. Y.; Dovichi, N. J. *J. Chromatogr. B* **1994,** *657*, 265.

(18) Gilman, S. D.; Ewing, A. G. *Anal. Chem.* **1995,** *67*, 58.

(19) Gooijer, C.; Mank, A. J. G. *Anal. Chim. Acta* **1999,** *400*, 281.

(20) Imasaka, T.; Ishibashi, N. *Anal. Chem.* **1990,** *62*, 363A.

(21) Mank, A. J. G.; Yeung, E. S. *J. Chromatogr. A* **1995,** *708*, 309.

(22) Rahavendran, S. V.; Karnes, H. T. *Anal. Chem.* **1997,** *69*, 3022.

(23) Gallaher, D. L.; Johnson, M. E. *Analyst* **1999,** *124*, 1541.

(24) Higashijima, T.; Fuchigami, T.; Imasaka, T.; Ishibashi, N. *Anal. Chem.* **1992,** *64*, 711.

(25) Jansson, M.; Roeraade, J.; Laurell, F. *Anal. Chem.* **1993,** *65*, 2766.

(26) Okazaki, T.; Imasaka, T.; Ishibashi, N. *Anal. Chim. Acta* **1988,** *209*, 327.

(27) Kaneta, T.; Komatsubara, T.; Shiba, H.; Imasaka, T. *Anal. Sci.* **1998,** *14*, 1017.

(28) Pankov, J. I.; Berkeyheiser, J. E.; Marsuka, H. P.; Wittke, J. *Solid State Commun.* **1970,** *8*, 1051.

(29) Strite, S.; Morkoc, H. *J. Vac. Sci. Technol. B* **1992,** *10*, 1237.

(30) Nakamura, S. *Jpn. J. Appl. Phys.* **1991,** *30*, 1620.

(31) Nakamura, S.; Senoh, M.; Iwasa, N.; Nagahama, S. *Jpn. J. Appl. Phys. Lett.* **1995,** *34*, 797.

(32) Nakamura, S.; Senoh, M.; Nagahama, S.; Iwasa, N.; Yamada, T.; Matsushita, T.; Sugimoto, Y.; Kiyoku, H. *Appl. Phys. Lett.* **1996,** *69*, 4056.

Chapter Two – Detection of NDA-Labeled Amino Acids*

2.1 Introduction

Unfortunately, despite the numerous advantages of laser induced fluorescence detection in CE, most analytes of interest exhibit little or no native fluorescence. For instance, of the twenty amino acids only tryptophan and tyrosine have any appreciable native fluorescence [1,2]. However, expensive UV lasers are necessary for their excitation. Alternatively, a fluorescent probe or label can be used to derivatize the analytes of interest. The highly fluorescent fluorescein and rhodamine families of probes have been used extensively for LIF detection in CE [3-6]. However, these probes are intrinsically fluorescent, thus creating the need to separate any unreacted probe from the labeled analytes. These probes are also likely to form unwanted fluorescent side-products, which can further complicate separations. These attributes of conventional probes have led to the development of fluorogenic probes. These probes are not intrinsically fluorescent but form fluorescent products when reacted with appropriate functional groups, such as primary amines.

Structures of some common fluorogenic reagents for primary amines and their fluorescent products are shown in Figure 2-1. Perhaps the classic fluorogenic reagent is *o*-phthalaldehyde (OPA) in the presence of 2-mercaptoethanol (2-ME). Reaction of OPA and 2-ME with primary amines yields a product with an excitation maximum near 340 nm [7-9]. In 1987, de Montigny *et al.* at Kansas synthesized naphthalene-2,3-dicarboxaldehyde (NDA), an analogue of OPA [10]. When primary amines are derivatized

* A portion of the work described in this chapter has been published as "Violet (405 nm) Diode Laser for Laser Induced Fluorescence Detection in Capillary Electrophoresis", Melanson, J.E.; Lucy, C.A., 2000, *Analyst*, 125, 1049-1052.

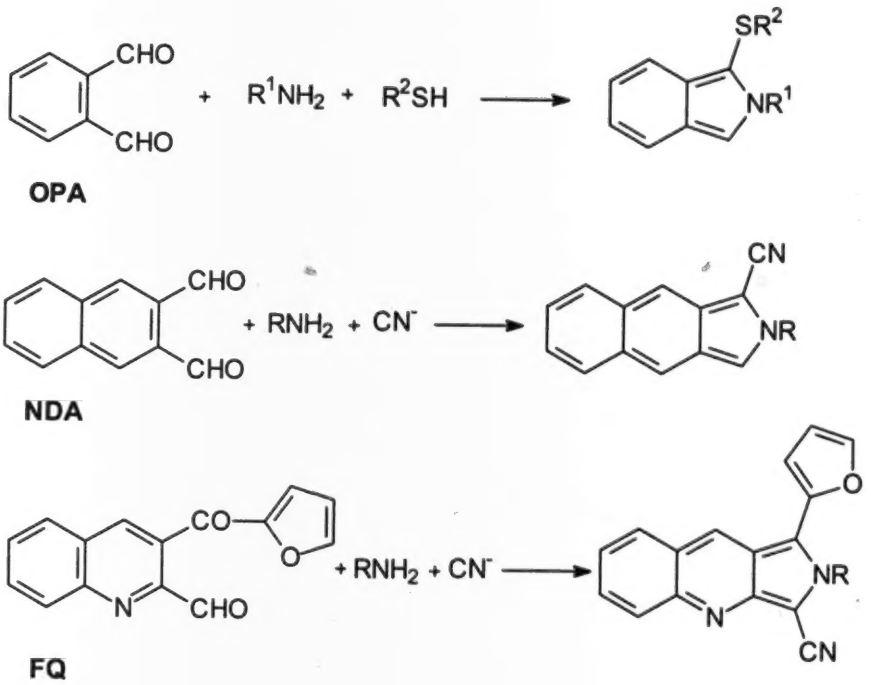

Figure 2-1. Structures of some common fluorogenic probes.

with NDA in the presence of cyanide (CN^-) the fluorescent product exhibits excitation bands in the visible region near 420 and 440 nm, as described in references [10, 11] and shown in Figure 2-2. As well as having higher quantum efficiencies than OPA/2-ME derivatives, NDA/CN^- derivatives offer superior stability [10]. Specifically, OPA/2-ME derivatives degrade rapidly ($t_{1/2}$ = 1.5 h) while NDA/CN^- derivatives experience less than 10% loss in fluorescence in 10 h [10]. Also shown in Figure 2-1 is 3-(2-furoyl)quinoline-2-carboxaldehyde (FQ) which is an example of a reagent that has been tailored for excitation by the 488-nm line of the argon ion laser [12]. Probes like FQ have the disadvantage of being licensed to a particular company and are thus roughly 10 to 100 times more expensive than the classic OPA or NDA reagents.

Traditionally, the 442-nm line of the HeCd laser has been employed for excitation of NDA-labeled derivatives [13-16]. Unfortunately, the HeCd laser has inferior stability and shorter lifetime compared to the similarly or lower priced argon ion or HeNe lasers. This has lead to a decline in its popularity in recent years. As an alternative, Roeraade and co-workers reported the use of a custom-built frequency-doubled diode laser operating at 424 nm for the detection of NDA-labeled amino acids [17]. However, a practical version of this laser is not commercially available and frequency-doubling is not a trivial task. Thus recent use of NDA as a fluorogenic label for LIF detection has been limited.

The violet diode laser may represent a viable alternative to the HeCd for the excitation of NDA-derivatives. The fluorescence excitation and emission spectra of NDA-labeled glycine in borate buffer (pH 9.5) are shown in Figure 2-2. This excitation spectrum possesses bands near 420 and 440 nm, which agree well with the literature

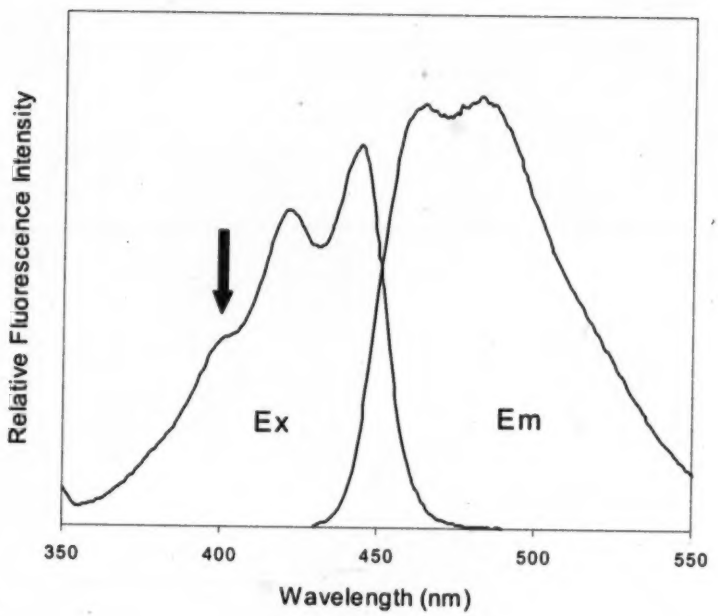

Figure 2-2. Fluorescence excitation (Ex) and emission (Em) spectra of NDA-labeled glycine in pH 9.5 borate buffer. The arrow indicates the point of excitation with the violet diode laser.

values for glycine of 419 and 442 nm [11] (in phosphate buffer, pH 7, 60% CH_3CN). It should be noted that this is not an accurate excitation spectrum since the spectrofluorometer used does not correct for the decline in intensity of the Xe-arc lamp upon approaching the near-UV. The 420-nm band should appear ~ 10% more intense than the 440-nm band [11, 18]. In addition to the two major bands, there also exists a band near 400 nm, which appears as a shoulder off of the 420-nm band. The 400-nm band is not well characterized but it has been previously observed [18]. The 400-nm band has an intensity of roughly 65% of that of the 420-nm band and roughly 70% of that of the 442-nm band [18]. It should also be noted that all NDA-amino acid adducts have roughly the same excitation/emission maxima and differ by only ~ ± 2 nm. Therefore the excitation of NDA-labeled amino acids at 400 nm is only marginally less efficient than at 442 nm. However, the more effective filtering of scattered excitation light at 400 nm may offset this. Specifically, a 500-nm (FWHM = 25 nm) band-pass filter will most likely transmit more light at 442 nm than at 400 nm (assuming elastic scattering). Thus a lower background signal may be expected with excitation at the shorter wavelength.

In this chapter, the first application of the violet diode laser for laser induced fluorescence detection in capillary electrophoresis is described. The laser is evaluated using both a commercial and a home-built LIF detector. NDA-labeled amino acids were chosen as a simple test mixture.

2.2 Experimental

2.2.1 Apparatus

Fluorescence spectra were obtained on a Shimadzu RF-5301 PC Spectrofluorometer (Columbia, MD, USA) controlled by RF-530XPC Personal Fluorescence software on a Pentium PC. Laser power measurements were performed with a Newport 835 optical power meter (Irvine, CA, USA) or a PocketPower™ handheld power meter (Melles Griot, Irvine, CA).

2.2.2 Commercial CE-LIF System

A P/ACE 2100 (Beckman Instruments, Fullerton, CA, USA) equipped with a LIF detector was used. A schematic of the optical setup is shown in Figure 2-3. To briefly summarize, laser light from an optical fiber travels through a hole in the beam-block and then onto the capillary. Fluorescence is collected at 180° by an ellipsoidal mirror and focused back past the optical fiber, through an emission filter and then onto the photomultiplier tube. A hole in the center of the ellipsoidal mirror allows any unscattered laser light to pass through. Data acquisition and control was performed using P/ACE Station software (Beckman) for Windows 95 on a 486 PC. Untreated silica capillaries (Polymicro Technologies, Phoenix, AZ, USA) with an inner diameter of 50 μm, outer diameter of 365 μm, and a total length of 57 cm (50 cm to the detector) were used. The capillary was thermostated at 25°C for all experiments. The laser beam was coupled to the LIF detector through a 1.5-m multi-mode fiber patchcord with a 100/140-μm (core/cladding) diameter and SMA 906 connectors (Oz Optics Inc., Carp, ON, Canada). Fluorescence was collected through a 500-nm band pass filter, with a 25-nm full-width-

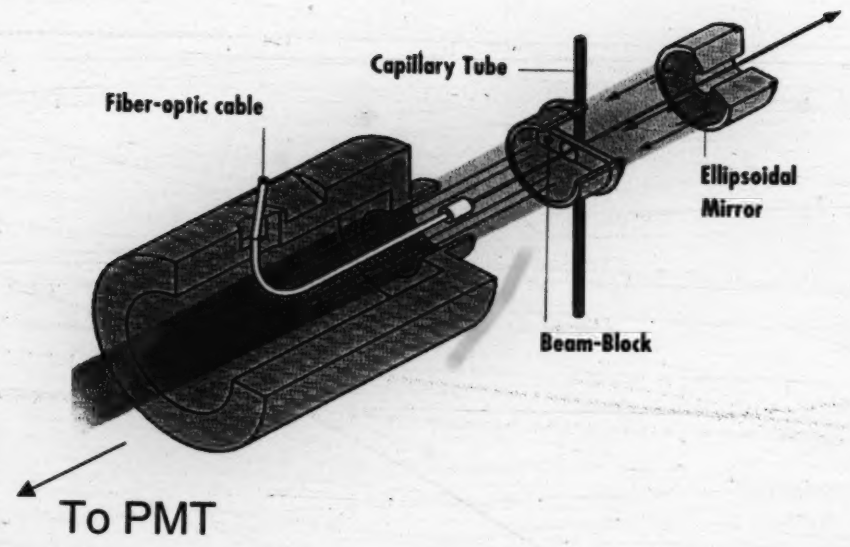

Figure 2-3. Schematic of the optical setup of the Beckman LIF detector.

at-half-maximum (Omega Optical, Brattleboro, VT, USA). The data acquisition rate and detector response time (rise time) were set at 10 Hz and 0.1 s, respectively, for separation optimization experiments to achieve optimal efficiency while 5 Hz and 1 s were used to reduce background noise in determining detection limits.

The laser diode (shown in Figure 1-5) was purchased from Nichia Corporation (Tokyo, Japan). Individual diodes lase at a wavelength of 405 ± 10 nm. This particular diode was rated by the manufacturer to emit at 400 nm with an output power of 5 mW, under an operating current of 48 mA at 25°C, with beam divergences in the parallel ($\theta_{\parallel}$) and perpendicular ($\theta_{\perp}$) directions of 7.5° and 32.3°, respectively. A ± 6 V power supply built in-house was employed and delivered a current of 47.4 mA, resulting in an output of 3.5 mW (less than typical to prolong life of diode). An automatic power control (APC) function was integrated into the circuit to monitor light output through a photodiode and adjust the operating current accordingly to maintain constant output power.

The 5.6-mm diameter laser diode was placed into an aluminum housing. A focusing lens was mounted onto the aluminum housing approximately 1 mm from the diode head. The focusing lens was plano-convex with a 5-mm diameter and 6-cm focal length. The diode housing with optics was then inserted into a 3.5-cm diameter by 7.5-cm long finned aluminum heat sink to provide passive temperature control. Onto the heat sink, a fiber optic bulkhead was mounted (SMA 905/906 receptacle; Amphenol Canada Corp., Scarborough, ON). The distance of the diode head with respect to the bulkhead was then optimized to achieve optimal focusing into the fiber, resulting in a transmission efficiency of approximately 30 %. Laser power was adjusted to deliver ~ 1 mW out of the fiber. No beam-correcting optics were employed.

2.2.3 High-sensitivity LIF detector

A Model 300 Crystal CE System (ATI Unicam) was used to supply high voltage and perform pressure rinses and injections. Untreated fused silica capillaries (Polymicro Technologies, Phoenix, AZ, USA) with a length of 65 cm (60 cm to the detector), an inner diameter of 50 μm, and an outer diameter of 365 μm were used.

For excitation, a 400-nm diode laser was used, built in-house with the Nichia laser diode as described above in Section 2.2.2 but with minor modifications. The diode was inserted into a laser diode collimator (Oz Optics Ltd., Carp, ON). The collimator was then placed into a finned aluminum heat sink with a length of 7.5 cm and a diameter of 3.5 cm. No beam-correcting optics were employed. A schematic of the laser is shown in Figure 2-4. The ± 6 V power supply and drive electronics were housed in a box outside of the laser body (heat sink) to avoid unnecessary heat generation. The current supplied to the diode was variable and a LCD displayed the approximate power output based on calibration data of output power (light intensity; mW) as a function of input current. Normal operating current of the laser at maximum output power (5 mW) was 48 mA so a safety feature was built into the circuit to cut off power to the laser if the current exceeded 50 mA.

A schematic of the optical setup is shown in Figure 2-5. The laser beam was passed through a 400-μm pinhole (Melles Griot) that sat inside the 6.3× (0.20 NA) microscope objective (Melles Griot) which focused the beam onto the capillary. Laser power was adjusted to deliver ~ 0.25 mW onto the capillary. Fluorescence was collected at 90° with a 40× (0.65 NA) microscope objective (Melles Griot), passed through a 1-mm

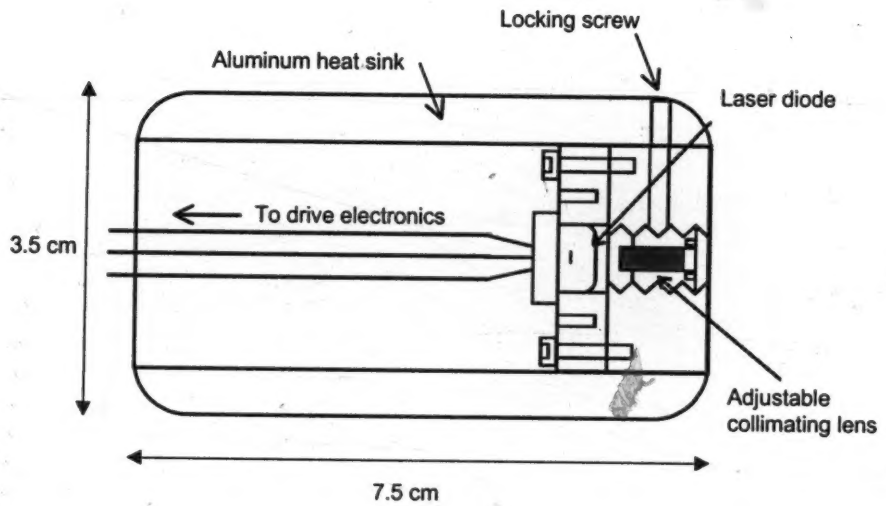

Figure 2-4. Side view schematic of the violet diode laser.

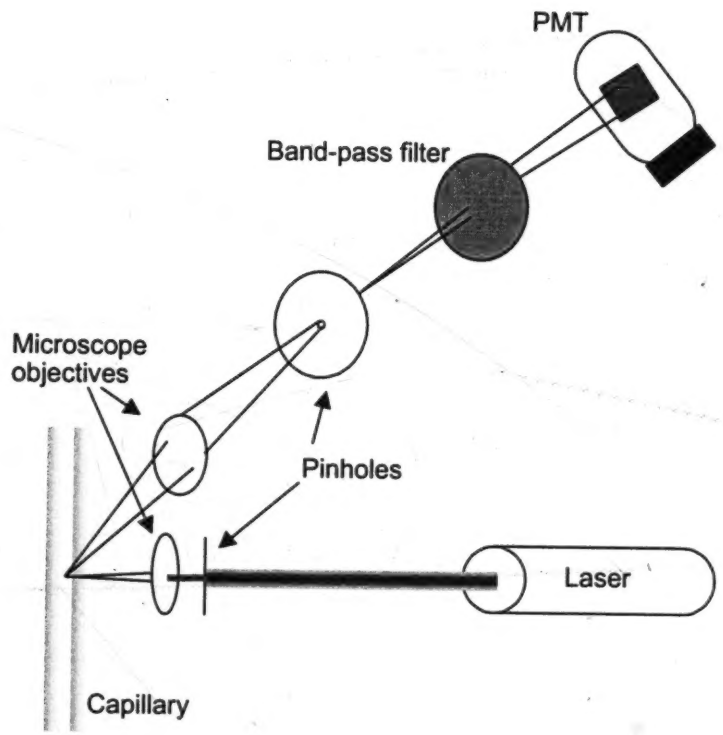

Figure 2-5. Schematic of the laser induced fluorescence detector.

pinhole (Melles Griot) for spatial filtering, and then through a 500-nm band-pass filter (500DF25, Omega). The photomultiplier tube (PMT) used was a Hamamatsu R3896 (Hamamatsu Corporation, Bridgewater, NJ, USA) which is a 28-mm diameter side-on variety. The PMT was driven by a regulated high-voltage power supply (HC123-01, Hamamatsu) that was controlled with a 12 V DC power supply built in-house. The PMT was operated at 600 V unless otherwise noted. The current signal from the PMT was passed through a current-to-voltage converter, amplified by 10^8, then passed through an 8^{th} order, 25 Hz, low-pass filter. The analog signal was sent to a BNC-2120 connector accessory (National Instruments, Austin, TX, USA) then collected at 5 Hz by a PCI-6023E data acquisition board (National Instruments) using Virtual Bench Logger version 2.51 software (National Instruments) on a Celeron 400 MHz PC. Data analysis was performed with Igor Pro version 3.12 software (Wavemetrix Inc., Oregon, USA).

2.2.4 Reagents

All solutions were prepared in Nanopure 18 MΩ water (Barnstead, Chicago, Il, USA). Buffers were prepared from reagent grade boric acid (BDH) and the pH was adjusted using sodium hydroxide (BDH, Toronton, ON). Sodium dodecyl sulfate (98 %) was obtained from Aldrich (St. Louis, MO, USA). The amino acid standard mixture designed specifically for fluorescence detection (Cat.# A 2161) was purchased from Sigma (St. Louis, MO, USA). Concentrations of all components were 25 μM ± 4% except for cystine at 12.5 μM ± 4. The three amino acids not included in the mixture were tryptophan, asparagine, and glutamine. Individual L-amino acids for peak identification were also obtained from Sigma (Cat # LAA-21). Naphthalene-2,3-dicarboxaldehyde (NDA) was purchased Molecular Probes (Eugene, OR, USA) and

sodium cyanide was obtained from Sigma. NDA was dissolved in A.C.S. grade acetonitrile (Fisher, Fair Lawn, NJ, USA).

2.2.5 Derivatization procedure

The derivatization procedure used was adapted from that of Ueda *et al.* [14]. To 700 µl of borate buffer (100 mM, pH 9.5) in a 1.5 ml polypropylene vial, 100 µl of sodium cyanide solution (10 mM in borate buffer) and 100 µl of the amino acid standard mixture (25 µM each, 2.5 µM after 1/10 dilution) were added and mixed. Next, 100 µl of NDA solution (1 mM in acetonitrile) were added and the vial was capped, shaken, and the reaction was allowed to proceed at room temperature for 30 min. The reaction mixture was then injected immediately into the capillary, or was quenched by a 1/10 dilution with borate buffer when using the commercial instrument or by a 1/100 dilution when using the high-sensitivity instrument. All concentrations of NDA-amino acid discussed below are based on the initial amino acid concentration in the reaction mixture and thus assume 100% labeling efficiency.

2.2.6 Separation conditions – MEKC using commercial CE-LIF

New capillaries were flushed with 0.1 M NaOH for 10 min at 20 p.s.i (138 kPa) before use. A 5-min pressure rinse at 20 p.s.i. with the separation buffer (100 mM borate – 50 mM SDS at pH 9.5) was performed before each injection. Injections were executed hydrodynamically at 0.5 p.s.i. (3.45 kPa; 60.5 Pa/cm) for 3 s. Separations were performed with an applied potential of 15 kV (263 V/cm) with a voltage ramp time of 30 s.

2.2.7 Separation conditions – MEKC and CZE using high-sensitivity CE-LIF

Capillaries were pre-conditioned similarly to those in Section 2.2.6. The separation buffer was modified for MEKC to 25 mM borate – 50 mM SDS at pH 9.5 in an attempt to reduce Joule heating in the capillary of the high-sensitivity instrument since the capillary was not thermostated. For CZE experiments, 25 mM borate at pH 9.5 was used as the buffer. Injections were performed hydrodynamically at 50 mbar (5 kPa; 76.9 Pa/cm) for 3 s. Separations were performed with an applied potential of 20 kV (308 V/cm) with a voltage ramp of 6 kV/s.

2.3 Results and Discussion

2.3.1 Detection of NDA-labeled amino acids with MEKC using commercial CE-LIF

The charge on the NDA-labeled amino acids at pH 9.5 varies from near-zero for arginine to –2 for glutamic acid and aspartic acid, while all others carry a charge of –1. These compounds carrying a charge of –1 cannot be adequately separated by conventional CZE (shown in Section 2.3.3). Thus micellar electrokinetic chromatography (MEKC) was employed. However, since most analytes are charged, a combination of both CZE and MEKC will be responsible for the separation. The MEKC aspect of the separation will be further complicated since the negatively charged analytes will be experiencing electrostatic repulsion with the SDS micelles, while simultaneously allowing their hydrophobic moiety to partition into the micelles.

Separation conditions were adapted from those of Ueda *et al.* [14]. Displayed in Figure 2-6 is the separation of a standard mixture of NDA-labeled amino acids in 100 mM sodium borate – 50 mM SDS buffer at pH 9.5 at a concentration of 250 nM. Of the

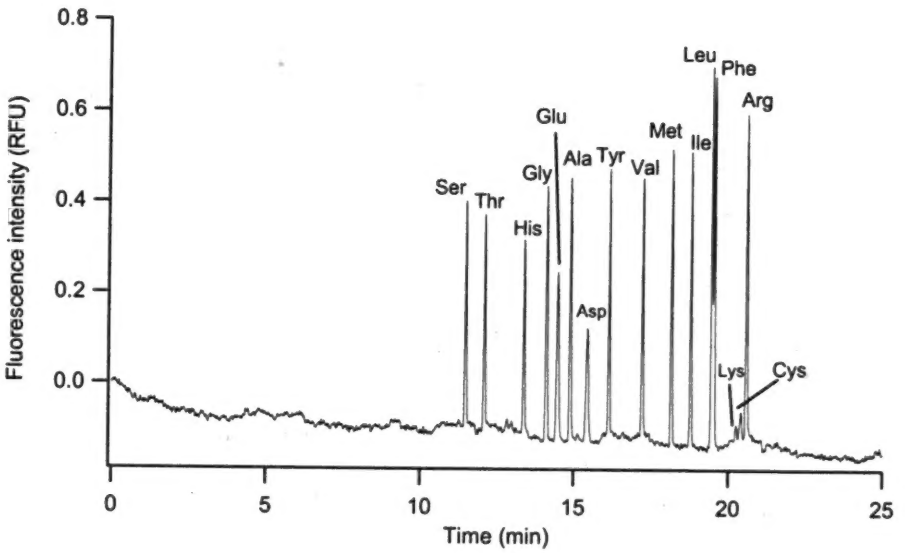

Figure 2-6. MEKC separation of NDA-amino acids using commercial CE-LIF instrument. Experimental conditions: 57-cm capillary (50 cm to detector); 15 kV applied; 100 mM borate-50 mM SDS buffer, pH 9.5; 250 nM amino acid mixture shown; RFU = relative fluorescence units.

mono-labeled compounds carrying a charge of −1, the polar amino acids serine (Ser) and threonine (Thr) migrate to the detector first, while the more hydrophobic amino acids leucine (Leu) and phenylanaline (Phe) migrate last. The doubly-labeled lysine (Lys) and cystine (Cys) migrate after Phe due to increased hydrophobicity. With a charge of −2, glutamic acid (Glu) and aspartic acid (Asp) have intermediate migration times. One would expect Glu and Asp to migrate to the detector first due to their increased repulsion from the SDS micelles. However, this is apparently offset by their larger electrophoretic mobilities. Arginine (Arg) has the longest migration time, owing to its net charge of zero. Thus arginine experiences the least amount of electrostatic repulsion with the SDS micelles. Proline was not detected since it does not possess a primary amine group. Peaks for the di-labeled amino acids such as Lys and Cys were considerably smaller than the others due to intra-molecular quenching [10]. Specifically, di-labeled lysine has a quantum efficiency of fluorescence (Φ_f) of 0.02 while mono-labeled amino acids exhibit Φ_f of 0.75 to 0.80 in aqueous solvent [11]. Baseline separation was achieved for the 14 mono-labeled amino acids, except for Leu and Phe which were only partially resolved. These two peaks could have been separated with the addition of cyclodextrins to the electrophoretic buffer [14], but this was not investigated since the focus of this study was on detection.

Quantitative studies were only performed for Asp and Arg. These amino aicds are somewhat representative of the mixture as Asp yielded the least intense peak of the mono-labeled amino acids and Arg yielded the most intense well-resolved peak. A linear detector response using peak area was achieved over a concentration range of 25 nM to 2.5 μM for each (Asp: slope = 97000 ± 460, intercept = – 0.0011 ± 0.00066, R^2 =

0.99998; Arg: slope = 180000 ± 1900, intercept = – 0.0045 ± 0.0028, R^2 = 0.99988). Limits of detection (LOD) were determined by calculating the S/N at 25 nM and then extrapolating for the concentration at 3 × S/N. LOD values were 8 nM and 3 nM for Asp and Arg, respectively. Note that these values are based on the concentration of the native amino acids added to the reaction mixture. For the di-labeled lysine and cystine, LOD values were roughly 10-fold higher. This limit of detection achieved was slightly poorer than that quoted by Ueda *et al.* (0.24 nM) using the 442-nm line of the HeCd laser [14] and comparable to that obtained by Roeraade and co-workers (5.9 nM) employing a frequency-doubled diode laser at 424 nm [17].

2.3.2 Detection of NDA-amino acids with MEKC using high-sensitivity CE-LIF

To better reflect the sensitivity achievable for NDA-labeled amino acids with the violet diode laser, the experiment was repeated with a custom-built LIF detector. The same experimental conditions were employed except the separation buffer was modified to 25 mM borate – 50 mM SDS at pH 9.5 (lowered from 100 mM borate) in an attempt to reduce Joule heating since the capillary was not thermostated. Shown in Figure 2-7 is the separation of the NDA-labeled amino acids at a concentration of 25 nM. It is obvious that the efficiency is significantly poorer than that shown in Figure 2-6. Despite the reduction in ionic strength of the buffer, Joule heating is prevelant. The most highly retained compounds (i.e. t_{mig} > 12 min) undergo the most severe band broadening, which is consistent with previous literature reports [19]. Modification of the conditions (i.e. reduce voltage, reduce SDS concentration) may have led to improved results. But again, the focus of this study was on detection so this route was not explored. Despite the poor

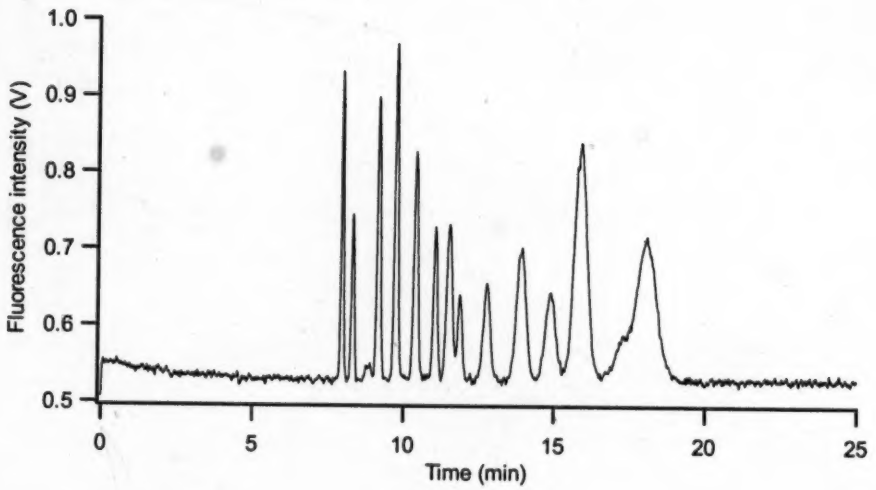

Figure 2-7. MEKC separation of NDA-amino acids using the high-sensitivity CE-LIF instrument. Experimental conditions: 65-cm capillary (60 cm to detector); 20 kV applied; 25 mM borate-50 mM SDS buffer, pH 9.5; 25 nM amino acid mixture shown; peak identities as in Figure 2-6.

peak shapes, signal-to-noise is dramatically improved over that achieved with the commercial instrument. Specifically, serine (sharp peak in both cases) at a concentration of 25 nM yielded a S/N of 130 using the home-built system (Figure 2-7) while the commercial system yielded a S/N of only 8.5 at the same concentration. However, the poor efficiency will undoubtedly compromise limits of detection, so a fair comparison between the two detection schemes is not possible under these conditions.

2.3.3 Detection of NDA-amino acids with CZE using high-sensitivity CE-LIF

To better evaluate the performance of the high-sensitivity LIF detector, the NDA-amino acid mixture was separated by CZE. It was anticipated that without the need for SDS in the electrophoretic buffer, the current generated in the capillary would be greatly reduced, thus minimizing Joule heating.

Shown in Figure 2-8 is a CZE separation of the NDA-amino acid mixture in 25 mM borate buffer at pH 9.5 at a concentration of 10 nM. As observed in Figure 2-8 and discussed above in Section 2.3.1., CZE is not capable of separating all of the components. With roughly zero net charge, Arg migrates to the detector first. The slight peak tailing of Arg is due to its positively charged subsitutent (p$Ka \sim 12.5$) interacting with the capillary wall. The peak at ~ 5 min is a reaction by-product and is observed in the blank. The numerous peaks between between 5.6 and 6 min are the compounds carrying a charge of −1, many of which are overlapping as seen by the inflated heights of the peaks at 5.6 and 5.7 min. No attempt was made to identify these peaks. The acidic amino acids Glu and Asp are well resolved and migrate to the detector much later due to their greater electrophoretic mobility opposing the EOF.

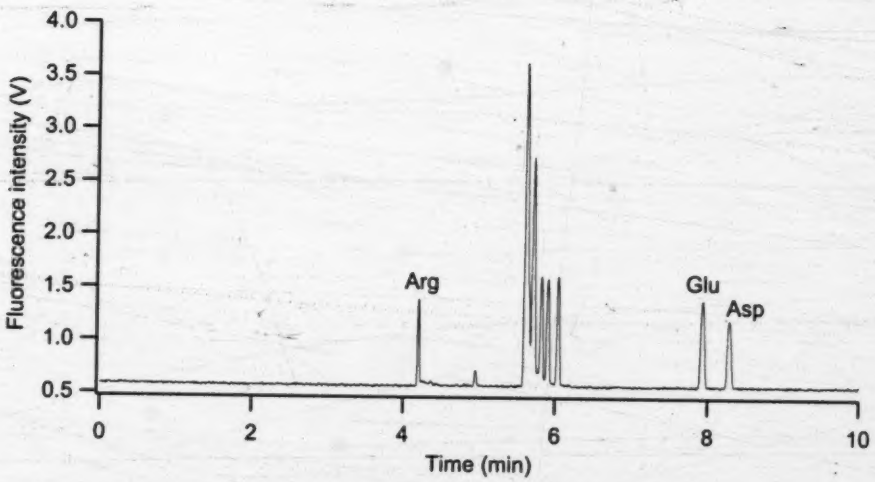

Figure 2-8. CZE separation of NDA-amino acids using the high-sensitivity CE-LIF instrument. Experimental conditions: 65-cm capillary (60 cm to detector); 20 kV applied; 25 mM borate, pH 9.5; 10 nM amino acid mixture shown.

For a visual comparison of sensitivity between the two instruments, the data shown in Figure 2-8 is for an injection of a 10-nM NDA-amino acid mixture, which is only slightly higher than the limit of detection achieved with the commercial instrument. Quantitative studies were only performed for the well-resolved Arg and Asp. Limits of detection were determined by calculating the S/N at 2.5 nM and then extrapolating for the concentration at 3 × S/N. LOD values were 0.3 nM and 0.4 nM for Arg and Asp, respectively. This represents at least a 10-fold improvement over that achieved with the commercial instrument. This sensitivity is now on par with Ueda *et al.* (0.24 nM) using the 442-nm line of the HeCd laser [14] and roughly 10-fold better than that obtained by Roeraade and co-workers (5.9 nM) employing a frequency-doubled diode laser at 424 nm[17].

2.3.5 Effect of laser power on signal-to-noise of NDA-amino acids

It is worth noting that the laser powers employed in these studies are relatively low. Roeraade and co-workers observed no increase in S/N beyond 0.3 mW of laser power [17]. They attributed this to photobleaching of the NDA-labeled amino acids, therefore light intensity in excess of 0.3 mW contributed only to scatter and thus increased background [17]. Consequently, only 0.25 mW of light was focused onto the inner-diameter of the capillary using the high-sensitivity detector. With the commercial system, 1 mW of light measured out of the fiber optic was determined optimal. This greater power was most likely required due to losses from fiber-to-fiber connections within the detector and poor focusing onto the capillary.

2.4 Conclusion

In this chapter, the violet diode laser was shown to be useful for the excitation of NDA-labeled amino acids. The detection limits for NDA labeled amino acids were comparable to those achieved with other laser systems such as the HeCd. Thus the violet diode laser is a viable alternative to the HeCd laser. Compared to the HeCd, the violet diode laser has a longer lifetime, is more compact, consumes less power, and can be purchased at less than half the cost of the HeCd.

The next stage of development will need to be the introduction of new derivatization reagents and applications tailored to the violet diode laser. There already exists a number of probes that would be compatible with the violet diode laser. Listed in Table 2-1 is a small sample of such probes that are offered by Molecular Probes for modification of amines. However, the number of such dyes is small relative to those compatible with the Ar ion laser. It is important to realize that it is not simply a coincidence that these probes have excitation maxima near 488 nm as derivatization reagents such as FQ were specifically designed for this wavelength [12]. Thus, one could envision that many probes could easily be tuned for excitation near 400 nm. However, researchers and chemical manufacturers must first be convinced that the violet diode laser is indeed an attractive alternative to gas-based lasers before investing the time and effort necessary into the development of new fluorescent probes.

Table 2-1. Fluorescent probes potentially compatible with the violet diode laser. All data from Molecular Probes.

Product Name	Excitation max. (nm)	Exctinction coeff. (M^{-1} cm^{-1})	Emission max. (nm)
Fluorescamine	380	7 800	464
2-anthracenesulfonyl chloride	382	4 000	421
7-hydroxycoumarin-3-carboxylic acid	386	29 000	448
Dapoxyl® carboxylic acid, succinimidyl ester	395	20 000	601
Cascade Blue® acetyl azide, trisodium salt	396	29 000	410
7-dimethylamino-4-methylcoumarin-3-isothiocyanate (DACITC)	400	36 000	476
7-diethylaminocoumarin-3-carboxylic acid	409	33 000	473
Cascade Yellow™ succinimidyl ester	409	24 000	558
Pacific Blue™ succinimidyl ester	416	36 000	451
7-hydroxycoumarin-3-carboxylic acid, succinimidyl ester	419	36 000	447

2.5 Literature cited

(1) Lee, T. T.; Yeung, E. S. *J. Chromatogr.* **1992,** *595*, 319.

(2) Timperman, A. T.; Oldenburg, K. E.; Sweedler, J. V. *Anal. Chem.* **1995,** *67*, 3421.

(3) Seiler, K.; Harrison, D. J.; Manz, A. *Anal. Chem.* **1993,** *65*, 1481.

(4) Takizawa, K.; Nakamura, H. *Anal. Sci.* **1998,** *14*, 925.

(5) Hutt, L. D.; Glavin, D. P.; Bada, J. L.; Mathies, R. A. *Anal. Chem.* **1999,** *71*, 4000.

(6) Chen, D. Y.; Dovichi, N. J. *J. Chromatogr. B* **1994,** *657*, 265.

(7) Roth, M. *Anal. Chem.* **1971,** *43*, 880.

(8) Hill, D. W.; Walters, F. H.; Wilson, T. D.; Stuart, J. D. *Anal. Chem.* **1979,** *51*, 1338.

(9) Lindroth, P.; Mopper, K. *Anal. Chem.* **1979,** *98*, 1667.

(10) deMontigny, P.; Stobaugh, J. F.; Givens, R. S.; Carlson, R. G.; Srinivasachar, K.; Sternson, L. A.; Higuchi, T. *Anal. Chem.* **1987,** *59*, 1096.

(11) Matuszewski, B. K.; Givens, R. S.; Srinivasachar, K.; Carlson, R. G.; Higuchi, T. *Anal. Chem.* **1987,** *59*, 1102.

(12) Beale, S. S.; Hsieh, Y. Z.; Wiesler, D.; Novotny, M. *J. Chromatogr.* **1990,** *499*, 579.

(13) Ueda, T.; Kitamura, F.; Mitchell, R.; Metcalf, T.; Kuwana, T.; Nakamoto, A. *Anal. Chem.* **1991,** *63*, 2979.

(14) Ueda, T.; Mitchell, R.; Kitamura, F.; Metcalf, T.; Kuwana, T.; Nakamoto, A. *J. Chromatogr. A* **1992,** *593*, 265.

(15) Amankwa, L. N.; Kuhr, W. G. *Anal. Chem.* **1993,** *65*, 2693.

(16) Gilman, S. D.; Ewing, A. G. *Anal. Chem.* **1995,** *67*, 58.

(17) Jansson, M.; Roeraade, J.; Laurell, F. *Anal. Chem.* **1993,** *65*, 2766.

(18) Shear, J. B.; Brown, E. B.; Webb, W. W. *Anal. Chem.* **1996,** *68*, 1778.

(19) Sepaniak, M. J.; Cole, R. O. *Anal. Chem.* **1987,** *59*, 472.

Chapter Three – Indirect Laser-Induced Fluorescence Detection Using a Violet Diode Laser *

3.1 Introduction

As discussed in the previous chapter, LIF detection usually requires derivatization of the analytes of interest with a fluorescent probe. This approach is well established for analytes containing highly reactive functional groups such as amines or thiols. In contrast, analytes such as inorganic ions or carboxylic acids are not so easily derivatized. For such compounds, indirect detection is frequently the best alternative.

Indirect detection is based on the displacement of an absorbing or fluorescing species present in the background electrolyte by the analyte, resulting in a decrease in signal intensity [1,2], as depicted in Figure 3-1. Indirect UV absorbance detection has seen widespread use for a variety of applications [3]. Despite its popularity, the sensitivity of indirect UV absorbance is generally poor (10^{-4} to 10^{-5} M) [4,5]. Indirect LIF detection is more sensitive than indirect UV absorbance [3,4], by at least an order of magnitude [6]. Yet, indirect LIF detection has seen very limited use since it was first reported in 1988 by Kuhr and Yeung [7,8]. The limited use of indirect LIF has been attributed to the high cost associated with lasers, and the lack of appropriate fluorescent probes [3]. However, the main reason behind this is most likely the power instability of conventional gas-based lasers [7] (typically 1% [9]).

The theoretical limit of detection for indirect LIF detection is given by [8]:

---

* A version of this chapter has been published as "Indirect Laser-Induced Fluorescence Detection Using a Violet Diode Laser", Melanson, J.E.; Boulet, C.A.; Lucy, C.A., 2001, *Analytical Chemistry*, 73, 1809-1813.

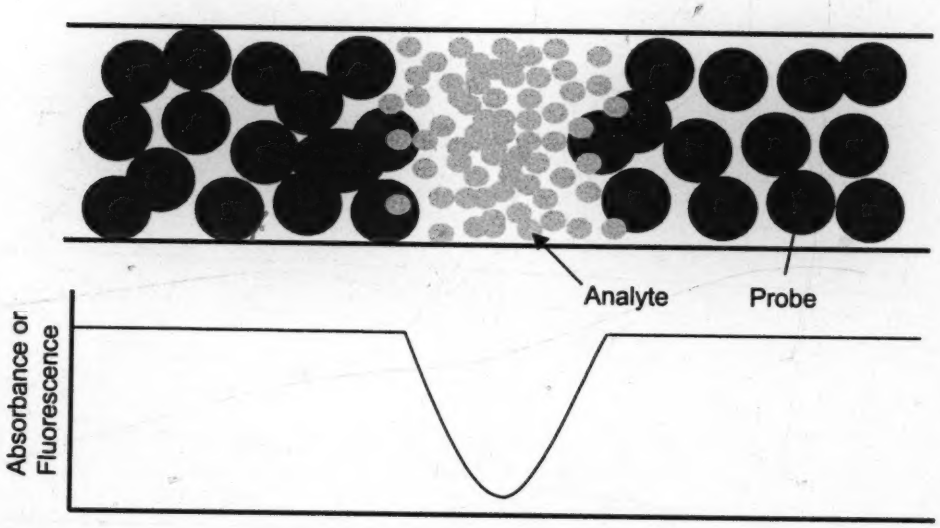

Figure 3-1. Depiction of the mechanism of indirect detection.

$$C_{LOD} = \frac{C_P \times s_{BN}}{T_R} = \frac{C_P}{T_R \times DR} \qquad \text{(Eqn. 3-1)}$$

where C_P is the concentration of the fluorescent probe, s_{BN} is the relative standard deviation of the background fluorescence fluctuations (noise), T_R is the transfer ratio (the number of probe molecules displaced by one analyte molecule), and *DR* is the dynamic reserve (ratio of the background fluorescence intensity to the noise; $= s_{BN}^{-1}$). Since fluorescence intensity is proportional to the excitation intensity, laser power fluctuations translate into baseline noise. Increased noise reduces the dynamic reserve, and thereby increases the limit of detection. Thus indirect LIF detection is especially sensitive to laser power fluctuations. In contrast, these laser power fluctuations are not as detrimental for direct LIF detection in which the background fluorescence is minimal.

To date, the majority of CE-indirect LIF applications have employed the HeCd laser operating at 325 nm [6-8] and at 442 nm [10], or the argon-ion laser operating in the UV (330-360 nm) [11-16], and at 488 nm [17-25]. Arguably, the most successful of these applications have all adopted some means of laser power stabilization [6, 8, 10, 11, 13]. Kuhr and Yeung observed an increase in DR from 299 to 10 439 upon employing laser power stabilization [8]. Similarly, Andersson *et al.* found laser power stabilization to be crucial to their work, reporting a *DR* of 1005 compared to 80 without stabilization [6]. Despite the obvious advantage of laser power stabilization, the drawbacks include increased instrument complexity and cost, and loss in laser power (up to 40 % [8]). Thus laser power stabilization has not been successful in increasing the popularity and utility of indirect LIF.

Diode lasers appear to be ideally suited for indirect detection owing to their greater power stability than gas-based lasers (typically 0.01 % vs. 1 % [9]). Unfortunately, relatively large probes containing extended conjugated systems are required since diode laser output has been limited to the red region (635 nm) of the electromagnetic spectrum. This is particularly problematic for indirect detection in which the probe must be compatible with the analytes of interest [3]. In indirect detection, the transfer mechanism is based on charge displacement. Thus both the probe and analyte should ideally carry the same charge. Further, the mobility of the probe and analyte must be similar to minimize electrodispersion [3] (*i.e.* peak asymmetry). So the choice of probes is rather limited at these long wavelengths.

Thus while diode lasers have been employed for excitation in numerous direct LIF applications in CE [26], only a handful of indirect LIF-CE applications have been reported. Lehotay *et al.* first demonstrated the utility of a diode laser (796 nm) for indirect detection in HPLC [27]. They attributed the large DR (> 1000) observed to the high power stability of the laser. Diode lasers (670 nm [28] and 750 nm [29]) have also been employed for indirect LIF detection in micellar electrokinetic chromatography (MEKC). For these chromatographic-based techniques, the transfer mechanism is based on differential partitioning into stationary phase of the analyte and probe and/or volumetric displacement [27]. This allows large probes of any charge to be effective, and the organic modifier or micellar phase could enhance the solubility of the probe.

To the best of our knowledge, only one study has employed a diode laser for indirect LIF detection in CZE [30]. Higashijima *et al.* used a 670-nm diode laser and methylene blue as probe to detect the amino acids glycine and proline [30]. A DR of 1300

was achieved without laser power stabilization but detection limits were a disappointing 1 mM [30]. Further, the large positively charged probe adsorbed so strongly onto the capillary wall that derivatization of the silanol groups was required [30].

The violet diode laser offers significant advantages for indirect LIF. Many commercially available probes are excited in the violet/blue region of the electromagnetic spectrum that are of moderate size and water-soluble. In this chapter, the utility of the violet diode laser for indirect detection in CZE is demonstrated. Novel indirect fluorescent probes are reported for the determination of high-mobility ions such as the inorganic ions and for determination of moderate mobility ions such as phosphonic acids. Finally, the baseline noise and dynamic reserve achieved with the diode laser are directly compared with those achieved using a HeCd laser.

3.2 Experimental

3.2.1 Apparatus

A P/ACE 2100 (Beckman, Fullerton, CA, USA) equipped with an LIF detector module was used for all experiments. Data acquisition and instrument control was performed with P/ACE Station software (Beckman) for Windows 95 on a 486 PC. Fluorescence spectra were obtained on a Shimadzu RF-5301 PC Spectrofluorometer (Columbia, MD, USA) controlled by RF-530XPC Personal Fluorescence software on a Pentium PC. Laser power measurements were performed with a PocketPower™ handheld power meter (Melles Griot, Irvine, CA, USA).

3.2.2 Violet diode laser setup

The diode laser was obtained from Power Technologies (Model # PPM04(LD1349)F1; Little Rock, AR, USA). Power Technologies packages violet laser diodes produced by Nichia Corporation (Tokyo, Japan). Nichia produces laser diodes with output of 405 ± 10 nm. The laser diode used in this work was rated by the manufacturer to lase at 415 nm with a typical power output of 5 mW. The laser was operated in constant current mode and was thermostated at 25°C. The laser was received equipped with a pre-aligned SMA fiber optic receptacle and was coupled to the LIF detector through a 1-m multimode fiber optic patchcord with a 100/140-μm (core/cladding) diameter and SMA 906 connectors (Polymicro Technologies, Phoenix, AZ, USA). The current supplied to the diode was adjusted to deliver 2 mW from the fiber (4 mW measured from the SMA receptacle; ~ 50% coupling efficiency). Fluorescence emission was collected through a 500-nm (500DF25) band pass filter (Omega Optical, Brattleboro, VT, USA) for the HPTS probe and a 650-nm filter (650DF25, Omega) for the TSPP probe.

3.2.3 HeCd laser setup

The single-wavelength HeCd laser operated at 325 nm with a power output of 5 mW and was equipped with a SMA fiber optic receptacle (Model # 3056-8M; Omnichrome, Irvine, CA). The laser beam was coupled to the LIF detector through a 1.5-m, high OH (designed for UV), multimode fiber patchcord with a 100/140-μm (core/cladding) diameter and SMA 906 connectors (Oz Optics Inc., Carp, ON, Canada). The optical power measured out of the fiber was 2 mW. Fluorescence was collected through a 400-nm (400BP20) band pass filter (Omega).

3.2.4 Reagents

All solutions were prepared in Nanopure 18-MΩ water (Barnstead, Chicago, IL, USA). 8-Hydroxypyrene-1,3,6-trisulfonic acid (HPTS; pyranine) was obtained from Molecular Probes (Eugene, OR, USA) and tetrakis-(4-sulphophenyl)porphine (TSPP) was purchased from Molecular Probes and Aldrich (under the name 5,10,15,20-tetraphenyl-21H,23H-porphine-p,p',p",p"'-tetrasulfonic acid, tetra sodium salt dodecahydrate; St. Louis, MO, USA). Sodium salicylate was obtained from Matheson Coleman & Bell (Norwood, OH, USA). L-glutamic acid was obtained from Aldrich and BIS-TRIS (bis[2-hydroxyethyl]imino-tris[hydroxymethyl]methane) from Sigma (St. Louis, MO, USA). Reagent grade HCl was obtained from Anachemia (Montreal, PQ, Canada). Sodium or potassium salts of the inorganic salts were from Fisher (Pittsburgh, PA, USA). Methylphosphonic acid (MPA), ethyl methylphosphonate (EMPA), and pinacolyl methylphosphonate (PMPA) were obtained from Aldrich while isopropyl methylphosphonate (IMPA) was synthesized at the Defense Research Establishment at Suffield (Suffield, AB, Canada).

3.2.5 Procedures

Untreated fused silica capillaries (Polymicro Technologies, Phoenix, AZ, USA) with a length of 27 cm (20 cm to the detector), an inner diameter of 50 μm, and an outer diameter of 365 μm were used. New capillaries were pre-conditioned with 0.1 M sodium hydroxide for 5 min followed by deionized water for 5 min, both at 138 kPa. Before each run, a 2-min rinse at 138 kPa with the separation buffer was performed. Injections were performed hydrodynamically using 3.45 kPa for 3 s. Data was collected at 10 Hz with a detector response time of 0.1 s. Capillaries were thermostated at 25°C in all experiments.

3.3 Results and discussion

3.3.1 Selection of indirect fluorescent probes

Numerous factors must be taken into consideration when selecting a probe for indirect detection. Firstly, the spectral properties of the probe must be compatible with the light source. In this case, probes compatible with the 415-nm line of the violet diode laser were considered. Secondly, the mobility of the probe must be comparable to that of the analytes to minimize electrodispersion [31].

Electrodispersion is caused by a difference in the electrophoretic mobility between the sample zone and the background electrolyte [31]. This mobility difference causes the local field strength to vary, and results in characteristic triangular peak shapes, illustrated in Figure 3-2 for cationic analytes. When the sample cation has a lower mobility than the buffer co-ion (cation), or probe in the case of indirect detection, the fast probe ion will outrun the sample ion and enter the sample zone from the trailing edge (Figure 3-2A). The varying local field causes ions to migrate at different velocities, and thus band broadening results. The sample ion, with a slower mobility, cannot cross the leading boundary into the fast moving buffer zone. Therefore, the result is a sharp leading edge and a diffuse trailing edge, resulting in a tailed peak. Figure 3-2B depicts the opposite case in which the sample cation has a higher mobility than the probe ion. The result is a sharp trailing edge and a diffuse leading edge, resulting in a fronted peak. In addition, electrodispersion is most prominent for high sample concentrations and low buffer concentrations, such as those used in indirect detection.

Matching the mobility of the probe with that of the analyte is inherently difficult since probes with excitation maxima near 400 nm or greater require rather large conjugated systems, while the desired analytes are relatively high-mobility anions. Thus the probes must be highly (negatively) charged to compensate for their large size.

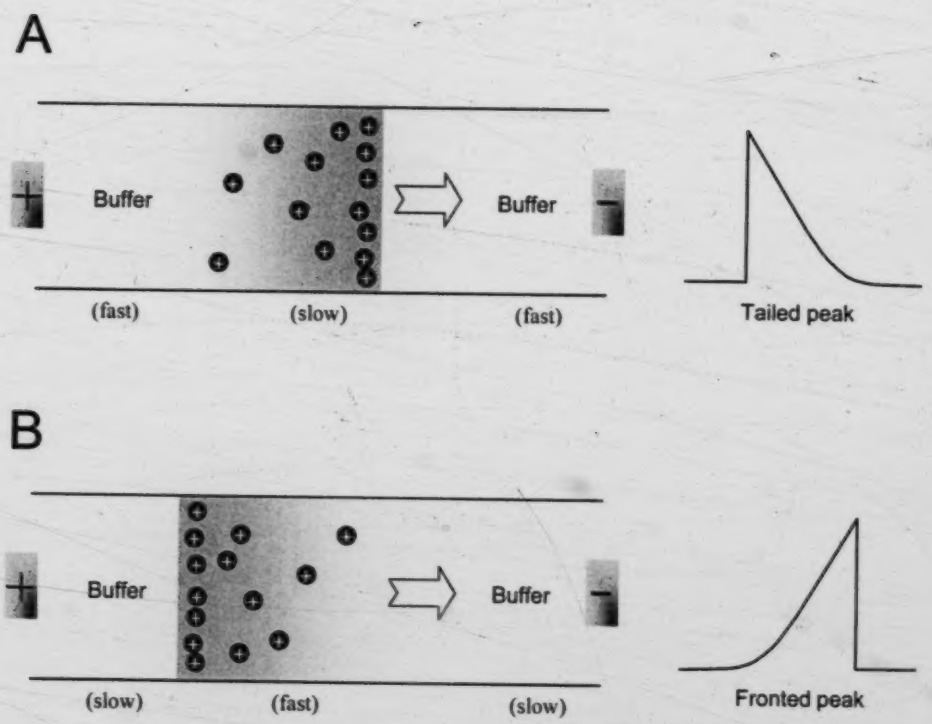

Figure 3-2. Schematic of the mechanism of electrodispersion when (A) the sample cation has a lower mobility than the buffer co-ion or probe and (B) the sample cation has higher mobility than the probe.

Fortunately, highly charged molecules tend to be water soluble, another desirable characteristic. Finally, perhaps the most important issue when selecting a fluorescent probe is cost. High-purity fluorescent probes tend be very expensive and are sold in rather small quantities (~ 5 mg). This is tolerable in direct LIF detection when only minute quantities are required as derivatization agents. However, such costs are impractical for indirect detection where the probe must be present in the background electrolyte. Several milliliters of buffer are generally required for a CE separation. Microliter-scale inlet and outlet vials can be used in CE, but this increases electrolysis effects [32] and reduces the lifetime of the buffer. Thus significant quantities (~ 100 mg) are required to perform any type of study or analyses. Therefore cost is an issue.

Based on the criteria described above, 8-hydroxypyrene-1,3,6-trisulfonic acid (HPTS; pyranine) and tetrakis-(4-sulphophenyl)porphine (TSPP) were selected as potential probes for indirect LIF detection. The structures of HPTS and TSPP are shown in Figure 3-3 and their spectral properties are listed in Table 3-1.

HPTS is a commonly used pH-indicator. Upon ionization of the phenol group (pK_a 7.0 [33]), its conjugation is extended, shifting its excitation maximum from 403 nm to 454 nm. Thus for this work pH of less than 5 were used to stabilize the HPTS mobility and to exploit the 403-nm excitation band. The sulphonate groups have $pK_a \sim -2$, and so are considered permanent negative charges. Thus, under our acidic conditions, HPTS carries a charge of –3, is highly water-soluble, and possesses an electrophoretic mobility of -6.8×10^{-4} cm^2/(Vs).

TSPP falls into a large class of compounds know as porphyrins. Porphyrins and their metal complexes play an important role in biological processes such as

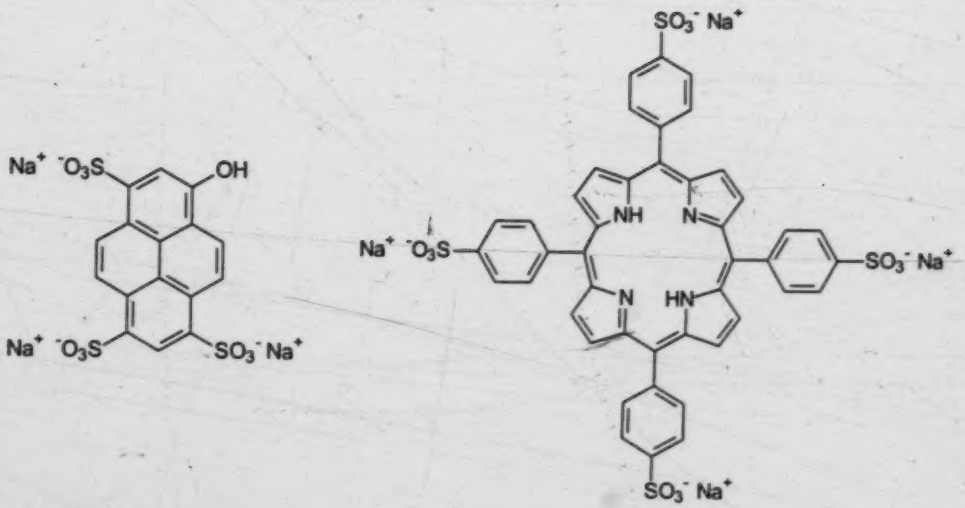

Figure 3-3. Structures of HPTS and TSPP.

Probe	pH	Excitation Max. (nm)	Extinction ($cm^{-1}M^{-1}$)	Emission max. (nm)
HPTS	4	403	20 000	511
	9	454	22 000	511
TSPP	<5	434	NA	NA
	7	413	460 000	645

Table 3-1. Spectral properties of HPTS and TSPP.

photosynthesis and oxygen transport. Porphyrins have been widely used in analytical chemistry, primarily for the spectrophotometric determination of metal ions [34]. Porphyrins possess a sharp and highly intense absorption band between 400 – 450 nm known as the Soret band. For TSPP, the Soret band at 413 nm has an extinction coefficient of 460 000 $cm^{-1}M^{-1}$. This extinction coefficient is roughly ten times greater than that for most standard fluorescent probes, and should translate into greater sensitivity for indirect LIF detection. Highly fluorescent probes allow C_P to be lowered while maintaining a large signal and therefore a large DR [1].

The net charge of TSPP varies from –4 at neutral pH to –2 under acidic conditions. Two ionizable nitrogens in its inner ring structure have pK_a 5.4 [35] which yield two positive charges under acidic conditions, resulting in a net charge of –2. Thus for this work, working well above the pK_a of the inner nitrogens was necessary to maximize the mobility of TSPP and enhance its analytical performance. The electrophoretic mobility of TSPP was measured to be -4.8×10^{-4} $cm^2/(Vs)$ under the optimized buffer conditions (pH 7.2) described below. TSPP was also fully water soluble at the concentrations studied.

3.3.2 Detection of inorganic anions with HPTS

3.3.2.1 Choice of buffering agent

As the magnitude of the EOF and the mobility of some analytes can vary with pH, control of the pH is critical in CZE. Further, electrolysis caused by the applied voltage can alter the pH within the electrolyte reservoirs [32]. Thus it is important that the electrolyte have adequate buffering capacity. However, buffering of electrolytes for indirect detection while maintaining high-sensitivity is a formidable task. In the case of

anion analysis, introduction of a buffering co-anion into the system (*i.e.*, phosphate, acetate, etc.) will lead to competitive displacement of the co-anions and the probe by the analyte [5]. This will decrease the transfer ratio T_R in equation 3-1 and thereby compromise sensitivity. Techniques to overcome this problem have included employing a slow moving buffering agent relative to the probe [5] or titrating the acid form of a probe with a buffering base to near the pK_a of the base [5].

Another alternative to buffering electrolytes for indirect detection is the use of amphoteric electrolytes, introduced by Haddad and co-workers [5]. At its isoelectric point (p*I*), an ampholyte exists in a zwitterionic form with a net charge of zero. An ampholyte will buffer at its p*I* when the pK_a values of the two buffering groups are roughly within 1 unit of the p*I* [5]. For instance, the ampholyte glutamic acid has two carboxylic acid groups with pK_a values of 2.19 and 4.25 and an amino group with pK_a 9.67. With a p*I* of 3.22, the carboxylate groups of glutamic acid provide adequate buffering capacity at its p*I*. With zero net charge, such zwitterions are ideal for indirect detection since they will not competitively displace the probe. Thus, the transfer ratio for indirect detection remains high. Further, zwitterionic buffers do not substantially increase the conductivity of the electrolyte and may be added in relatively large quantities to provide adequate buffering. In this study, the current generated during separations was < 2 μA. This is beneficial since Joule heating has been shown to produce random, low frequency oscillations in background fluorescence intensity, which is particularly harmful in indirect LIF detection [36]. Finally, previous work using this buffer for indirect UV detection yielded excellent migration time reproducibility. % RSD values ranged from 0.18 to 0.22 for the four

analytes studied over 30 consecutive runs with capillary conditioning between runs consisting of a simple 3-min buffer rinse[37].

3.3.2.2 Separation optimization

Inorganic anions are the primary analytes for which indirect detection is employed, so they were chosen as test analytes in this study. Figure 3-4 shows the separation of bromide, sulfate, nitrate, perchlorate, and chlorate using 10 μM HPTS in 10 mM glutamic acid buffer at pH 3.2. Baseline separation was achieved in less than 2 min on a 20-cm effective length capillary under a field strength of – 370 V/cm. At pH 3.2 the electroosmotic flow (EOF) was nearly suppressed in the forward direction with a residual of 2.0×10^{-4} $cm^2/(Vs)$. Thus the anions migrated counter-EOF. EOF modifiers such as surfactants were not employed to avoid possible precipitation of the probe [5]. A range of HPTS concentrations of 1 – 100 μM was investigated, and 10 μM was determined to be optimal. The probe concentration was kept low to maximize sensitivity (Equation 3-1) while maintaining good baseline stability (*DR*). Further, the 10-μM probe concentration chosen was comparable to that employed previously for high-sensitivity indirect LIF [1].

3.3.2.3 Figures of Merit

Linear calibration based on peak area was achieved for the inorganic anions over a range of 1 – 50 μM using the separation and conditions shown in Figure 3-4. Above 50 μM, electrodispersion was significant due to the low probe concentration and low conductivity of the buffer. This is an inherent problem of indirect detection when electrophoretic buffers are optimized for high-sensitivity [3]. Limits of detection were determined for bromide and chlorate by calculating the S/N at 5 μM and then performing a linear extrapolation for the concentration that would produce a peak with an intensity of

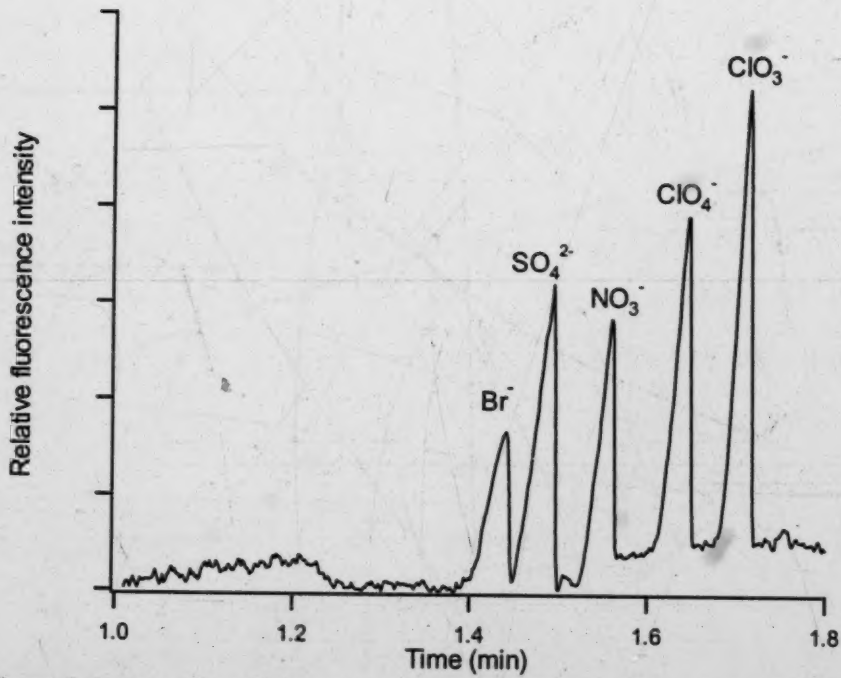

Figure 3-4. Separation of inorganic anions using HPTS. Experimental conditions: 27-cm capillary (20-cm to detector); – 10 kV applied; excitation at 415 nm. Buffer: 10 μM HPTS; 10 mM glutamic acid; pH 3.2. 10 μM Anions shown (system peak at 1.88 min not shown).

3 × S/N. Limits of detection were 0.6 μM for bromide (50 ppb) and 0.4 for μM for chlorate (30 ppb). The other anions would have LOD values intermediate to bromide and chlorate. The poorer LOD values observed for the higher mobility anions bromide, sulfate, and nitrate was due to the greater peak asymmetry (Fig. 3-4) resulting from the increasing mobility mismatch between these analytes and the probe (electrodispersion). Under the buffer conditions used in Figure 3-2, the mobility of HPTS was determined to be -6.8×10^{-4} cm^2/(Vs). This matches well with the absolute mobilities of ClO_3^- and ClO_4^-, which are 6.7×10^{-4} and 6.99×10^{-4} cm^2/(Vs) [38]. The absolute mobilities of bromide, sulfate and nitrate range from 7.4×10^{-4} to 8.3×10^{-4} cm^2/(Vs) [38].

The sensitivity achieved was comparable-to or better than that achieved previously for indirect LIF detection of inorganic anions [8, 11, 19, 23] and over an order of magnitude better than the generalized detection limit of 10^{-5} M for indirect absorbance detection [4]. The LOD values achieved in this study also compare favorably with ion chromatgraphy using eluant-suppressed conductivity detection, which generally yields LOD values for ions such as bromide, sulfate, and nitrate in the 5-10 ppb range, but generally at least an order of magnitude higher for chlorate and perchlorate [39].

3.3.3 Detection of phosphonic acids with TSPP

Small aliphatic acids represent another class of compounds for which indirect detection is commonly used. In particular, the analysis of chemical warfare (CW) agent degradation products has generated considerable interest in recent years [37, 40-44]. Fortunately, most CW agents degrade into harmless monoester and alkyl phosphonic acids after relatively short exposure to the environment, as shown in Figure 3-5. For instance, the nerve agent sarin undergoes a rapid hydrolysis to form isopropyl

methylphosphonate (IMPA; monoester), which then undergoes a much slower hydrolysis to form methylphosphonic acid (MPA; alkyl). Similarly, the nerve agent soman breaks down to pinocolyl methylphosphonate (PMPA) and VX degrades to ethyl methylphosphonate (EMPA), with MPA being the final product for each. Thus these degradation products can be safely analyzed in water or soil samples taken from suspected attack sites.

The phosphonic acids could not be detected using HPTS as the probe since the phosphonic acids co-migrated with the system peak at 1.88 min in Figure 3-4, and so could not be detected. Therefore the lower mobility TSPP (-4.8×10^{-4} cm^2/(Vs) under the optimized buffer conditions) was tested as the probe. Figure 3-6 shows the separation of PMPA, IMPA, EMPA, and MPA using 50 μM TSPP in 5 mM BIS-TRIS buffer at pH 7.2. Baseline separation was achieved in less than 2 min on a 20-cm effective length capillary under a field strength of 370 V/cm. The phosphonic acids migrated opposite the EOF. However, the EOF at pH 7.2 (7.6×10^{-4} cm^2/(Vs)) was greater than the analyte mobility. Thus the detector was positioned near the cathode.

TSPP solutions are extremely photo-sensitive and lower concentration buffers (1 – 10 μM) degraded quickly (within hours) even when shielded from light. Thus a probe concentration of 50 μM was chosen to increase buffer stability (several days) and reproducibility. This concentration was not high enough to compromise sensitivity (Equation 3-1).

Quantification studies were performed only with MPA as the other phosphonic acids are chemically unstable. Linear calibration using peak area was achieved for MPA over a range of 0.5 – 50 μM. The limit of detection was determined for MPA by

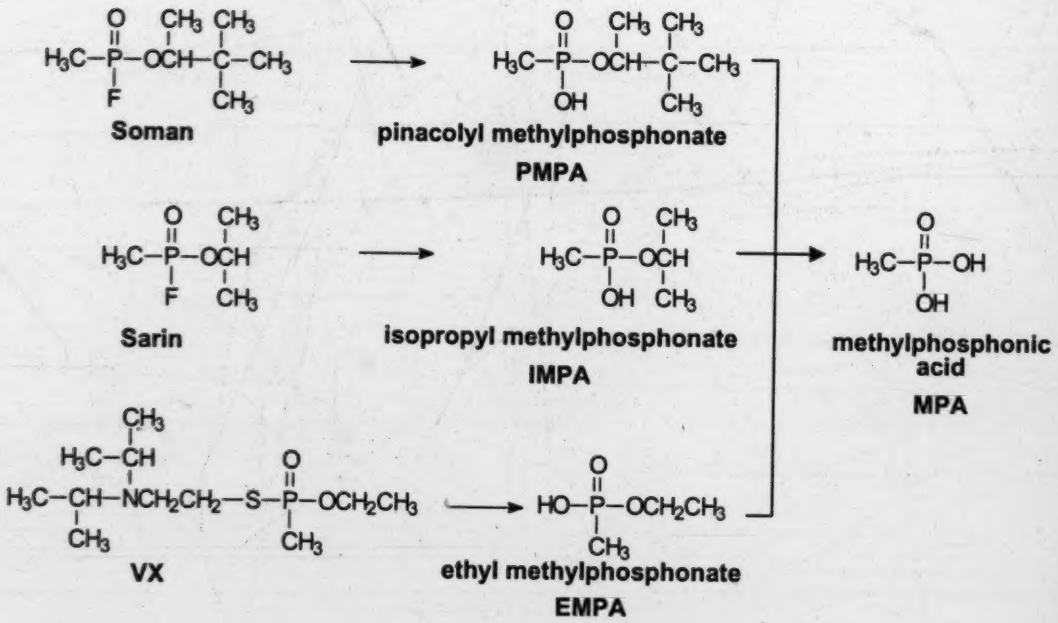

Figure 3-5. Degradation pathways of some common nerve agents.

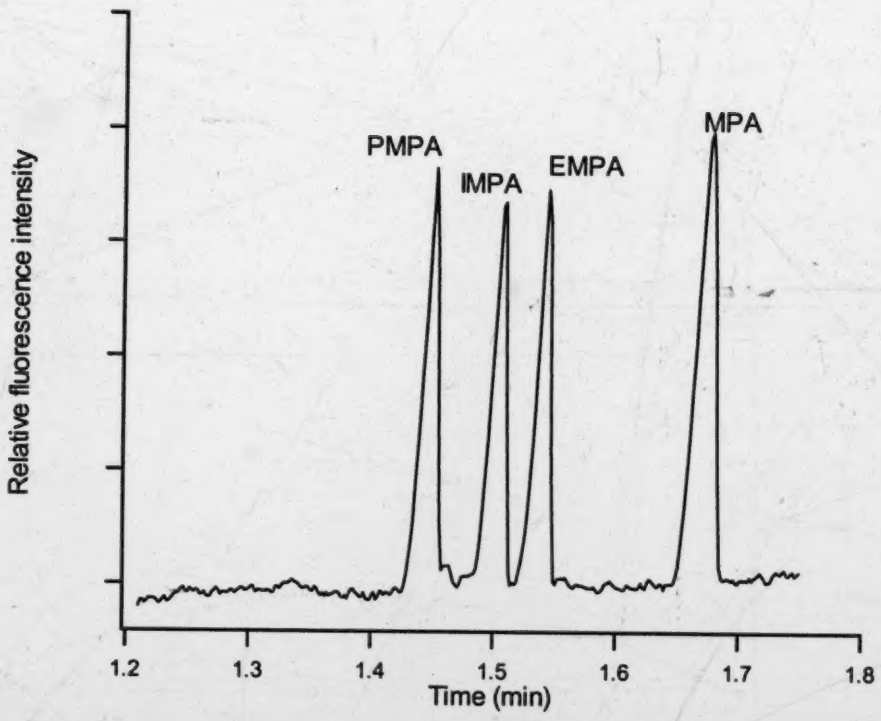

Figure 3-6. Separation of the chemical warfare agent degradation products: pinacolyl methylphosphonate (PMPA), isopropyl methylphosphonate (IMPA), ethyl methylphosphonate (EMPA), and methylphosphonic acid (MPA) using TSPP. Experimental conditions: 27-cm capillary (20-cm to detector); +10 kV applied; excitation at 415 nm. Buffer: 50 μM TSPP; 5 mM BIS-TRIS; pH 7.2 (adjusted with HCl). 10 μM Phosphonic acids shown (water peak at 1.18 min and system peak at 1.96 min not shown).

calculating the S/N at 1 μM and then performing a linear extrapolation for the concentration that would produce 3 × S/N. A LOD of 0.2 μM was achieved. Marginally higher LOD values would be expected for PMPA, IMPA, and EMPA, as they yielded slightly less intense peaks than MPA at the same concentration (Figure 3-6). The LOD of 0.2 μM represents roughly a ten-fold improvement in sensitivity over indirect absorbance techniques for these analytes using a similar hydrodynamic injection [37, 42]. Yet, the sensitivity of the TSPP indirect LIF was compromised by the addition of HCl to the buffer to adjust the pH. The chloride ions undoubtedly lead to competitive displacement of the probe, thus reducing the transfer ratio (Equation 3-1). As an alternative, the ampholyte histidine was tested as a buffer at pH 7.6 but yielded severe baseline perturbations and was not investigated further.

3.3.4 Baseline stability and dynamic reserve

As discussed above, laser power fluctuations translate into baseline noise and hinder sensitivity for indirect detection. According to Equation 3-1, increased baseline noise will reduce the dynamic reserve, thus increasing the limit of detection. *DR* values were calculated by selecting at least a 10-s portion (100 data points) of the baseline in Figure 3-4 and Figure 3-6, respectively. Thus these values were obtained using a buffer optimized for separation and sensitivity performance, and not optimized for maximum *DR*. *DR* values were calculated as the mean background fluorescence signal divided by the standard deviation of the signal over the baseline segment. The dynamic reserve thus observed were 1400 for the HPTS buffer system and 3300 for TSPP using the 415-nm violet diode laser.

These values of *DR* are comparable to those achieved previously with a 670-nm diode laser (1300 in ref. [30]) and also comparable to that achieved with a power-stabilized HeCd laser (1005 in [6], and up to 10 000 in ref. [8]). However, *DR* values from one laboratory cannot be justly compared to those from another lab since differences in the optical setups as well as in the method for determining *DR* will affect the results. For instance, Shamsi *et al.* reported *DR* values ranging from 1910 to 3380 over a range of different probe concentrations, but these values were determined by monitoring the background fluorescence during a pressure rinse of the capillary [23]. Background fluorescence is highly flow rate dependent due to photobleaching effects [8]. Thus, measuring the fluorescence intensity during a pressure (high flow rate) rinse may not accurately represent what occurs during a true separation. As a consequence, cross comparisons between laboratories may not be realistic.

To accurately compare the baseline stability achieved with diode lasers and gas-based lasers, a head-to-head study was performed using the 415-nm diode laser and a 325-nm HeCd laser (unstabilized, Sec. 3.2.3). Figure 3-7 shows a 20-s (200 data points) baseline segment void of any obvious perturbations and drift. The diode laser was tested with 2.5 μM TSPP as the probe, and the HeCd laser with 1 mM salicylate. Salicylate has been the predominant probe for indirect detection using a HeCd laser [7, 8]. Electrophoretic conditions were as described in Figure 3-6 and probe concentrations were adjusted to generate similar fluorescence intensity (constant shot noise). The TSPP concentration had to be kept much lower than that of salicylate due to the enormous extinction

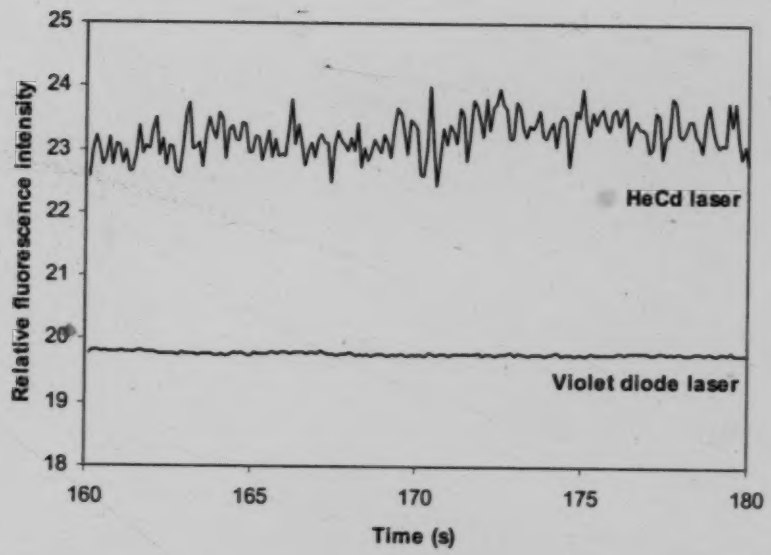

Figure 3-7. Comparison of baseline stability of 325-nm HeCd and 415-nm diode laser in indirect LIF detection. Experimental conditions and buffer as in Figure 3-6 except the probe concentrations were 2.5 μM TSPP with the diode laser 1 mM salicylate with the HeCd (probe concentrations adjusted to generate

coefficient of TSPP. These conditions should allow for a fair comparison, although perhaps slightly biased in favor of the HeCd since higher probe concentrations generally yield larger *DR* [1].

Figure 3-7 clearly illustrates the greater baseline stability achieved with the violet diode laser. The baseline noise calculated as the relative standard deviation of the fluorescence signal was 1.4 % for the HeCd and 0.091 % for the diode laser, yielding *DR* values of 74 and 1100, respectively. It should be noted that the *DR* observed for TSPP in this experiment is lower than that observed in Figure 3-6 (3300, as discussed above in this section). This lowering of *DR* with lower probe concentration is consistent with previous studies [23]. With constant laser power and detector shot noise in the violet diode laser and HeCd laser systems, it assumed that this is a true test of the effect of laser power stability on *DR* in indirect LIF detection.

3.4 Conclusions

This work demonstrates the potential of the violet diode laser for indirect LIF detection. The detection limits achieved herein for inorganic anions and chemical warfare degradation products are 0.1-0.8 μM. These are significantly greater than the 0.01 μM achieved in Sec. 2.3.1 with direct fluorescence detection on the same commercial instrument. However, while inferior to direct LIF in terms of sensitivity and simplicity, indirect LIF detection remains a viable alternative for analytes that are not easily derivatized. The high power stability and low cost of the violet diode laser make it an attractive alternative to indirect absorbance techniques.

In related work, we exploited the high stability of the violet diode laser for LIF detection of metal ions using the fluorogenic ligand 8-hydroxyquinoline-5-sulfonic acid (HQS) [45]. The high stability was advantageous since HQS was present in the background electrolyte for on-column complexation. Uncomplexed HQS generates relatively sufficient background fluorescence, so laser stability was critical as in indirect fluorescence detection.

3.5 Literature cited

(1) Yeung, E. S.; Kuhr, G. W. *Anal. Chem.* **1991,** *63*, 275A.

(2) Yeung, E. S. *Acc. Chem. Res.* **1989,** *22*, 125.

(3) Doble, P.; Haddad, P. R. *J. Chromatogr. A* **1999,** *834*, 189.

(4) Albin, M.; Grossman, P. D.; Moring, S. E. *Anal. Chem.* **1993,** *65*, 489A.

(5) Doble, P.; Macka, M.; Haddad, P. R. *J. Chromatogr. A* **1998,** *804*, 327.

(6) Andersson, P. E.; Pfeffer, W. D.; Blomberg, L. G. *J. Chromatogr. A* **1995,** *699*, 323.

(7) Kuhr, W. G.; Yeung, E. S. *Anal. Chem.* **1988,** *60*, 1832.

(8) Kuhr, W. G.; Yeung, E. S. *Anal. Chem.* **1988,** *60*, 2642.

(9) Gooijer, C.; Mank, A. J. G. *Anal. Chim. Acta* **1999,** *400*, 281.

(10) Garner, T. W.; Yeung, E. S. *J. Chromatogr.* **1990,** *515*, 639.

(11) Gross, L.; Yeung, E. S. *J. Chromatogr.* **1989,** *480*, 169.

(12) Hogan, B. L.; Yeung, E. S. *J. Chrom. Sci.* **1990,** *28*, 15.

(13) Gross, L.; Yeung, E. S. *Anal. Chem.* **1990,** *62*, 427.

(14) Hogan, B. L.; Yeung, E. S. *Anal. Chem.* **1992,** *64*, 2841.

(15) Xue, Q.; Yeung, E. S. *J. Chromatogr. A* **1994,** *661*, 287.

(16) Church, M. N.; Spear, J. D.; Russo, R. E.; Klunder, G. L.; Grant, P. M.; Andresen, B. D. *Anal. Chem.* **1998,** *70*, 2475.

(17) Richmond, M. D.; Yeung, E. S. *Anal. Biochem.* **1993,** *210*, 245.

(18) Chao, Y. C.; Whang, C. W. *J. Chromatogr. A* **1994,** *663*, 229.

(19) Marti, V.; Aguilar, M.; Yeung, E. S. *J. Chromatogr. A* **1995,** *709*, 367.

(20) Desbene, A. M.; Morin, C. J.; Mofaddel, N. L.; Groult, R. S. *J. Chromatogr. A* **1995,** *716*, 279.

(21) Huang, Y. M.; Whang, C. W. *Electrophoresis* **1998,** *19*, 2140.

(22) Jin, L. J.; Wang, T.; Li, S. F. Y. *Electrophoresis* **1999,** *20*, 1856.

(23) Shamsi, S. A.; Danielson, N. D.; Warner, I. M. *J. Chromatogr. A* **1999,** *835*, 159.

(24) Ruiz-Calero, V.; Puignon, L.; Glaceran, M. T. *J. Chromatogr. A* **2000,** *873*, 269.

(25) Munro, N. J.; Huang, Z.; Finegold, D. N.; Landers, J. P. *Anal. Chem.* **2000,** *72*, 2765.

(26) McWhorter, S.; Soper, S. A. *Electrophoresis* **2000,** *21*, 1267.

(27) Lehotay, S. J.; Pless, A. M.; Winefordner, J. D. *Anal. Sci.* **1991,** *7*, 863.

(28) Kaneta, T.; Imasaka, T. *Anal. Chem.* **1995,** *67*, 829.

(29) Wallenborg, S. R.; Bailey, C. G. *Anal. Chem.* **2000,** *72*, 1872.

(30) Higashijima, T.; Fuchigami, T.; Imasaka, T.; Ishibashi, N. *Anal. Chem.* **1992,** *64*, 711.

(31) Hjerten, S. *Electrophoresis* **1990,** *11*, 665.

(32) Macka, M.; Andersson, P.; Haddad, P. R. *Anal. Chem.* **1998,** *70*, 743.

(33) Wolfbeis, O. S. *Anal. Chem.* **1986,** *58*, 2874.

(34) Biesaga, M.; Pyrzynska, K.; Trojanowicz, M. *Talanta* **2000,** *51*, 209.

(35) Kano, K.; Tanaka, N.; Minamizono, H.; Kawakita, Y. *Chem. Lett.* **1996,** *11*, 925.

(36) Bailey, C. G.; Wallenborg, S. R. *Electrophoresis* **2000,** *21*, 3081.

(37) Melanson, J. E.; Wong, B. L. Y.; Lucy, C. A.; Boulet, C. A. *J. Chromatogr. A* **2001,** *920*, 359.

(38) Lucy, C. A. *J. Chromatogr. A* **1999,** *850*, 319.

(39) Johnson, E. L. In *Ion Chromatography*; Tarter, J. G., Ed.; Marcel Dekker: New York, 1987, pp 1.

(40) Pianetti, G. A.; Taverna, M.; Baillet, A.; Mahuzier, G.; Baylocq-Ferrier, D. *J. Chromatogr.* **1993,** *630*, 371.

(41) Mercier, J. P.; Morin, P.; Dreux, M.; Tambute, A. *J.Chromatogr. A* **1996,** *741*, 279.

(42) Nassar, A. F.; Lucas, S. V.; Jones, W. R.; Hoffland, L. D. *Anal. Chem.* **1998,** *70*, 1085.

(43) Nassar, A. F.; Lucas, S. V.; Myler, C. A.; Jones, W. R.; Campisano, M.; Hoffland, L. D. *Anal. Chem.* **1998,** *70*, 3598.

(44) Nassar, A. F.; Lucas, S. V. *Anal. Chem.* **1999,** *71*, 1285.

(45) Vos, C. J.; Melanson, J. E.; Lucy, C. A. *Anal. Sci.* **2001,** *17*, 225.

Chapter Four – Analyses of Urinary Porphyrins

4.1 Introduction

Porphyrias are a class of liver disorders caused by disruptions in heme biosynthesis. Different porphyrias are caused by specific enzyme deficiencies. For instance, porphyria cutanea tarda (PCT) results from deficiency of the enzyme uroporphyrinogen decarboxylase. A simple means of diagnosing PCT is to monitor by-products of heme biosynthesis, such as urinary porphyrins [1]. Specifically, patients suffering from PCT excrete elevated levels of hetpacarboxylic acid porphyrins and uroporphyrins (8 -COOH) while healthy individuals excrete predominantly coproporphyrins (4 -COOH groups). Therefore the diagnosis of certain porphyrias can be achieved by monitoring the relative abundance of these urinary porphyrins excreted. Structures of these urinary porphyrins and related compounds are shown in Figure 4-1.

Urinary porphyrins have been determined by such techniques as flow-injection analysis (FIA) [2, 3] and immunoassay [4]. These techniques are useful for preliminary screening of excess porphyrin production but do not yield the characteristic pattern or porphyrin profile and thus do not provide enough information for the diagnosis of the porphyrias.

High performance liquid chromatography (HPLC) has been the method of choice for urinary porphyrin analyses in recent years [5, 6]. Analysis times are in the 30-min range and gradient elution is required due to the highly varying hydrophobicity of the urinary porphyrins [6, 7]. Detection schemes such as chemiluminescence [8] and mass spectrometry (MS) [8] have been implemented successfully, but absorbance and fluorescence have

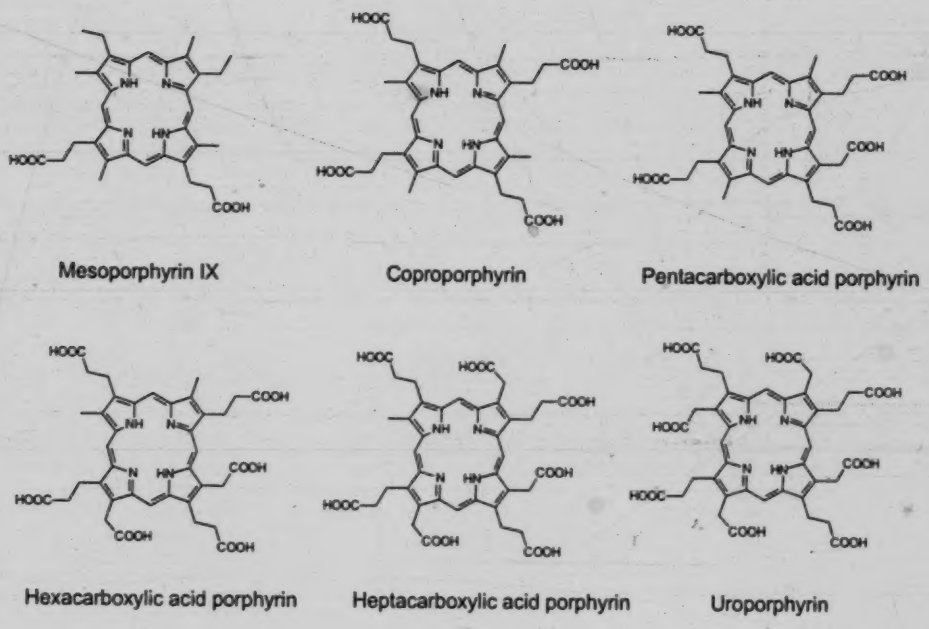

Figure 4-1. Structures of urinary porphyrins.

developed into the standard methods of detection [5, 6]. Both absorbance and fluorescence exploit the porphyrins' highly intense Soret or *B*(0,0) band in the 400-nm region which have molar extinction coefficients ranging from 200 000 to 400 000 M^{-1} cm^{-1} [9]. An absorption spectrum of a urinary porphyrin (uorporphyrin) is shown in Figure 4-2. Sensitivity is reasonable with limits of detection for fluorescence in the 0.2 to 2 nM range [7, 10] and that for absorbance roughly 2- to 10-fold higher [7]. However, this sensitivity is only marginally sufficient since normal levels of urinary porphyrins in urine are in the low-nM range [11]. Therefore sample preparation techniques are generally required to pre-concentrate or clean-up the sample [5-7]. The most popular of these techniques is esterification of the urinary porphyrins. Typically esterification requires a 24 h reaction in a dark room, followed by solvent extraction [6, 7]. Thus fairly rigorous sample preparation is required to compensate for the lack of sensitivity of these methods.

Capillary electrophoresis (CE) coupled with fluorescence detection appears to be ideally suited for the analysis of urinary porphyrins. However, sensitivity has been generally poor, with limits of detection in the 10 – 80 nM range [10, 12, 13]. These detection limits do not compete with current HPLC methods discussed above. The poor sensitivity achieved with CE is due to the lack of an appropriate light source for fluorescence excitation. A practical laser for the 400-nm region has not been available. Consequently, continuous sources such as the Xe arc [10] or high-pressure mercury lamp [13] have been used for excitation. The output of these lamps is not easily focused and is therefore not very compatible with the small dimensions of CE. In the only known CE-LIF report, Sweedler and co-workers achieved 1 – 10 nM detection limits using 15 mW of the 488-nm line of an Ar ion laser [12]. In this study, the authors could not exploit the highly

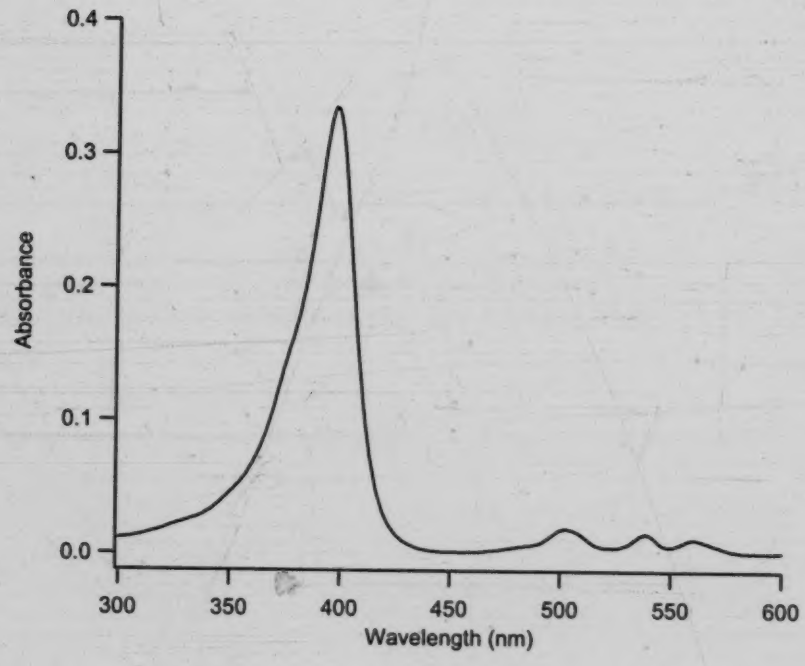

Figure 4-2. Absorption spectrum of a typical porphyrin (uroporphyrin) in 10 mM CHES - 75 mM SDS at pH 10.

intense Soret band of the porphyrins at this wavelength but instead used the second most intense band centered near 500 nm (Figure 4-2).

For the work described in this chapter, the violet diode laser is employed for excitation in the detection of urinary porphyrins in capillary electrophoresis. Operating at 400 nm, the laser is ideally suited for porphyrin analyses and fills a void in the array of laser lines available.

4.2 Experimental

4.2.1 Apparatus

Optimization of the urinary porphyrin CE separation was performed on a P/ACE 2100 (Beckman, Fullerton, CA, USA) equipped with a LIF detector. Untreated fused silica capillaries (Polymicro Technologies, Phoenix, AZ, USA) with a length of 57 cm (50 cm to the detector), an inner diameter of 50 μm, and an outer diameter of 365 μm were used. Capillaries were thermostated at 25°C in all experiments. A 415-nm diode laser (Power Technologies Inc.; Model # PPM04(LD1349)F1; Little Rock, AR,) was used for excitation, as was described in Section 3.2.2. Fluorescence emission was collected through a 600-nm (600DF50) band-pass filter (Omega Optical, Brattleboro, VT, USA).

All other experiments employed a Model 300 Crystal CE System (ATI Unicam) equipped with a home-built LIF detector, as described in Section 2.2.3. Untreated fused silica capillaries (Polymicro Technologies, Phoenix, AZ, USA) with a length of 65 cm (60 cm to the detector), an inner diameter of 50 μm, and an outer diameter of 365 μm were used. For excitation, a 400-nm diode laser was used, built in-house as described in

detail in Section 2.2.3. The laser beam was passed through a 400-μm pinhole (Melles Griot) that sat inside the 6.3× (0.20 NA) microscope objective (Melles Griot) which focused the beam onto the capillary. Laser power was adjusted to deliver ~ 0.25 mW onto the capillary. Fluorescence was collected at 90° with a 40× (0.65 NA) microscope objective (Melles Griot), passed through 1-mm pinhole (Melles Griot) for spatial filtering, and then through a 600-nm band-pass filter (600DF50, Omega).

4.2.2 Reagents

All solutions were prepared in deionized (18 MΩ) water (Nanopure filtration system, Barnstead, Chicago, IL, USA). Buffers were prepared with 2-[*N*-cyclohexylamino]ethanesulfonic acid (CHES; pK_a = 9.3; Sigma), sodium dodecyl sulfate (SDS; 99 %; Aldrich), and the pH was adjusted using sodium hydroxide (BDH). The porphyrin marker kit (Product # CMK-1A, Porphyrin Products, Logan, UT, USA) contained 10 nmol of each of the type I carboxylic acid porphyrins (4, 5, 6, 7, 8 –COOH groups) in solid form. The structures of these are shown in Figure 4-1. Mesoporphyrin IX is not a biological porphyrin but is also included in the mixture as a representative dicarboxylic acid porphyrin. The mixture also contains two isomers of the hexacarboxylic acid porphyrin.

4.2.3 Procedures

New capillaries were flushed with 0.1 M NaOH for 10 min at 1000 mbar and then water for 5 min at 1000 mbar before use. Injections were performed hydrodynamically at 50 mbar for 6 s. Optimized buffer conditions consisted of 10 mM CHES-75 mM SDS at pH 10. Separations were performed with an applied potential of 25 kV (385 V/cm). Porphyrin standards and urine samples were diluted with the separation buffer and were

shielded from light whenever possible. Buffers were purged with N_2 before use to remove dissolved oxygen, which is known to be an efficient quencher of fluorescence.

4.3 Results and discussion

4.3.1. Separation of the urinary porphyrins

4.3.1.1 Literature Methods

Given their high charge, urinary porphyrins appear to be ideally suited for separation by CE. However, only a handful of CE studies have been reported [10, 12, 14]. The common theme to all of these studies is the use of buffer additives such as surfactants and/or organic modifier to solubilize the porphyrins. Weinberger *et al.* reported an excellent CE method with a buffer consisting of 20 mM CAPS – 100 mM SDS at pH 11 [10]. The rationale behind the use of elevated pH was most likely to maximize the negative charge on the capillary wall to enhance electrostatic repulsion between the porphyrins and the capillary wall. In initial studies employing 10 % methanol for solubilization, the authors observed loss of resolution and peak broadening over several runs [10]. This was attributed to adsorption of porphyrins onto the capillary wall [10]. Therefore 100 mM SDS was added to the buffer system to compete with the porphyrins for any hydrophobic sites on the capillary wall and/or enhance the solubility of the porphyrins [10]. Ultimately, the 10 % methanol was dropped from their buffer system to avoid the migration time drift associated with methanol evaporation [10].

4.3.1.2 Method Optimization

Initial studies herein were based on the method of Weinberger *et al.* [10]. However, it was anticipated that the concentrated buffer (i.e. 100 mM SDS, pH 11) might cause

excessive Joule heating within our homebuilt instrument, as it does not possess any active cooling system. Significant broadening was observed on this instrument using a similar buffer system, as described in Chapter 2. Thus employing a lower SDS concentration, if possible, appeared advantageous. Further, pH 11 seems unnecessarily high to maximize repulsion between the carboxylated porphyrins and the capillary surface since the silanol groups (-SiOH) are generally considered to be fully ionized at pH 8 or 9 ($pK_a \sim 5.6$ [15]).

The effect of SDS concentration on the separation of the urinary porphyrins was investigated. These effects are not well documented and are therefore somewhat interesting. It should be mentioned that all of the SDS concentrations studied are above the critical micelle concentration (CMC) of SDS, which is generally in the range of 2 – 6 mM in most buffers employed in CE [16]. Figure 4-3 demonstrates the effect of SDS on the separation of the porphyrin mixture in 10 mM CHES buffer at pH 10. Without SDS (bottom trace), the migration order was as expected given the counter-EOF conditions. That is, the lowest charged porphyrin (mesoporphyrin IX, 2) migrated to the detector first, and the highest charged porphyrin (uroporphyrin, 8) migrated last. All peaks were very broad and asymmetrical except for the coproporphyrin (4) peak (N = 240 000).

At 25-mM SDS, a change in migration order is apparent in Figure 4-3, with mesoporphyrin IX now migrating after coproporphyrin. The coproporphyrin peak is lower in efficiency than for 0 mM SDS, whereas all other peaks increase in efficiency. The efficiency increase is proportional to the charge, with the highly charged uroporphyrin (– 8) producing an extremely sharp peak (N= 7 800 000). This efficiency is much higher than any model would predict and can only be explained by some type of band-focusing phenomenon. At 50 mM SDS, the migration order was as in 25

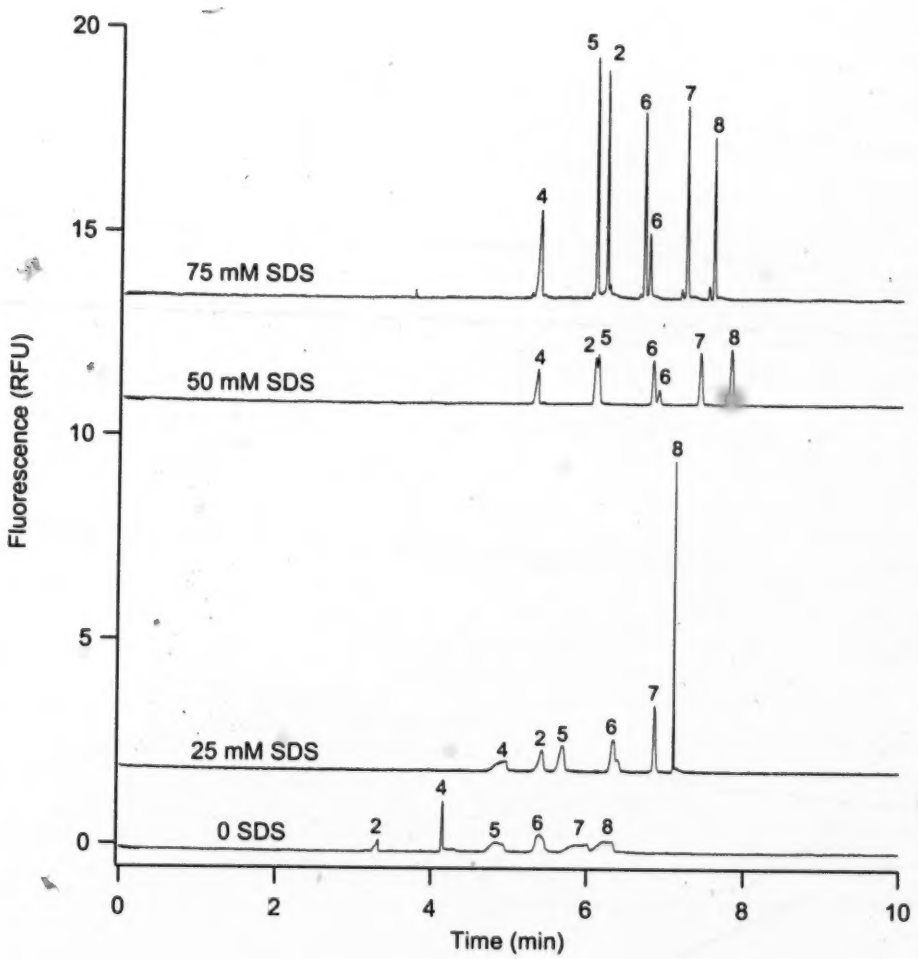

Figure 4-3. The effect of SDS concentration on the urinary porphyrin separation. Experimental conditions: Beckman 2100 CE-LIF instrument; 57-cm capillary (50 cm to detector); 20 kV applied; 10 mM CHES buffer with variable SDS concentration, pH 10; 1 μM porphyrin mixture shown; peaks identified by their number of carboxylic acid groups; RFU = relative fluorescence units.

mM SDS, but with mesoporphyrin IX now co-migrating with pentacarboxyl porphyrin. All peaks showed reasonable efficiency (N = 85 000 – 230 000). Thus, the less highly charged porphyrins are increasing in efficiency with increasing SDS and uroporphyrin is experiencing a dramatic loss with increasing SDS. With the increase in efficiency, separation of the two isomers of hexacarboxyl porphyrin was achieved.

At 75 mM SDS, mesoporphyrin IX migrates after pentacarboxyl porphyrin. Also, the migration times of the more highly charged porphyrins appear shorter. This quicker migration seems counter-intuitive since one would expect any retention the SDS is causing to increase with increasing SDS concentration. However, migration times are not an accurate indicator for porphyrin-micelles interactions in this case. The increased ionic strength at 75-mM SDS will reduce both electroosmotic flow and electrophoretic mobility. In this case, the more highly charged porphyrins experience a greater reduction in electrophoretic mobility relative to the less highly charged ones (counter-EOF). This is consistent with previous investigations of the effect of ionic strength on multiply-charged analytes [17]. Good peak shapes were observed for all porphyrins except coproporphyrin, which exhibited fronting. Higher SDS concentrations were not investigated as the goal of this study was to reduce the SDS concentration from that previously used, and the separation at 75 mM SDS was adequate. To summarize, the optimal buffer conditions consisted of 10 mM CHES – 75 mM SDS at pH 10.

4.3.1.3 Porphyrin Mobility Behaviour

Section 4.3.1.2 demonstrated that high concentrations of SDS are indeed required for efficient separation of the urinary porphyrins and more importantly that the method of

Weinberger *et al.* [10] could not be significantly improved. However, the anomalous behaviour of some of the porphyrins is worthy of discussion.

The migration shifts of mesoporphyrin IX (peak 2 in Fig. 4-3) are easily explained by its greater hydrophobicity and thus greater MEKC behaviour relative to other porphyrins. As shown in Figure 4-1, Mesoporphyrin IX has both of its carboxylic acid groups on adjacent indole groups. This leaves the opposite side of the molecule free to interact with the SDS micelles. All of the other porphyrins have a more uniform charge distribution and interact minimally with the micelles.

Perhaps the most interesting behaviour of the porphyrins was that of coproporphyrin, (peak 4 in Fig. 4-3). It produced by far the sharpest peak (N = 240 000) of any of the porphyrins in the absence of SDS. Upon addition of SDS, coproporphyrin experienced a loss in efficiency as a result of peak fronting. This is consistent with the observations of Weinberger *et al.* [10]. They eliminated the peak fronting by increasing the capillary temperature to 45 °C, which they claim enhanced the solubility of coproporphyrin [10]. However, this explanation is not consistent with the high efficiency observed in the absence of SDS.

A possible explanation for the high efficiency achieved in the absence of SDS may be that coproporphyrin forms dimers in solution which enhances its solubility [18]. From the structure of coproporphyrin in Figure 4-1, one could envision that one coproporphyrin molecule could stack on top of another such that the carboxylic acid groups of the top molecule would fit between those of the bottom molecule. This favorable conformation would allow interaction of the hydrophobic porphyrin backbones while minimizing electrostatic repulsion between carboxylic acid groups. Upon addition

of SDS to the buffer, these dimers may have broken down, thus explaining coproporphyrin's poorer solubility at 25 mM SDS. For the more highly charged porphyrins, electrostatic repulsion would most likely limit dimer formation. Mesoporphyrin IX most likely forms dimers or other aggregates, but these may not carry a high enough net charge to solubilize the aggregates.

4.3.2 Calibration and detection limits

Figure 4-4 shows the separation of a 500 pM urinary porphyrin mixture under the optimized buffer conditions described in Section 4.3.1.2 using the high-sensitivity LIF detector. The efficiency of the separation in Figure 4-4 (N= 105 00 – 135 000) is comparable to that observed in Figure 4-3 (75 mM SDS). Thus it does not appear that Joule heating is having as severe an impact on the separation as it was with the NDA-labeled amino acids in Chapter 2 using a similar buffer system. This is further evidence that the porphyrins have little MEKC-type retention since Joule heating is more detrimental to highly retained analytes in MEKC [19].

Calibration curves were obtained for only the clinically relevant coproporphyrin and uroporphyrin, as shown in Figure 4-5. Linear calibration was achieved over a range of 50 pM to 1 nM (coproporphyrin: slope = 0.0146 ± 0.00021, intercept = 0.000241 ± 0.00012, R^2 = 0.9996; uroporphyrin: slope = 0.0190 ± 0.00064, intercept = – 0.00016 ± 0.00036, R^2 = 0.998). The linear ranges in Figure 4-5 extend over the normal levels for porphyrin in diluted urine samples (Section 4.3.3 below).

Limits of detection (LOD) were determined by calculating the S/N at 50 pM and then extrapolating for the concentration that would produce a peak with an intensity of 3 × S/N. An LOD of 20 pM was determined for coproporphyrin. This LOD represents an

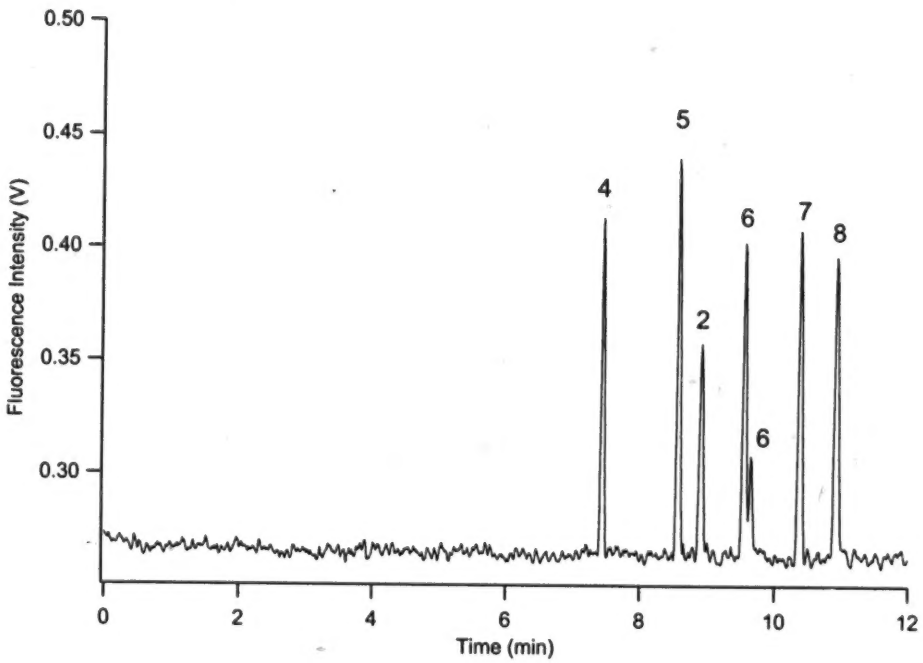

Figure 4-4. Optimized separation using the high-sensitivity instrument. Experimental conditions: 65-cm capillary (60 cm to detector); 25 kV applied; 10 mM CHES - 75 mM SDS buffer, pH 10; 500 pM porphyrin mixture shown; peaks identified by their number of carboxylic acid groups.

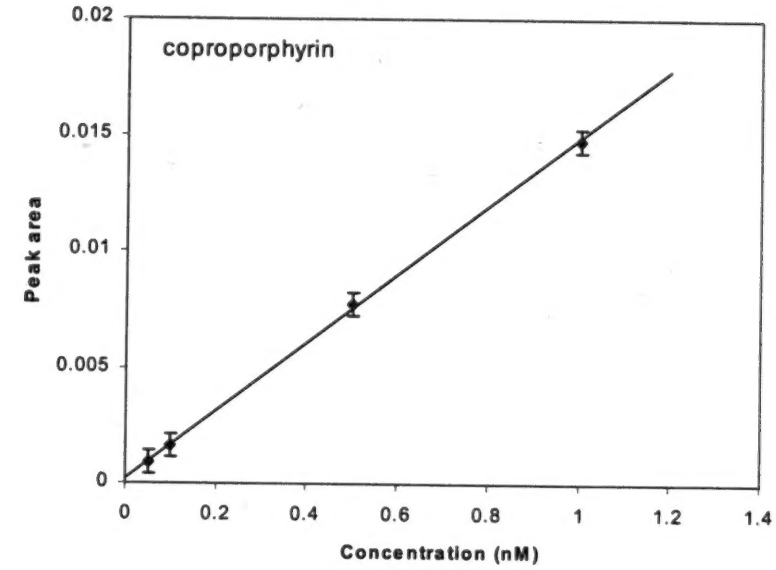

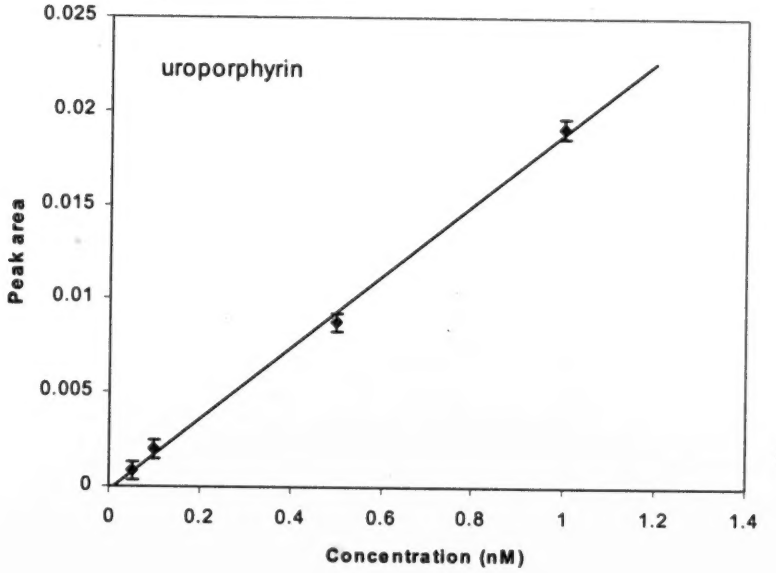

Figure 4-5. Calibration curves for coproporphyrin (top) and uroporphyrin (bottom).

improvement in sensitivity of almost 3 orders of magnitude over previous reports of CE-fluorescence analyses of this same porphyrin mixture [10, 12, 13]. Using a 75-W xenon arc lamp at 400 nm with a custom-built optical fiber based detector, Weinberger *et al.* achieved LODs of 80 nM [10]. Similarly, Li and co-workers quoted an LOD of 10 nM using a 100 W high-pressure mercury lamp at 405 nm with an epi-fluorescence microscope for on-column detection [13]. In the only known CE-LIF report, Sweedler and co-workers achieved LODs ranging from 1 – 10 nM using the 488-nm line of an Ar ion laser coupled with a commercial LIF detector [12]. In this study, the authors could not exploit the highly intense Soret band of the porphyrins at this wavelength but instead used the second most intense band near 500 nm (Figure 4-2).

The LOD of 20 pM achieved in this work also compares quite favorably with previously reported HPLC methods for determining urinary porphyrins. LODs of 1 – 2 nM [10] and 0.2 nM [7] have been reported. Perhaps the lowest LOD reported to date is that of Ausio *et al.* who quoted 70 pM using LC-MS in single-ion-monitoring (SIM) mode (~ 100× higher in scanning mode) [7]. However, esterification (24-h process) of the urinary porphyrins was required to facilitate ionization before detection by MS and the LOD quoted was achieved using porphyrin-ester standards [7].

4.3.3 Detection of porphyrins in urine

Due to the high sensitivity achieved for the urinary porphyrins, the method was tested on a urine sample from a healthy individual. The normal uroporphyrin concentration in urine ranges from 5 – 35 nM [11]. This is well above the LOD for this method. Thus urine could be diluted before analyses. Dilution of the sample would help

minimize matrix effects, particularly de-stacking of the sample due to the high ionic strength of urine [20].

Figure 4-6 shows the separation of the urine sample from a healthy individual after a 1/10 dilution with the separation buffer. Coproporphyrin and uroporphyrin are easily observed at this dilution factor. Further, the porphyrin profile is consistent with that of a healthy individual, as the coproporphyrin level is roughly 10-fold higher than that of uroporphyrin [5, 7]. No attempt was made to identify the numerous peaks observed at 5-7 min. They are most likely porphyrins or porphyrin-based molecules since not many other molecules would be expected to absorb light near 400 nm and then fluoresce near 600 nm. The presence of this fairly intense and marginally interfering set of peaks suggested that further dilution of the urine sample might be advantageous.

Figure 4-7 shows a blow-up of the 7 to 12 min region of the separation shown in Figure 4-6 for the 1/10 dilution (top trace) along with that for a 1/100 diluted sample (bottom trace). Both peaks are still observed after the 1/100 dilution, but that of uroporphyrin is approaching the LOD. The tail of the mass of peaks that interfered with coproporphyrin at the 1/10 dilution is not observed at the 1/100 dilution. A further advantage of a greater dilution factor is that lowering the concentration of matrix components such as proteins would undoubtedly make for a more robust method. Proteins in the sample could potentially adsorb irreversibly to the capillary surface that could alter the EOF, resulting in hysteresis effects [20]. However, the SDS in the separation buffer would help to prevent protein adsorption [21]. Regardless, the greater dilution factor is advantageous.

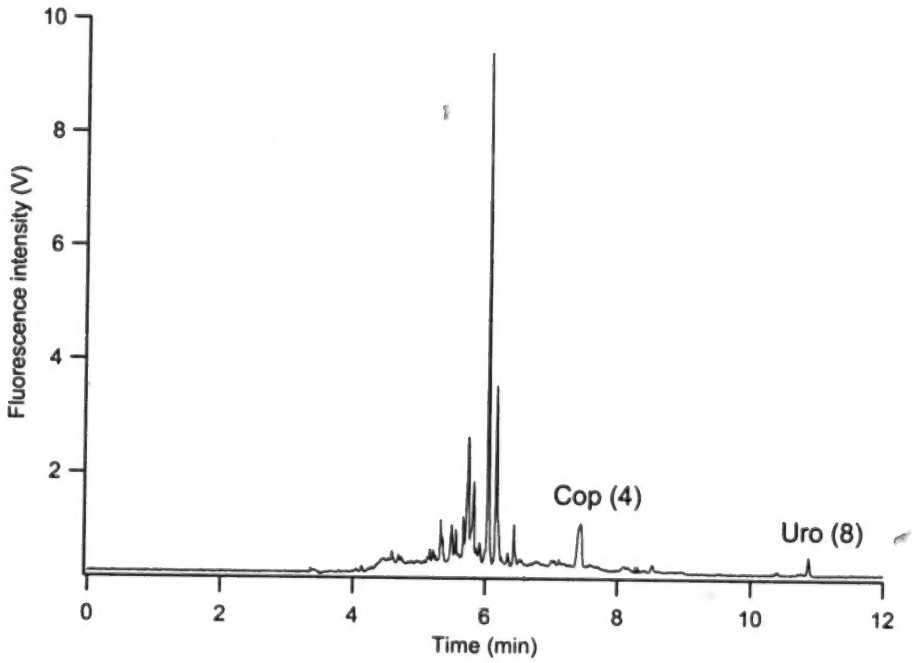

Figure 4-6. Separation of 1/10 diluted urine sample. Experimental conditions as in Figure 4-3.

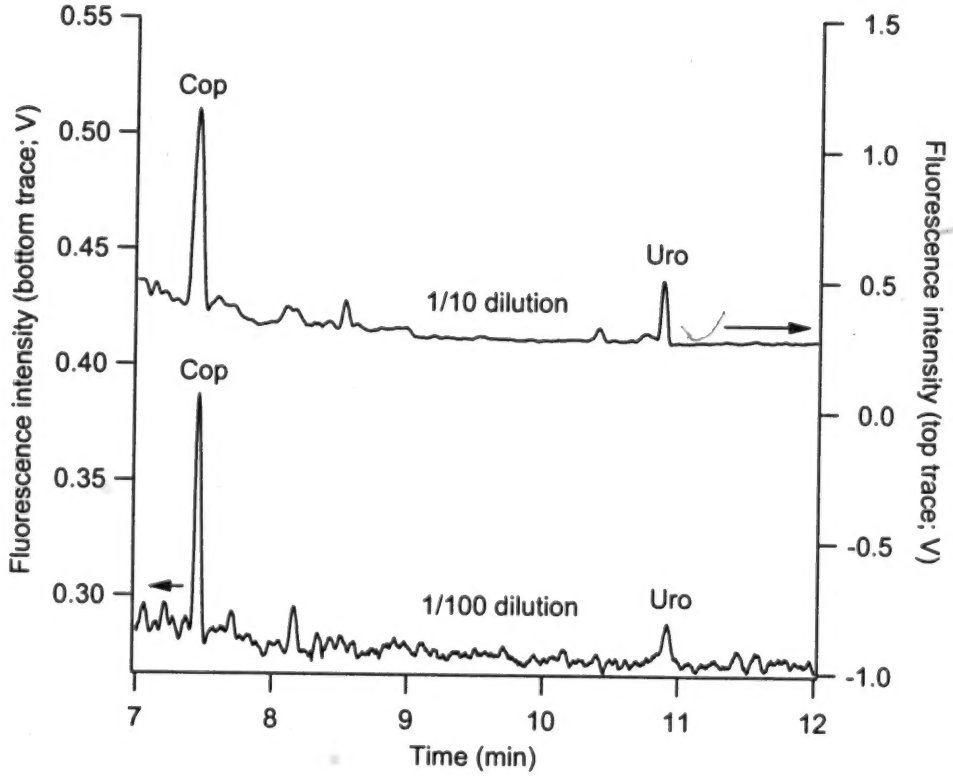

Figure 4-7. Blow-up of 7 to 12 min region of the separation of 1/10 diluted urine (top trace; right y-axis) and 1/100 diluted urine sample (bottom trace; left y-axis).

It is quite apparent that both the coproporphyrin and uroporphyrin peaks in the diluted urine sample (Figure 4-7) are broader than those in the standard mixture (Figure 4-3). This is likely due to the natural occurrence of type III isomers of these two porphyrins. In normal subjects, uroporphyrins consist of about 65 % type I and 35 % type III isomers, while coproporphyrins are the opposite, being 60 % type III and 40 % type I [5]. Compared to the type I porphyrins used in the standard, the type III isomers differ only by the position of one carboxylic acid group. These isomers have slightly different electrophoretic mobilities and are partially separated under the conditions used in this work, resulting in broader peaks. Therefore this methodology cannot discriminate between type I and type III isomers of coproporphyrin and uroporphyrin, which is consistent with previous studies using a similar buffer system [10].

Levels of coproporphyrin and uroporphyrin in the urine sample were quantified. Using peak areas obtained from the 1/100 diluted urine sample and the calibration curves, the concentrations in the original sample were determined to be 34 nM for coproporphyrin and 5.6 nM for uroporphyrin. These concentrations represent the total porphyrin concentrations (type I and III isomers). The total uroporphyrin concentration is within the range of 5 – 35 nM for normal urine specimens [11]. Since the 5.6 nM is at the low end of this range, the 1/100 dilution may be practical since the majority of samples would contain greater concentrations of uroporphyrin. However, the actual concentrations of the porphyrins are not as important for clinical diagnosis as is the relative abundance or "porphyrin profile" [6].

Ideally, a urine sample from a patient suffering porphyria cutanea tarda (PCT) would have been analyzed to further validate the method. However, such a sample was

not available as the clinical diagnostics lab at the University Hospital has recently disposed of its urine archives and a sample will not be available until a new PCT patient is diagnosed (still waiting). As discussed above, the porphyrin profile for a PCT patient is the reverse of that for a healthy patient. Uroporphyrin and heptacarboxylic acid porphyrin are the predominant porphyrins excreted and these are present at levels roughly 10-fold than higher than is coproporphyrin in healthy individuals [5, 7]. Therefore the diagnosis of PCT patients is much less analytically challenging than the confirmation that a person is healthy, so this method could easily be used for samples of patients suffering from PCT.

4.4 Conclusions

The violet diode laser is a useful tool for the analysis of urinary porphyrins. Using the laser coupled with the custom-built LIF detector, a gain in sensitivity of nearly 3 orders of magnitude over previous reports [10, 12, 13] was achieved. This high sensitivity allows for up to a 100-fold dilution of urine prior to analysis, compared to the pre-concentration steps required in previous methods.

4.5 Literature cited

(1) Doss, M.; Schermuly, E. In *Porphyrins in Human Diseases*; Doss, M., Ed.; S. Karger: Basel, 1976, pp 189.

(2) Huie, C. W.; Aiken, J. H.; Williams, W. R. *Anal. Chim. Acta.* **1991,** *254*, 189.

(3) Fang, Q.; Du, M.; Huie, C. W. *Anal. Chem.* **2001,** *73*, 3502.

(4) Matveeva, E. G.; Savitsky, A. P.; Gomez-Hens, A. *Anal. Chim. Acta.* **1998,** *361*, 27.

(5) Lim, C.; Peters, T. *Clin. Chim. Acta.* **1984,** *139*, 55.

(6) Lim, C. K.; Li, F. M.; Peters, T. J. *J. Chromatogr.* **1988,** *429*, 123.

(7) Ausio, X.; Grimalt, J. O.; Ozalla, D.; Herrero, C. *Anal. Chem.* **2000,** *72*, 4874.

(8) Lin, M.; Huie, C. *J. Liq. Chromatogr.* **1997,** *20*, 681.

(9) Gouterman, M. In *The Porphyrins*; Dolphin, D., Ed.; Academic Press: New York, 1978; Vol. III, Physical Chemistry, Part A, pp 1.

(10) Weinberger, R.; Sapp, E.; Moring, S. *J. Chromatogr.* **1990,** *516*, 271.

(11) Eales, L. In *The Porphyrins*; Dolphin, D., Ed.; Academic Press: New York, 1978; Vol. VI, Biochemistry, Part A, pp 665.

(12) Wu, N.; Li, B.; Sweedler, J. V. *J. Liq. Chromatogr.* **1994,** *17*, 1917.

(13) Zhang, Y.; Lee, H. K.; Li, S. F. Y. *Talanta* **1998,** *45*, 613.

(14) Bowser, M. T.; Sternberg, E. D.; Chen, D. D. Y. *Electrophoresis* **1997,** *18*, 82.

(15) Schwer, C.; Kenndler, E. *Anal. Chem.* **1991,** *63*, 1801.

(16) Wiedmer, S. K.; Riekkola, M. *Rev. Anal. Chem.* **1999,** *18*, 67.

(17) Li, D.; Fu, S.; Lucy, C. A. *Anal. Chem.* **1999,** *71*, 687.

(18) Morales-Rojas, H.; Yatsimirsky, A. K. *J. Phys. Org. Chem.* **1999,** *12*, 377.

(19) Sepaniak, M. J.; Cole, R. O. *Anal. Chem.* **1987,** *59*, 472.

(20) Shihabi, Z. K. In *Handbook of Capillary Electrophoresis*; Landers, J. P., Ed.; CRC Press: Boca Raton, 1997, pp 457.

(21) Verzola, B.; Gelfi, C.; Righetti, P. G. *J. Chromatogr. A* **2000,** *874*, 293.

Chapter 5 – Trace Analysis of Myoglobin after Reconstitution with a Fluorescent Porphyrin

5.1 Introduction

As we enter the post-genome era, the determination of proteins is arguably the greatest challenge facing analytical chemists today. Most attention in the literature has been given to the emerging field of 'proteomics', in which the identity and function of all of an organism's proteins is sought. However, the determination of certain proteins or certain classes of proteins is also of interest to researchers. For instance, such determinations are useful for clinical diagnosis of specific conditions or diseases.

Despite the success of capillary electrophoresis in the field of genomics, two fundamental problems have hindered the performance of CE for protein analyses. Firstly, proteins possess multiple amine groups (cationic) which cause proteins to adsorb onto the capillary surface. This problem is being overcome by the development of capillary coating procedures. The second problem, and the one discussed herein, is the issue of detection.

Although proteins do possess an intrinsic UV absorbance due to the aromatic tryptophan, tyrosine, and phenylanaline residues, sensitivity is generally poor. Limits of detection are usually in the low-micromolar range and sensitivity is dependent on the number of aromatic groups a protein possesses [1].

Alternatively, labeling proteins with fluorescent probes has been employed [2]. Amine reactive probes such as 5-furoylquinoline-3-carboxaldehyde (FQ) [1] and 6-aminoquinolyl-*N*-hydroxysuccinimidyl carbamate (6-AQC) [3] have been used. However, since proteins generally have multiple reactive sites, heterogeneity of the reaction

products is observed. For instance, for a protein with *n* free amine groups (# of lysine residues + N-terminus), there are $2^n - 1$ possible reaction products [4]. Myoglobin has 19 lysine residues. Thus there are 1 048 575 possible products upon derivitization. As each of these products has a different electrophoretic mobility, multiple peaks would be expected [5]. In practice, a single extremely broad peak is usually observed [5]. Recently, attempts have been made to drive the labeling reaction to completion [3]. SDS was employed to denature the proteins and thus make all their reactive sites accessible to the labeling reagent [3]. However, this methodology was only effective for small proteins which possess only a few lysine groups, such as lysozyme with only 6 lysine groups [3]. Therefore, labeling of proteins remains a fundamental hurdle that must be overcome for CE-LIF to be useful in proteomics.

Exploiting the native fluorescence of proteins is an attractive alternative to labeling. Sub-nanomolar detection limits have been reported by exploiting the intrinsic fluorescence of proteins [6]. However, this fluorescence is mainly from tryptophans within the protein. Tryptophan requires excitation at ~ 280 nm. As a consequence, UV lasers are required. Unfortunately, these lasers tend to be very bulky and rather expensive. A few proteins possess native fluorescence in the visible region of the spectrum. For instance, green fluorescent protein (GFP; *Aequorea victoria*; jellyfish) contains a fluorophore formed by the cyclization of the Ser65-Tyr66-Gly67 tripeptide [7]. GFP has been extensively used in molecular and cell biology applications [7]. In addition, GFP has been used as a model protein in fundamental studies in capillary electrophoresis [5, 8].

This chapter explores the potential of using a large class of proteins known as heme proteins which contain an intrinsic fluorophore that might be useful for LIF

detection in CE and other applications. These proteins contain a heme group, which is a porphyrin molecule similar to those determined in Chapter 4. Thus, the violet diode laser presents an opportunity for highly sensitive detection of heme proteins. The primary challenge for this approach is that the porphyrin of the heme group contains a central metal atom, which is an efficient quencher of fluorescence. The model protein for these studies is myoglobin, as it is biologically important and yet is simple in structure.

5.2 Experimental

5.2.1 Apparatus

A Model 300 Crystal CE System (ATI Unicam) equipped with a home-built LIF detector was used, as described in Section 2.2.3. Untreated fused silica capillaries (Polymicro Technologies, Phoenix, AZ, USA) with a length of 65 cm (60 cm to the detector), an inner diameter of 50 μm, and an outer diameter of 365 μm were used. For excitation, a homebuilt 400-nm diode laser was used. A detailed description of this laser is given in Section 2.2.3. The laser beam was passed through a 400-μm pinhole (Melles Griot) that sat inside the 6.3× (0.20 NA) microscope objective (Melles Griot) which focused the beam onto the capillary. Laser power was adjusted to deliver ~ 0.25 mW onto the capillary. Fluorescence was collected at 90° with a 40× (0.65 NA) microscope objective (Melles Griot), passed through 1-mm pinhole (Melles Griot) for spatial filtering, and then through a 600-nm band-pass filter (600DF50, Omega).

5.2.2 Reagents

Myoglobin and *apo*-myoglobin (both horse skeletal) were obtained from Sigma. Protoporphyrin IX and Zn(II)-protoporphyrin IX were from Aldrich. Boric acid, sodium hydroxide, and magnesium chloride were obtained from BDH. Zinc(II) chloride and HPLC-grade methanol were from Fisher.

5.2.3 Reconstitution procedure

The procedure used for reconstitution was a modified version of a literature method [9]. 10 μM stock solutions of protoporphyrin IX and Zn(II)-protoporphyrin IX were prepared in 50% methanol/50% 25-mM borate buffer at pH 9.5. About 1 h of vigorous stirring was required to completely dissolve the porphyrins. Porphyrin solutions were shielded from light whenever possible. 14-μM stock solutions of *apo*-myoglobin were prepared by dissolving 56 nmol of *apo*-myoglobin in 4 ml of water.

In a 1.5-ml amber polypropylene microcentrifuge tube, an appropriate volume of 25 mM borate buffer was added such that the final volume was 1 ml. Next, an appropriate volume of *apo*-myoglobin solution was added, followed by the porphyrin solution. This mixture was then vortexed at 2000 r.p.m for ~ 10 s and allowed to sit at room temperature in the dark for 30 min. The reaction mixture was then injected directly into the capillary without dilution.

5.2.4 Separation conditions

New capillaries were flushed with 0.1 M NaOH for 10 min at 1000 mbar and then then water for 5 min at 1000 mbar before use. Injections were performed hydrodynamically at 50 mbar for 6 s. Optimized buffer conditions consisted of 25-mM

borate at pH 9.5. Separations were performed with an applied potential of 20 kV (308 V/cm).

5.3 Results and discussion

5.3.1 Structure of myoglobin

Myoglobin is an oxygen-binding protein of muscle cells. It is a relatively small (MW = 16,700; horse skeletal) protein and consists of single polypeptide chain of 153 amino acid residues of known sequence. Myoglobin folds such that most of the hydrophobic amino acid side chains are oriented toward the interior of the molecule. This creates a very dense hydrophobic core or pocket that is typical of globular proteins. Inside this hydrophobic pocket sits a porphyrin ring known as the heme group. Shown in Figure 5-1 is the three dimensional structure of myoglobin [10] with the polypeptide backbone (no side chains shown for clarity) shown in a ribbon representation and the heme group in ball-and-stick format.

The heme group of myoglobin consists of a protoporphyrin IX (PPIX) molecule in which an Fe (III) atom is bound by the four pyrrole-nitrogens of the porphyrin. The structure of the heme group of myoglobin is shown in Figure 5-2A. The heme group is held in the inner pocket of myoglobin by two main forces. Firstly, the iron atom of the heme group forms a coordinate bond to a nitrogen atom of the five-membered ring of histidine residue 93. As shown in Figure 5-2B, the iron atom can form two coordinate bonds that run perpendicular to the four in the plane of the porphyrin ring; one to the histidine residue; and the other serves as the binding site for oxygen. Secondly, the heme group is held in place by the hydrophobic interaction between the porphyrin and the

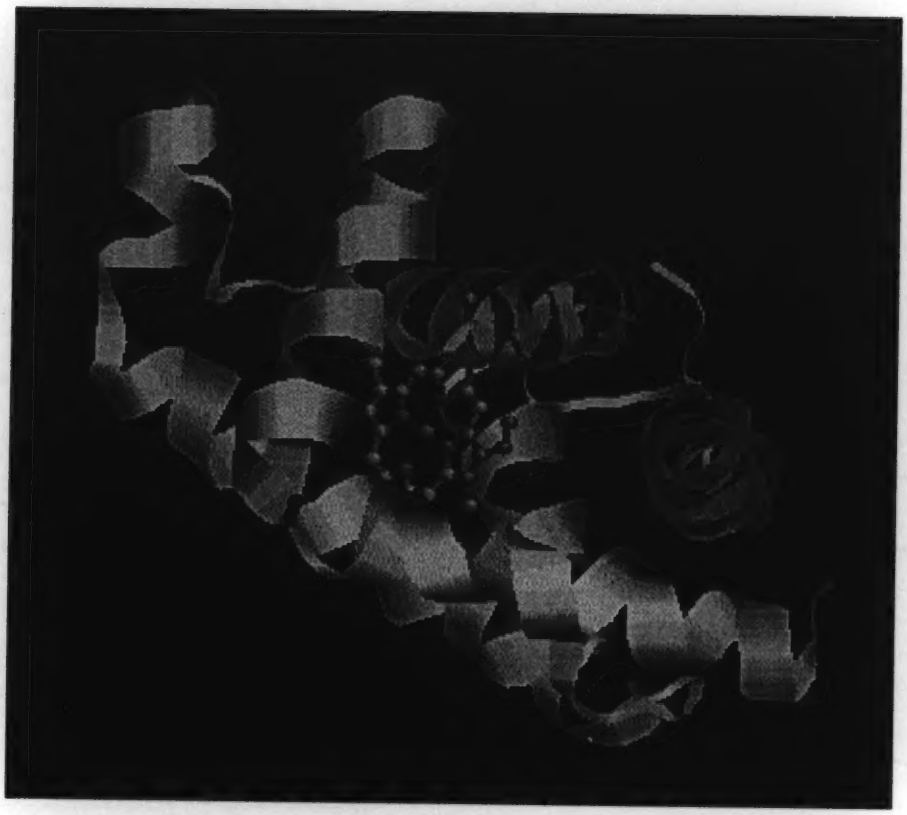

Figure 5-1. Three dimensional structure of myoglobin with the polypeptide backbone shown in a ribbon representation and the heme group in ball-and-stick format (no side chains shown for clarity). Source: ref. 9.

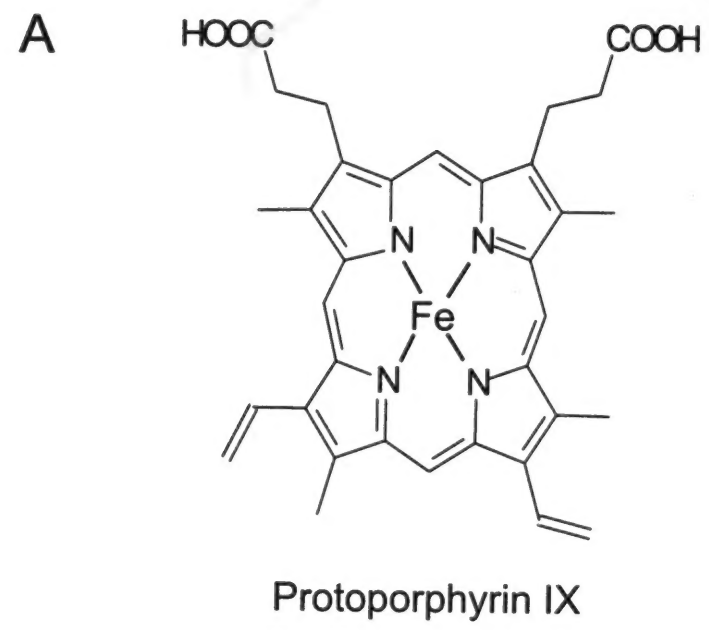

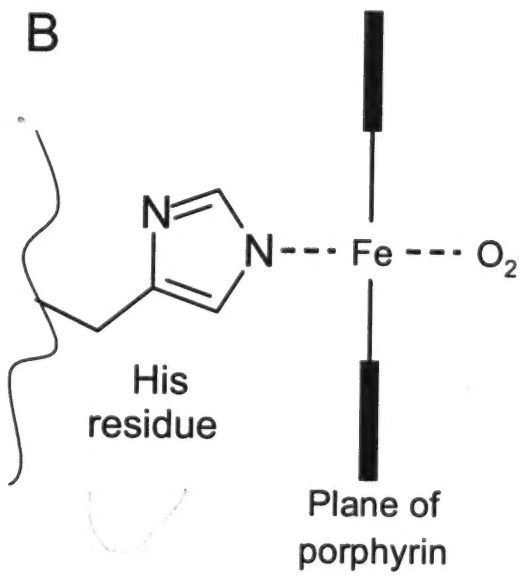

Figure 5-2. A) Structure of the heme group of myoglobin (Fe-protoporphyrin IX) porphyrins. B) Coordination of the Fe atom in the heme group of myoglobin.

hydrophobic residues of the inner pocket of myoglobin. PPIX is a very hydrophobic porphyrin with only two carboxylic acid groups (Figure 5-2A). The relative importance of these two forces is ambiguous in the literature and will be a topic of further discussion below.

5.3.2 Optical properties of the heme group

Protoporphyrin IX in its free-base form is a highly fluorescent porphyrin with excitation and emission maxima at 400 nm (Soret band) and 619 nm, respectively (10 mM phosphate; pH 7.4) [11]. An analogue of mesoporphyrin IX, PPIX gives a similar fluorescence response to the porphyrins described in Chapter 4 upon excitation with the violet diode laser. However, when bound to iron, PPIX exhibits normal absorption behaviour, but is essentially non-fluorescent. Fe(III) is a paramagnetic metal (unpaired electrons). As such, iron is an effective quencher of fluorescence. Although this quenching is usually considered 100 % efficient, very weak fluorescence ($\Phi_f \sim 4 \times 10^{-6}$) has been reported for some Fe-porphyrin complexes [12]. For comparison, *normal* fluorescence for metalloporphyrins exhibit Φ_f between 0.001 and 0.2 [13].

Figure 5-3 shows an electropherogram of 5 μM of native (Fe-containing) horse skeletal myoglobin in borate buffer at pH 9.5. The multiple peaks observed between 5 and 6 minutes are most likely due to isoforms of myoglobin. Horse myoglobin is known to have a major isoform (p*I* 7.4) and a minor isoform (p*I* 6.9) which have been separated by gel electrophoresis [14]. These peaks were also observed using UV absorbance detection (λ = 214 nm) under the same experimental conditions. The intensity of the peaks in Figure 5-3 are over 1500 times lower than one would expect to achieve for an equimolar concentration of free-base PPIX (no Fe) using similar buffer conditions to

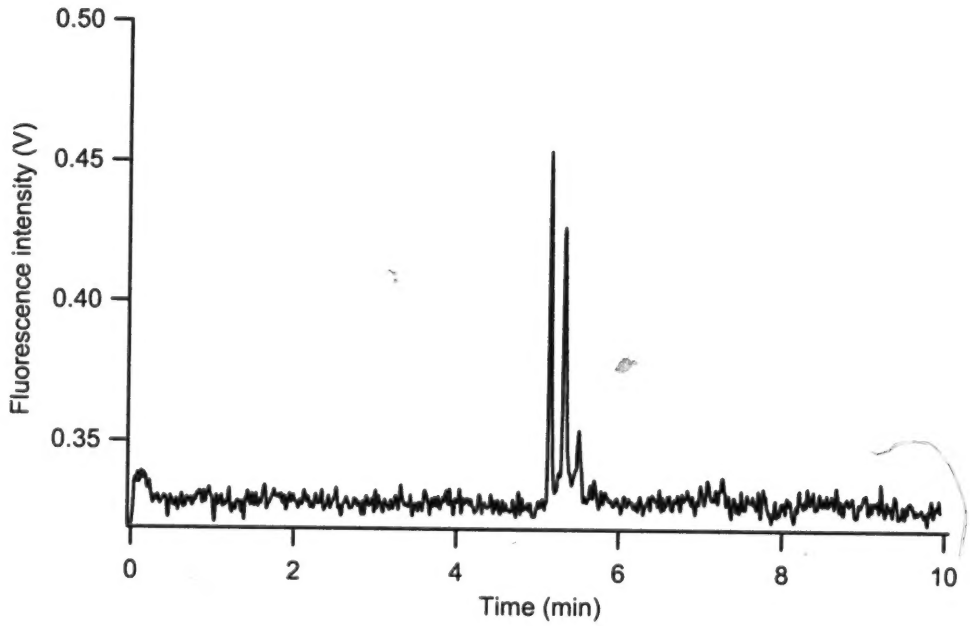

Figure 5-3. Electropherogram of 5 μM native (Fe-containing) horse skeletal myoglobin in borate buffer at pH 9.5.

those employed in Chapter 4. Specifically, 100 nM PPIX yielded a peak with a height of over 5 V (same relative scale as Figure 5-3). This reduction in signal correlates well with the reduced quantum yield for porphyrins that contain iron ($\sim 4 \times 10^{-6}$) [12]. Irreversible protein adsorption to the capillary wall may have also played a minor role in the apparent loss of signal. Protein recovery studies performed in our laboratory suggest that roughly 50 % of the myoglobin could be lost to the capillary wall under the conditions used in Figure 5-3. This issue will be discussed in greater detail in Section 6.2.1.1. With a limit of detection of 0.2 μM, native myoglobin fluorescence with excitation at 400 nm offers little advantage over absorbance detection in either the UV or 400-nm region. However, the fact that any fluorescence was observed is interesting in that it contradicts many previous reports and demonstrates the potential for trace detection of heme proteins.

5.3.3 Demetalation or transmetalation of the heme

Enhancing the fluorescence of the heme group of myoglobin is essential in order to make LIF a viable alternative to direct absorbance detection. A simple solution would be to remove the Fe atom from the porphyrin. However, porphyrins bind metals extremely strongly, with stability constants in the 10^{29} range [15]. Thus, extremely harsh conditions must be used to *demetalate* prophyrins. For instance, the standard method for demetalation of Fe-porphyrins calls for treatment with 100 % H_2SO_4 for 24 h [15]. In this procedure, protonation of the nitrogens of the inner porphyrin ring reduces the porphyrin's affinity for the metal. These harsh conditions are obviously not compatible with proteins such as myoglobin in which the heme group is held noncovalently. Undoubtedly denaturation would result, with the consequent loss of the heme group.

Another possible method for enhancing the fluorescence of myoglobin would be to exchange the iron for a different metal ion. This procedure is known as *transmetalation*. Whereas metals such as Fe quench fluorescence, porphyrins containing closed shell metals exhibit relatively strong fluorescence. The quantum yields of closed shell metal-porphyrins are generally inversely proportional to the molecular weight of the metal. Thus, lighter metals such as Mg(II) and Zn(II) typically yield the most intense fluorescence with generalized quantum yield of 0.25 and 0.04, respectively [13]. Unfortunately, the standard methods of transmetalation of heme groups also require rather harsh conditions, similar to those for demetalation. These exhaustive methods have been used for metal substitution in cyotchrome *c* [16, 17], where the heme group is covalently bound to the protein backbone. However, most of these methods were developed by biochemists that required quantitative reactions and pure products to perform studies on the protein structure and function.

To be analytically useful, the transmetalation need not be quantitative. Thus I explored whether the iron atom could be partially substituted using much less harsh conditions. Mg(II) and Zn(II) were added in excess to 5-μM myoglobin solutions and allowed to react for several hours in an attempt to shift the equilibrium and allow displacement of Fe. Molar ratios up to 1000:1 (metal:myoglobin) and light heating (50°C; non-denaturing conditions) was used to facilitate the reaction. In all cases, no enhancement in fluorescence was observed. Separations appeared essentially as shown in Figure 5-3. Thus, attempts at transmetalation by simple addition of Mg(II) and Zn(II) in large excess were futile. In retrospect this is not surprising, as the heme group of myoglogin is heavily shielded from aqueous solution, as shown in Figure 5-1. In fact, the

hydrophobic interior of myoglobin is so dense and compact that crystallographic data has shown that there is only sufficient space for four water molecules [18].

5.3.4 Reconstitution of myoglobin with a fluorescent porphyrin

An alternative to the removal or substitution of the Fe atom of the heme group is to exchange the entire heme group with a different porphyrin. This technique is known as *reconstitution*. Literature methods exist specifically for myoglobin [9]. Reconstitution of myoglobin generally consists of a denaturation step followed by extraction or ion-exchange chromatography to separate the myoglobin from the free heme group. Myoglobin without the heme group is known as *apo*-myoglobin. *Apo*-myoglobin can then be reacted with the porphyrin of choice at near-neutral pH and room temperature. The reaction is spontaneous and is almost complete within 5 min and totally complete within 2.5 h [9].

To facilitate these initial studies, apo-myoglobin was obtained commercially. As the denaturing and extraction steps are well established, they could be added into the overall procedure at a later stage. *Apo*-myoglobin is inherently in a denatured state since the heme group is required for protein folding [9]. Free-base PPIX and Zn-PPIX were also available commercially and were evaluated as potential fluorescent porphyrins for reconstitution with *apo*-myoglobin. The fluorescence excitation and emission maxima for PPIX and Zn-PPIX in aqueous solution are summarized in Table 5-1. Table 5-1 also includes the fluorescent characteristics of these porphyrins bound within hemoglobin, which like myoglobin encapsulates porphyrins in a hydrophobic environment [9].

Table 5-1. Fluorescence excitation and emission maxima for PPIX and Zn-PPIX in aqueous buffer (10 mM phosphate; pH 7.4) and bound within hemoglobin. Source: ref. 10.

Porphyrin	Wavelength of maxima (nm)	
	Excitation (Soret)	Emission
PPIX in buffer	400	619
PPIX-globin	403	625
Zn-PPIX in buffer	406	584
Zn-PPIX-globin	423	594

5.3.4.1 Reconstitution of *apo*-myoglobin with PPIX

Injection of 70 nM *apo*-myoglobin (not shown) resulted in no fluorescence response, as expected. Injection of 100 nM PPIX resulted in a strong peak at 7 min, as shown in the upper trace of Figure 5-4. The PPIX peak in Figure 5-4 is much broader (N = 27,500) than achieved for the urinary porphyrins in Chapter 4 (e.g., Figure 4-4). However, as was discussed in Section 4.3.1, it was necessary to add significant concentrations of SDS to the buffer to fully solubulize the porphyrins. SDS was not added to the buffer in this work as it would denature the myoglobin, thereby causing it to lose the porphyrin.

Figure 5-4 (bottom trace) is the separation of the reaction mixture of 70 nM *apo*-myoglobin with 100 nM PPIX. The *apo*-myoglobin and PPIX were mixed and allowed to react for 30 min at room temperature. The peak at 7 min due to PPIX is a third the height of that of 100 nM of free PPIX (upper trace), consistent with expectation. The two peaks at 5.3 and 5.5 min likely correspond to the reconstituted myoglobin as their migration times coincide with those of native myoglobin in Figure 5-3. Whereas three peaks were observed for the native myoglobin standard (Fe-containing) in Figure 5-3, only two were observed for the reconstituted myoglobin in Figure 5-4. One possible explanation is that the *apo*-myoglobin sample is more pure (fewer isoforms) than the myoglobin standard and therefore yields fewer peaks. Attempts to determine *apo*-myoglobin under similar CE conditions using UV absorbance detection were futile. Presumably this was due to the *apo*-myoglobin being its unfolded form and thus adsorbing more strongly to the capillary wall. Another possible explanation for the myoglobin patterns observed in Figures 5-3 and 5-4 is that the reconstitution reaction was

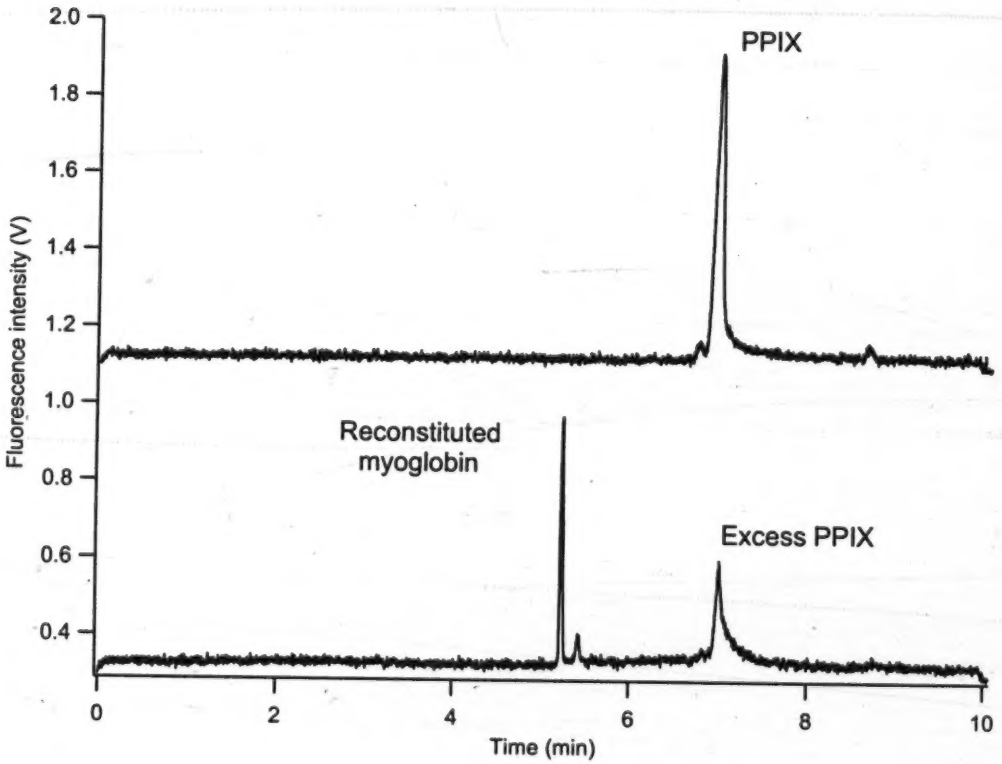

Figure 5-4. The separation of the reaction mixture of 70 nM *apo*-myoglobin with 100 nM PPIX (bottom trace) and the injection of 100 nM PPIX (top trace).

selective for certain isoforms. However, no such reaction bias has been discussed in the extensive literature on reconstitution of proteins [9].

The efficiencies for the reconstituted myoglobin peaks in Figure 5-4 are > 120 000. These are comparable to those of the native myoglobin in Figure 5-3. The sharpness of the myoglobin peaks in Figure 5-4 indicate that the protein is remaining folded throughout the electrophoretic run. If the protein was unfolding and losing PPIX while migrating the length of the capillary, the myoglobin peaks would be heavily tailed as has been previously observed in noncovalent labeling of proteins [19]. This suggests that even without a central metal atom, PPIX can form relatively stable complexes with myoglobin. This is consistent with previous work that suggested that the porphyrin-myoglobin interaction is largely hydrophobic in nature and is not dependent on the Fe-histidine ionic bond [9].

The relative areas of the PPIX peaks of both traces in Figure 5-4 can be used as an estimate of the reaction yield. The peak area of PPIX in the bottom trace (0.025) is approximately 30.5% of that of the PPIX peak in the control run (0.081). Assuming binding of PPIX by apomyoglobin is strictly 1:1, and taking into account the 30% excess of PPIX in the reaction mixture, the reaction yield is essentially 100%. For further evidence , the sum of the peak areas in the bottom trace of Figure 5-4 should equal that of the PPIX peak in the control experiment. Using corrected peak areas ($A_{corr} = A/t_m$; corrects for velocity differences through the detection window), the sum of the areas of the peaks in the bottom trace (0.008) falls short of that of the PPIX peak in the control experiment (0.012). This apparent loss of PPIX in the reaction mixture with *apo*-myoglobin is partially explained by a slight red-shift of the excitation spectrum of PPIX

upon entering the highly hydrophobic environment of the myoglobin interior (Table 5-1). In fact, a shift in the excitation maximum to 403 nm has been reported for PPIX-hemoglobin, compared to 400 nm for PPIX in aqueous solution (Table 5-1) [11]. Another possible source of this apparent loss of PPIX is protein adsorption to the capillary wall (discussed in Section 5.3.4.2 below). Regardless, the reaction is nearly 100% complete in 30 min. This is consistent with literature methods that claim that the reaction is almost complete in 5 min and totally complete in 2.5 h [9].

5.3.4.2 Reconstitution of apomyoglobin with Zn-PPIX

Figure 5-5 (bottom trace) shows the separation of the reaction mixture of 70 nM *apo*-myoglobin with 100 nM Zn-PPIX. The top trace in this same figure is the electropherogram for 100 nM Zn-PPIX. In general, reconstitution with Zn-PPIX yielded comparable results to those achieved with PPIX. The two peaks representing myoglobin are essentially identical in migration time to those in Figure 5-4. In the top trace of Figure 5-5, the second smaller peak migrating just after the major peak might be an impurity of free-base PPIX. With a lower mass, it would be consistent for PPIX to migrate to the detector after Zn-PPIX (counter-EOF).

As with PPIX, comparing the areas of the Zn-PPIX peaks of both traces in Figure 5-5 suggested that reaction went essentially to completion. The peak area of the excess Zn-PPIX in the bottom trace (0.011) is approximately 30.1% of the overall peak area in the control run of the top trace (0.036). The roughly 25 % lower intensity for the myoglobin peaks and the Zn-PPIX peaks compared to those in Figure 5-4 may be attributed to the red-shift of the Soret band for Zn-PPIX relative to PPIX (Table 5-1) or that Zn-PPIX has a slightly lower Φ_f than PPIX [13].

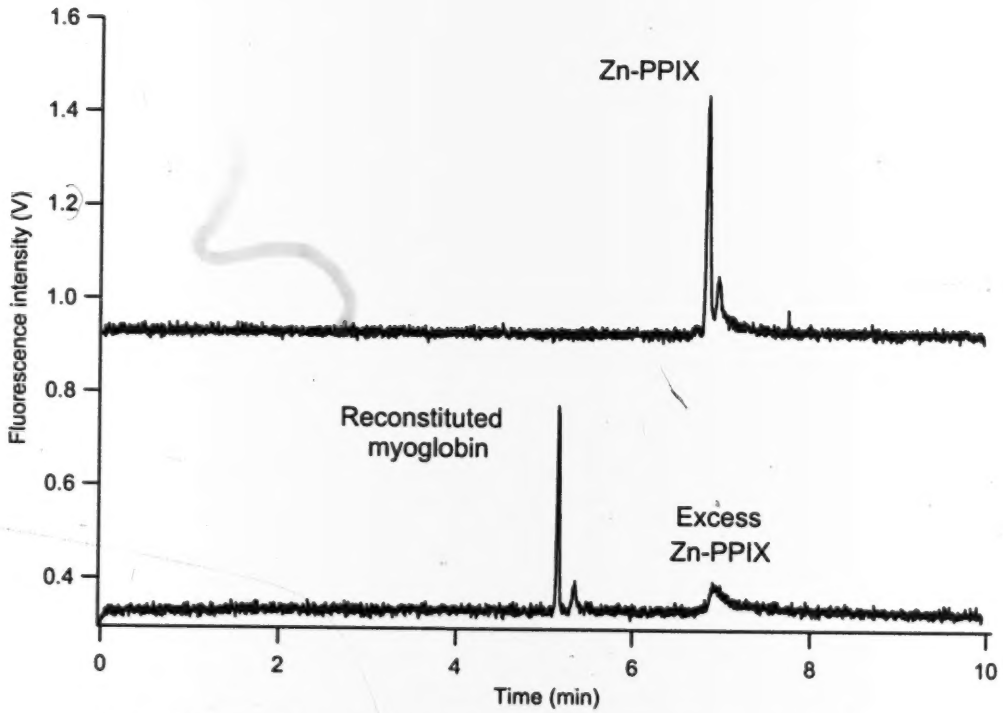

Figure 5-5. The separation of the reaction mixture of 70 nM *apo*-myoglobin with 100 nM Zn-PPIX (bottom trace) and the injection of 100 nM Zn-PPIX (top trace).

The performance of PPIX and Zn-PPIX in the reconstitution of *apo*-myoglobin was roughly identical in this initial study. However, using Zn-PPIX may be advantageous. Using Zn-PPIX over PPIX would greatly reduce the risk of picking up trace metal impurities such as Fe. This would become ever more important when dealing with real samples. Alternatively, if PPIX were used it would be necessary to add a scavenger chelate such as EDTA to the reaction mixture and buffer.

5.3.4.3 Potential sensitivity for reconstituted myoglobin

Figure 5-6 shows the separation of the reaction mixture of 7 nM *apo*-myoglobin with 10 nM Zn-PPIX. The secondary myoglobin peak is likely below the detection limit and so is not detected. Similarly, no peak associated with the excess porphyrin is present at 7 min. From the peak in Figure 5-6, the limit of detection was calculated to be 1 nM based on 3 S/N. This represents roughly 2 two order of magnitude improvement in sensitivity relative to that by achieved by native heme group fluorescence (Figure 5-3) and absorbance techniques. Also, this LOD is only slightly poorer than the 0.5 nM achieved for myoglobin with multi-labeling techniques using a sheath-flow detection cell [1].

The area of the peak for 7 nM in Figure 5-6 (area = 0.0014) is roughly 10 % of the size of that for 70 nM myoglobin in Figure 5-5 (area = 0.014), indicating that the response is linear. Scaling up the reaction to 700 nM *apo*-myoglobin and 1 μM Zn-PPIX was problematic due to the limited solubility of Zn-PPIX. This issue will be investigated in futures studies.

It should be noted that significant protein adsorption to the capillary was likely occurring throughout these experiments. Although capillary coatings have been

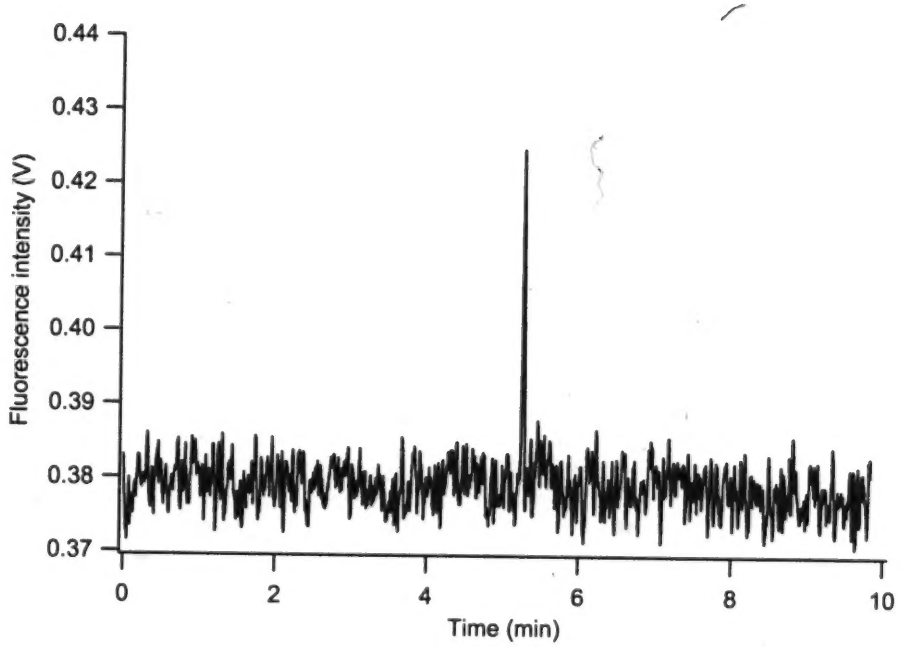

Figure 5-6. The separation of the reaction mixture of 7 nM *apo*-myoglobin with 10 nM Zn-PPIX.

developed in our laboratory to counteract this problem, even specific for myoglobin [20], these coatings were not employed to eliminate the chance of the coating material causing protein denaturation (loss of porphyrin). These coatings will be discussed in the Future Work section of the following chapter.

5.4 Conclusions

This preliminary work demonstrates the potential for sensitive detection of heme proteins using the violet diode laser for LIF detection. The possibilities of this technology are numerous, a few of which will be discussed in the next chapter.

5.5 Literature cited

(1) Pinto, D. M.; Arriaga, E. A.; Craig, D.; Angelova, J.; Sharma, N.; Ahmadzadeh, H.; Dovichi, N. J. *Anal. Chem.* **1997,** *69*, 3015.

(2) Krull, I. S.; Strong, R.; Sosic, Z.; Cho, B. Y.; Beale, S. C.; Wang, C. C.; Cohen, S. *J. Chromatogr. B* **1997,** *699*, 173.

(3) Liu, H.; Cho, B. Y.; Strong, R.; Krull, I. S.; Cohen, S.; Chan, K. C.; Issaq, H. J. *Anal. Chim. Acta* **1999,** *400*, 181.

(4) Zhao, J. Y.; Waldron, K. C.; Miller, J.; Zhang, J. Z.; Harke, H.; Dovichi, N. J. *J. Chromatogr.* **1992,** *608*, 239.

(5) Craig, D. B.; Dovichi, N. J. *Anal. Chem.* **1998,** *70*, 2493.

(6) Lee, T. T.; Yeung, E. S. *J. Chromatogr.* **1992,** *595*, 319.

(7) Misteli, T.; Spector, D. L. *Nat. Biotechnol.* **1997,** *15*, 961.

(8) Stastna, M.; Radko, S. P.; Chrambach, A. *Electrophoresis* **2001,** *22*, 66.

(9) Sano, S. *Reconstitution of Hemoproteins*; Academic Press: New York, 1978.

(10) PDB *Protein Data Bank, http://www.rcsb.org/pdb/.*

(11) Lamola, A. A.; Yamane, T. *Science* **1974,** *186*, 936.

(12) Adar, F.; Gouterman, M.; Aronowitz, S. *J. Phys. Chem.* **1976,** *80*, 2184.

(13) Gouterman, M. *Optical Spectra and Electronic Structure of Porphyrins and Related Rings*; Academic Press: New York, 1978.

(14) Tulp, A.; Verwoerd, D.; Benham, A.; Jalink, K.; Sier, C.; Neefjes, J. *Electrophoresis* **1998,** *19*, 1171.

(15) Phillips, J. N. *Rev. Pure Appl. Chem.* **1960,** *10*, 35.

(16) Vanderkooj, J. M.; Erecinska, M. *Eur. J. Biochem.* **1975,** *60*, 199.

(17) Ye, S.; Shen, C.; Cotton, T. M.; Kostic, N. M. *J. Inorg. Biochem.* **1997,** *65*, 219.

(18) Kendrew, J. C. *Sci. Am.* **1961,** *205*, 96.

(19) Legendre, B. L.; Soper, S. A. *Appl. Spec.* **1996,** *50*, 1196.

(20) Melanson, J. E.; Baryla, N. E.; Lucy, C. A. *Anal. Chem.* **2000,** *72*, 4110.

Chapter Six – Conclusions and Future Work

6.1 Conclusions

In this thesis, the violet diode laser has been shown to be a promising alternative to conventional gas-based lasers for laser induced fluorescence detection in capillary electrophoresis. The high stability of the violet diode laser is particularly advantageous for indirect fluorescence detection. Further, the detection of porphyrins and related compounds will be a significant niche for the violet diode laser for fluorescence applications.

Though still relatively expensive for a diode laser ($2 000 - $5 000 US), the cost of the violet diode laser will undoubtedly drop in the future. The economic windfall offered by the high-volume electronics market (*i.e.*, DVD players) will help drive prices down. Nichia now offers their violet laser diodes (395 – 415 nm) with powers of 5 and 30 mW. They have also begun to sell evaluation samples of their new 5 mW blue laser diodes (430 – 445 nm). For both the blue and the violet diodes, the desired wavelength can be specified upon ordering for fine-tuning applications.

Introduction of the violet diode laser into CE-LIF is just part of a larger trend toward the use of compact, inexpensive, and low-power lasers in the fields of chemistry and biotechnology. Low powered, frequency tripled and quadrupled Nd:YAG lasers operating at 355 and 266 nm, repectively, are now commercially available and have been employed for LIF detection in CE [1]. Similarly, use of a new hollow cathode metal vapor laser (NeCu) working at 248.6 nm has been reported in CE-LIF [2]. These lasers can be purchased for ~ $10 000 US, several times less than that required for full frame Ar/Kr

lasers that were previously required for UV excitation. Similarly, the new solid-state, 488-nm Sapphire laser by Coherent [3] threatens to render the Ar-ion laser obsolete for low-power applications such as fluorescence excitation.

6.2 Future work

The bulk of the future work stemming from this thesis will focus on extending the capabilities of the violet diode laser for the detection of heme proteins. The preliminary work described in Chapter 5 set the groundwork for numerous potential projects.

6.2.1 Myoglobin

6.2.1.1 Implementation of 'non-denaturing' capillary coatings

As discussed in Chapter 5, significant adsorption of reconstituted myoglobin to the capillary wall was likely occurring. Although the buffer pH (9.5) employed was more than two units above the pI of myoglobin (7.4), the protein carried only a slight net negative charge. In fact, a calculation of the overall charge of myoglobin at pH 9.5 taking into account the pK_a values of all of the amino acid substituents (and N- and C-terminus) of the entire protein sequence yielded a net charge of only ~ -2. In practice, this protein is essentially neutral and is just as likely to be attracted to the negatively charged capillary surface than it is repelled. In retrospect, increasing the pH to 10 to 10.5 to partially deprotonate the basic lysine groups (pK_a = 10.69) would have undoubtedly reduced adsorption. However, this higher pH might also denature myoglobin, which would have made detection with the violet diode laser impossible.

Capillary coatings have been a major theme of our research group over the past several years [4]. In particular, surfactant-based coatings have been developed to prevent protein adsorption. However, these coatings have been traditionally dynamic in nature

such that a relatively high concentration of surfactant (above the critical micelle concentration (CMC); low mM range) must be present in the background electrolyte to establish an equilibrium between surfactants in solution and those at the surface. Analyte-surfactant interactions are unavoidable with these coatings, and in the case of proteins, these interactions may lead to denaturation.

In studies not included in this thesis, I pioneered a coating procedure that eliminates these analyte-surfactant interactions by using the double-chained surfactant (didodecyldimethylammonium bromide; DDAB) [5, 6]. The bilayer formed with DDAB adheres to the capillary surface so strongly that excess surfactant can be flushed out of the capillary prior to performing separations. Protein recoveries in excess of 98 % have been achieved. Dr. Liang Li's group has also demonstrated that these coatings are compatible with off-line MALDI-TOF-MS of proteins after separation by capillary electrophoresis.

DDAB coatings are positively charged. Thus acidic conditions which would make myoglobin cationic would be employed. Using pH ~ 4 would begin to protonate the aspartic acid ($pK_a = 3.90$) and glutamic acid ($pK_a = 4.42$) residues and maximize the electrostatic repulsion between the protein and the capillary wall. These mildly acid conditions should not denature myoglobin.

6.2.1.2 Extension of reconstitution procedure to *holo*-myoglobin

Using the *Apo* form of myoglobin for reconstitution in Chapter 5 was a simple means of testing the potential of the violet diode laser for selective protein detection. However any practical analytical method will start with the *holo* form of the protein, which is the protein with the heme group intact.

As mentioned in Section 5.3.4, current methods of reconstitution involve a separation or extraction to isolate *apo*-myoglobin after denaturation. Biochemists require this separation/extraction step to obtain pure *apo*-protein for subsequent bio-physical studies. Such an exhaustive and labour-intensive sample preparation is unattractive from an analytical standpoint. Fortunately, for analytical applications such purity is not necessary. For example, after denaturation of *holo*-myoglobin, a 100-fold excess of the fluorescent porphyrin (Zn-PPIX) could be added to the protein. Thus, upon reconstitution, the fluorescent porphyrin would be a hundred times more likely to be taken up by the protein. Essentially, the protein would be quantitatively converted to the fluorescent form. Upon analysis, any residual myoglobin in the Fe form would cause negligible interference. The signal from the Fe form would be roughly 10^5-fold lower than the analytical signal of interest given the 10^2-fold lower abundance and the 10^3-fold lower fluorescence intensity (Section 5.3.2). Further, with a mass difference of only 10 AMU it is unlikely that the Zn and Fe form of myoglobin would be separated. Thus any residual signal from the Fe form would only add to the myoglobin signal.

A suitable denaturation/renaturation technique would have to be developed. Thermal denaturation of myoglobin at 90 °C for 20 min could be employed [7]. Once denatured, excess Zn-PPIX would be added and reconstitution would take place upon cooling. Alternatively, a quicker means to denature and renature the protein may be to use pH. A small volume of HCl could be used to bring the pH of the reaction buffer down to 1.5 – 2 to denature. Excess Zn-PPIX would then be added, followed by the addition of NaOH to bring the pH back to up to 9.5 to allow for reconstitution. Potential

problems with this technique include the limited solubility of Zn-PPIX and dealing with the large excess of Zn-PPIX injected into the capillary.

6.2.1.3 Enhancement of native (Fe) myoglobin fluorescence

Although the reconstitution procedure described above is fairly straightforward, it is still less attractive than simply exploiting myoglobin's native fluorescence. However, as shown in Section 5.3.2, the limit of detection for native myoglobin is relatively poor (0.2 μM) due to quenching of fluorescence by the central Fe atom of the heme group.

A potential method of enhancing the fluorescence of native myoglobin would be to reduce the Fe atom of the heme group. Whereas Fe(III) is paramagnetic, Fe(II) contains only paired electrons. Thus the quenching efficiency of Fe(II) would be expected to be lower than that of Fe(III). Regardless, neither form of Fe has either empty or full *d* orbitals so even Fe(II)-myoglobin would not be expected to exhibit Φ_f comparable with that of Zn(II) or Mg(II).

The degree to which fluorescence would be enhanced is likely to be only 1 order of magnitude at best. Literature suggests that the Φ_f of Fe(II)-hemoglobin is only twice that of Fe(III) hemoglobin [8]. However, this is only an approximation based on the excited electronic state lifetime (τ_e) of 6 fs for Fe(II)-hemoglobin compared to 3 fs for Fe(III) hemoglobin (assuming $\Phi_f \alpha \tau_e$) since no fluorescence was observed for either of these complexes [8]. Similarly, Fe(II)-cytochrome b_5 has a τ_e of 100 fs while Fe(III)-cytochrome b_5 has τ_e of ~ 10 fs [8]. In this study, the fluorescence was intense enough to be measured in the case of Fe(II)-cytochrome b_5 and a Φ_f of 4×10^{-6} was estimated [8]. Cytochrome b_5 is a protein analogous to myoglobin in that contains a single protoporphyrin IX heme group.

Thus only marginal gains in sensitivity would be predicted for reduction of Fe in the heme. Ultimately, the sensitivity would still be poorer than that possible with UV/tryptophan based native fluorescence. However, this methodology would offer more selective detection and may be useful for rapid screening for myoglobin in complex mixtures such as urine [9]. Regardless, since myoglobin is easily reduced upon addition of dithionite [8] it may be a simple experiment worth pursuing.

6.2.2 Other proteins

Although Chapter 5 dealt exclusively with myoglobin, a wide range of other proteins exist that could be detected in a similar fashion. Only a couple of these proteins will be discussed briefly below.

6.2.2.1 Hemoglobin

Similar to myoglobin, hemoglobin is an oxygen-binding protein consisting of four polypeptide chains (tetramer). Each of the four subunits has a hydrophobic pocket containing a Fe-PPIX heme group. High-sensitivity detection of hemoglobin could be useful for post exposure monitoring of chemical warfare agents. Currently MALDI-TOF-MS is required to detect adducts formed between agents such as mustard gas with the N-terminal valines of hemoglobin [10]. Defense Research Canada has been enthusiastic during preliminary discussions regarding this project, and a proposal is currently being drafted.

6.2.2.2 Cytochromes

Cytochromes are a large class of electron transfer proteins of the mitochondrial inner membrane. In particular, cytochrome *P*-450 consists of a single polypeptide chain with a single Fe-PPIX heme group, and is thus similar to myoglobin. Cytochrome *P*-450

is important in the bio-metabolism of many pharmaceuticals. Merck Frosst has expressed interest in our technology for detecting a series of cytochrome *P*-450 covalent adducts.

6.3 Literature cited

(1) Chan, K. C.; Muschik, G. M.; Isaaq, H. J. *Electrophoresis* **2000,** *21*, 2062.

(2) Zhang, X.; Sweedler, J. V. *Anal. Chem.* **2001,** *ASAP*.

(3) http://www.coherentinc.com/cohrLasersDPSS/html/sapphire.html .

(4) Melanson, J. E.; Baryla, N. E.; Lucy, C. A. *Trend. Anal. Chem.* **2001,** *20*, 365.

(5) Melanson, J. E.; Baryla, N. E.; Lucy, C. A. *Anal. Chem.* **2000,** *72*, 4110.

(6) Baryla, N. E.; Melanson, J. E.; McDermott, M. T.; Lucy, C. A. *Anal. Chem.* **2001,** *73*, 4558.

(7) Park, Z. Y.; Russell, D. H. *Anal. Chem.* **2000,** *72*, 2667.

(8) Adar, F.; Gouterman, M.; Aronowitz, S. *J. Phys. Chem.* **1976,** *80*, 2184.

(9) Marshall, T.; Williams, J.; Williams, K. M. *J. Chromatogr. B* **1991,** *569*, 323.

(10) Price, E. O.; Smith, J. R.; Clark, C. R.; Schlager, J. J.; Shih, M. L. *J. Appl. Tox.* **2000,** *20*, S193.

APPENDIX - Curriculum Vitae

Personal information

Date of birth: September 28, 1976
Place of birth: Moncton, New Brunswick
Languages spoken and written: English and French

Education history

07/1999-12/2001	University of Alberta Edmonton, Alberta Ph.D.
05/1998-06/1999	University of Calgary Calgary, Alberta MSc. Program (did not complete)
09/1994-04/1998	Dalhousie University Halifax, Nova Scotia BSc. (Advanced major in chemistry)

Scholarships and awards received

Scholarship/Award	Value	Location of Tenure	Year(s)
NSERC Post-Doctoral Fellowship	$ 35 000 /year for 2 years	ETH - Zurich	2002/03
Mary Louise Imrie Graduate Student Travel Award	$ 800	Boston, MA	2001
HPCE 2001 Student Travel Award	US$ 400	Boston, MA	2001
IICS 2000 Student Travel Award	US$ 800	Nice, France	2000
HPLC 2000 Student Travel Award	US$ 400	Seattle, WA	2000
Walter H. Johns Graduate Fellowship	$ 3 992 /year for 2 years	University of Alberta	2000/01
NSERC PGS-B (Graduate) Scholarship	$ 19 100 /year for 2 years	University of Alberta	2000/01
Tuition Scholarship	$ 1 500	University of Alberta	1999
Graduate Entrance Scholarship	$ 1 000	University of Alberta	1999
Graduate Research Scholarship	$ 2 000	University of Calgary	1999
Fee Remission Scholarship	$ 500	University of Calgary	1998/99
Belle Crowe Scholarship	$ 350	Dalhousie University	1997/98
Eastern Conference High School Hockey League Academic Athlete of the Year	$ 1 000	Dalhousie University	1994/95

Refereed publications

8. Nicole E. Baryla, Jeremy E. Melanson, Mark T. McDermott, and Charles A. Lucy, "Characterization of Surfactant Coatings in Capillary Electrophoresis by Atomic Force Microscopy", *Analytical Chemistry*, **2001**, 73, 4558-4565.

7. Jeremy E. Melanson, Nicole E. Baryla, and Charles A. Lucy, "Dynamic Capillary Coatings for Electroosmotic Flow Control in Capillary Electrophoresis", *Trends in Analytical Chemistry*, **2001**, 20, 365-374. (Invited review article.)

6. Jeremy E. Melanson, Brian L.-Y. Wong, Charles A. Lucy, and Camille A. Boulet, "High-Sensitivity Determination of Chemical Warfare Agent Degradation Products by Capillary Electrophoresis - Indirect UV Detection", *Journal of Chromatography A*, **2001**, 920, 359-365.

5. Jeremy E. Melanson, Charles A. Lucy, and Camille A. Boulet, "Indirect Laser-Induced Fluorescence Detection for Capillary Electrophoresis Using a Violet Diode Laser", *Analytical Chemistry*, **2001**, 73, 1809-1813.

4. Cheryl J. Vos, Jeremy E. Melanson, and Charles A. Lucy, "Violet Diode Laser for Metal Ion Determination by Capillary Electrophoresis - Laser Induced Fluorescence", *Analytical Sciences*, **2001**, 17, 225-227. (Invited paper in special issue dedicated to "Young Generation in Analytical Sciences".)

3. Jeremy E. Melanson and Charles A. Lucy, "Violet (405 nm) Diode Laser for Laser Induced Fluorescence Detection in Capillary Electrophoresis", *Analyst*, **2000**, 125, 1049-1052.

2. Jeremy E. Melanson, Nicole E. Baryla, and Charles A. Lucy, "Double-Chained Surfactants for Semi-Permanent Wall Coatings in Capillary Electrophoresis", *Analytical Chemistry*, **2000**, 72, 4110-4114.

1. Jeremy E. Melanson and Charles A. Lucy, "Ultra-Rapid Analysis of Nitrate and Nitrite by Capillary Electrophoresis", *Journal of Chromatography A*, **2000**, 884, 311-316.

Conference presentations

11. Jeremy E. Melanson and Charles A. Lucy, "Violet (405 nm) Diode-Laser Induced Fluorescence Detection of Proteins in Capillary Electrophoresis", *High Performance Capillary Electrophoresis* (HPCE 2001), Boston, MA, Jan. 13-18, 2001. (poster)

10. Jeremy E. Melanson, Charles A. Lucy, Robert T. Poirier and Camille A. Boulet, "Modes of Detection for Chemical Warfare Agent Degradation Products in Capillary

Electrophoresis" *The International Chemical Congress of Pacific Basin Societies* (Pacificem 2000), Honolulu, Hawaii, Dec. 14-19, 2000. (oral)

9. Jeremy E. Melanson and Charles A. Lucy, "Violet Diode Laser Presents Opportunities for Sensitive and Selective Detection in Ion Analysis", *International Ion Chromatography Symposium* (IICS 2000), Nice, France, Sept. 11-14, 2000. (oral)

8. Charles A. Lucy, Nicole E. Baryla, and Jeremy E. Melanson, "Surfactant Coatings for Electroosmotic Flow Control in Capillary Zone Electrophoresis", *International Ion Chromatography Symposium* (IICS 2000), Nice, France, Sept. 11-14, 2000. (oral)

7. Nicole E. Baryla, Jeremy E. Melanson, and Charles A. Lucy, "Atomic Force Microscopy Studies of Surfactant Wall Coatings in Capillary Electrophoresis", *International Conference on Analytical Sciences and Spectroscopy* (ICASS 2000), Winnipeg, Manitoba, August 13-16, 2000. (oral)

6. Charles A. Lucy, Cheryl Vos, and Jeremy E. Melanson, "Capillary Electrophoresis-Laser Induced Fluorescence using a Violet Diode Laser", *International Conference on Analytical Sciences and Spectroscopy* (ICASS 2000), Winnipeg, Manitoba, August 13-16, 2000. (oral)

5. Jeremy E. Melanson and Charles A. Lucy, "Laser Induced Fluorescence Detection of Chemical Warfare Agent Degradation Products in Capillary Electrophoresis", *High Performance Liquid Chromatography* (HPLC 2000), Seattle, Washington, June 24-30, 2000. (poster)

4. Charles A. Lucy, Nicole E. Baryla, Jeremy E. Melanson and Ken K.-C. Yeung, "Surfactant Additives as Dynamic Coatings in Capillary Zone Electrophoresis", High Performance Liquid Chromatography (HPLC 2000), Seattle, Washington, June 24-30, 2000. (oral)

3. Jeremy E. Melanson, Nicole E. Baryla, and Charles A. Lucy, "Semi-Permanent Wall Coatings in Capillary Electrophoresis formed using Double Chained Cationic Surfactants", *Canadian Society for Chemistry National Meeting & Exhibition* (CSC 2000), Calgary, AB, May 28-31, 2000. (oral)

2. Jeremy E. Melanson and Charles A. Lucy, "Double-Chained Cationic Surfactants for Electroosmotic Flow Reversal in Capillary Electrophoresis", The *Federation of Analytical Chemistry and Spectroscopy Societies* (FACSS) annual meeting held in conjunction with 45th *International Conference on Analytical Sciences and Spectroscopy*, Vancouver, BC, Oct. 1999. (poster)

1. Jeremy E. Melanson and Charles A. Lucy, "Ultra-Rapid Analysis of Nitrate and Nitrite by Capillary Electrophoresis", *International Ion Chromatography Symposium*, San Jose, California, Sept. 1999. (poster)